Modelling of an Integrated Gas and Electricity Network with Significant Wind Capacity

Meysam Qadrdan

School of Engineering

Cardiff University

Acknowledgements

DECLARATION

This work has not previously been accepted in substance for any degree and is not concurrently submitted in candidature for any degree.

Signed .... (candidate)   Date ....

This thesis is being submitted in partial fulfillment of the requirements for the degree of PhD.

Signed .... (candidate)   Date ....

This thesis is the result of my own independent work/investigation, except where otherwise stated. Other sources are acknowledged by explicit references.

Signed .... (candidate)   Date ....

I hereby give consent for my thesis, if accepted, to be available for photocopying and for interlibrary loan, and for the title and summary to be made available to outside organisations.

Signed .... (candidate)   Date ....

Abstract

The large scale integration of wind generation capacity into an electricity network poses technical as well as economic challenges. In this research, three major challenges introduced by wind including non-correlated power output from geographically dispersed wind farms, wind variability and wind uncertainty were studied. In order to address each of the aforementioned challenges an appropriate modelling approach and case studies were used.

The impacts of power output from dispersed wind farms on the Great Britain transmission reinforcement were studied using an optimal DC load flow combined with a power generation model. It was shown that Western and Eastern HVDC links play a crucial role to bypass the Scotland to England transmission bottleneck.

The impacts of wind variability on the GB gas and electricity network were investigated through application of the Combined gas and Electricity Network (CGEN) Model. Additional gas storage capacity was shown to be an efficient option to compensate for wind variability.

Two-stage and multi-stage stochastic programming models were developed to examine the impact of wind forecast uncertainty on the GB electricity and gas networks. Stochastic modelling approaches were shown to be efficient methods for scheduling and operating the system under wind uncertainty.

The key contributions of this thesis are the investigation of the impacts of wind generation variability on the gas network, and development of two-stage and multi-stage stochastic programming models of integrated gas and electricity network.

Contents

List of Figures

List of Tables

Nomenclature

Abbreviations and Acronyms

bcm	Billion Cubic Meters
$CCGT$	Combined Cycle Gas urbine
DM	Deterministic Model
ED	Economic Dispatch
GW	Gigawatt
h	Hour
$HVDC$	High Voltage Direct Current
LNG	Liquefied Natural Gas
MSM	Multi-stage Stochastic Model
MW	Megawatt
PFM	Perfect Foresight Model
SSA	Singular Spectrum Analysis
$SVPF$	Single Valued Point Forecast
TSM	Two-stage Stochastic Model
TWh	Terawatt hour
UC	Unit Commitment
$UKCS$	United Kingdom Continental Shelf
WPF	Wind Power Forecast

Constants

R	Gas constant
Re	Reynolds number
Z	Gas compressibility

Subscripts

b	Electrical busbar
c	Gas compressor
g	Gas terminal

i	Power generator
k	Thermal plants
l	Transmission line
m	Gas node
q	Gas pipe
t	Time
u	Gas storage facility
z	Level of possible wind power outcome at each time step

Superscripts

ι	Gas injection
ω	Gas withdrawal
av	Superscript av indicates average amount of a variable
f	Fuel cost of power generation
n	Superscript n indicates the standard condition
s	Scenario
sd	Shut-down
sp	Spot price
su	Start-up
ue	Unserved electricity
ug	Unserved gas
var	Variable cost of power generation

Parameters

α	Polytropic exponent
β	Gas turbine fuel rate coefficient of a compressor
$\Delta\left(\phi^s, \phi^{s'}\right)$	Distance between scenarios s and s'
Δw	Distance between every two adjacent levels of wind power (MW)
η	Efficiency
$\mathbb{E}[.]$	Expected value of a function
$\boldsymbol{\Phi}$	Set of wind power forecast scenarios
$\mathbf{N}(\mu, \sigma)$	Normal probability distribution function with mean value of μ and standard deviation of σ
$\mathbf{U}(a, b)$	Uniform probability distribution function with lower and upper bounds of a and b, respectively
$\overline{P}$	Maximum generation capacity of a thermal plants (MW)
$\overline{P}^w$	Upper bound of possible wind power outcome at each time step (MW)
$\overline{R}$	Maximum power ramp-up (MW/h)

ϕ	Wind power forecast scenario
π^s	Probability of scenario s
$\pi_{z,t}$	Probability of wind power level z at time t
ρ	Gas density, assuming standard conditions (kg/m^3)
$\underline{P}$	Minimum power generation of a thermal plants (MW)
$\underline{P}^w$	Lower bound of possible wind power outcome at each time step (MW)
$\underline{R}$	Maximum power ramp-down (MW/h)
$\underline{r}^{up}$	Minimum reserve requirement to support generator outages and forecast errors in electrical demand (MW)
$\widetilde{P}^w$	Possible wind power outcome at every time step (MW)
A	Pipe cross sectional area (m^2)
C	Cost (č£č)
C_{TC}	Maximum cold start-up cost (h)
CDT	Cool-down time (h)
D	Pipe diameter (mm)
DT	Minimum down-time for thermal units (h)
$F(\mu, \sigma)$	Cumulative density function for wind power distribution
f	Friction factor in a pipe
H	Heat value of natural gas $(\sim 39MJ/m^3)$
M	Incidence matrix
N^w	Number of possible levels of wind power at each time step
N^{ds}	Desired number of scenarios
N^{rs}	Number of random scenarios that initially generated
TC	Cool-down time (h)
$Temp$	Gas temperature (K)
ts	Length of time step (h)
UT	Minimum up-time for thermal units (h)
$wu\%$	Percentage of wind generation contributing to up spinning reserve requirements

Variables

ν	ON/OFF state of thermal unit (1/0)
∂LP	Linepack changes (mcm/h)
τ	Amount of gas tapped by a compressor (mcm)
E	Stored electrical energy in a pumped storage unit (MWh)
LP	Gas linepack (mcm)
P	Power (MW)

p	Gas pressure ($Pascal$)
Q	Gas flow (mcm/h)
r	Spinning reserve (MW)
S	Gas storage level (mcm)
V	Volume of a pipe (m^3)
v	gas velocity through a pipe (m^3/s)

Chapter 1

Introduction

1.1 Background

The administrative structure and ownership of the power sector has undergone major changes in many countries during the last two decades. The driving forces behind this restructuring are environmental and security concerns regarding utilisation of fossil fuel as well as privatisation of the energy sector.

The generation mix in many countries is moving toward a greater share of gas-fired (especially CCGT) and renewable generation (mostly wind). The increase in gas-fired generation results in a large rise of total gas demand.

Currently, a considerable amount of electricity is generated through gas-fired power plants. According to the World Energy Outlook 2010 [3], the worldwide gas consumption in the power sector in 2008 was 4303 TWh. This amount is projected to increase to 7600 TWh by 2035. The increase in gas demand for electricity generation makes natural gas the only fossil fuel for which total demand is higher in 2035 than in 2008. Due to the rise in gas demand, gas network capacity will need to increase to supply fuel to new gas fired power plants. At the same time, indigenous gas production in OECD regions, especially in most European countries, is not increasing fast enough to meet

the dramatic rise in gas demand (Table 1.1) which compels these countries to continually increase gas importation via pipeline or in the form of LNG. The share of LNG in total gas trade is projected by IEA to rise from 31% in 2008 to 35% in 2020 and 42% in 2035 [3].

In Fig. 1.1 a schematic representation of gas and electricity interaction on a national level is illustrated which shows the power sector of gas importing countries influencing the large share of gas imports. The dependency on imported gas not only affects security of gas supplies, but also causes concerns regarding the security of the power system.

Table 1.1: Natural gas demand and production in OECD regions (bcm), IEA's new policies scenario [3].

	Gas demand		Gas production		Annual demand growth	Annual production growth
	2008	2035	2008	2035	2008-2035	2008-2035
Europe	555	628	307	206	0.5%	-1.5%
North America	815	913	797	846	0.4%	0.2%
Pacific	170	216	53	136	0.9%	3.6%
OECD	**1541**	**1758**	**1157**	**1188**	**0.5%**	**0.1%**
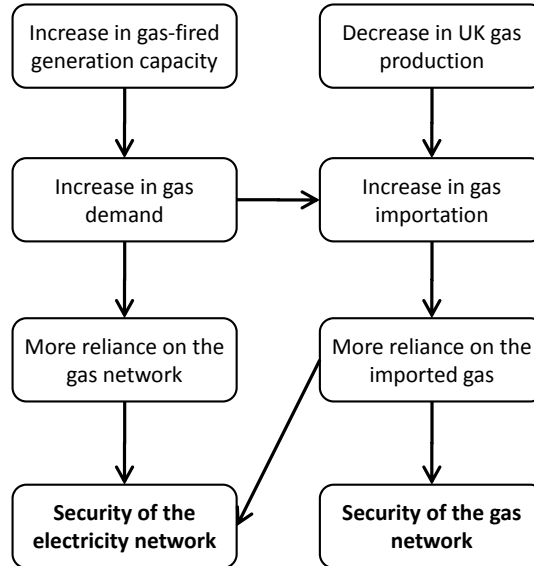
Figure 1.1: Gas and electricity sectors' interaction on a national level

The UK has ambitious plans to increase the share of electrical energy generated from renewables to more than 30% by 2020 [11]. Wind generation capacity is expected to contribute the majority of new renewable generation and be around 30 GW by 2020 [4; 11]. Other major changes in GB generation capacity mix are the expected decline of coal generation capacity due to the Large Combustion Plant Directive (LCPD) [12], and increase in gas-fired generation capacity (see Table 1.2).

Table 1.2: Connected generation capacity in "Gone Green" scenario (GW) [4]

Generation type	2009/2010	2020/2021
Coal-fired	28.4	19.8
Gas-fired	27.5	34.6
Nuclear	10.4	6.9
Wind	2.4	29.4
Oil	3.4	0
Pumped hydro	2.7	2.7
Hydro	1	1.1
Interconnector	2.1	4.2
Other	1.3	2.5
Total	**79.2**	**101.2**

Increase in the gas-fired generation capacity is happening along with a decline of UKCS gas reserves, as National Grid's trend analysis shows the percentage of UK gas that is imported will rise to 62-83% by 2020 [13].

1.2 Interdependencies between gas and electricity networks

Gas and electricity infrastructures are often modelled and analysed independently. However, in recent years researches regarding the integration of gas and electricity networks have been conducted as a consequence of the growing installation of gas-fired power plants [14; 15; 16]. The purposes of the mentioned researche are to analyse the techno-economic interdependencies between gas and electricity networks [17; 18] and to evaluate the security of the integrated system [15; 16; 19].

Since natural gas contributes a large share of the final cost of power generated by gas-fired plants, changes in the gas price has a significant impact on electricity prices. The larger the capacity of gas-fired generation, the stronger the link between gas and electricity markets are. Therefore, in a generation mix with a large share of gas-fired plants, a spike in gas price strongly influences electricity price and subsequently

economic competitiveness of the gas-fired plants in the electricity market. Over the long term, high gas price expectation impacts on power generation capacity expansion planning decisions [20]. For example, at the time that electric utility restructuring program was adopted and started in California gas price was assumed to remain well below US$3/MBtu, but then it rose dramatically to a level of US$4-5/MBtu [20]. Fontini and Paloscia [21] investigated the impacts of installing new CCGT plants on electricity price in Italy.

In an energy system with large capacity of gas-fired power plants, the capability of the gas network to supply the electrical gas demand to the power sector is crucial and affects the optimal operation of the electricity network [16; 22]. In such an integrated system, an interruption in the gas network not only constrains the ability to meet gas demand but could also disrupt electricity supplies [15]. Li et al. [22] analysed the impact of interdependency of electricity and natural gas networks on power system security using an integrated model. The model takes into account the natural gas network constraints in the optimal solution of security-constrained unit commitment. Role of dual-fuel gas generators to hedge price volatilities of natural gas and electricity is analysed. Shahidehpour et al. [23] investigated the impact of natural gas infrastructure contingencies on the operation of electricity networks. The impact of renewable sources of energy (hydro and PV) on power system security by reducing the dependence of the electricity network on the natural gas infrastructure is examined.

1.3 Challenges of significant wind power integration

Large scale integration of wind farms into the electricity network poses great technical challenges in operation of the network. There have been technical solutions proposed to deal with these challenges, but the economic feasibility of the solutions is a key issue. For example, large scale electrical storage is, technically, the first choice solution to

compensate for wind variability but given its high capital cost and low efficiency, it is not economically justifiable, except for especial purposes. In the following the most common challenges of wind farms integration are described.

1.3.1 Transmission capacity reinforcement

The impact of wind power on transmission networks depends on the locations of the wind farms and the load centres. Wind power affects the power flow in the network. It may change the power flow direction, reduce or increase power losses and introduce bottlenecks. Therefore, grid reinforcement may be necessary to maintain transmission adequacy [24].

Distribution of wind farms across GB is not uniform. A large capacity of wind generation is located in Scotland while the centre of power demand is in the south of England. Therefore, transmission reinforcement is required to ensure sufficient North-South transmission capacity. Hence, Western and Eastern HVDC links are proposed by the Electricity Network Strategy Group (ENSG) to be installed by 2020 [25].

1.3.2 Wind variability

Since wind is an intermittent source of energy, the amount of electricity generated by wind farms is variable. Such variability requires other generators to ramp up and down, as wind power varies, to balance the electricity demand. Gas-fired plants with their large generating capacity in GB are potential candidates to compensate for wind variability. This leads to more frequent as well as larger power swings by gas-fired generators which subsequently causes an increase in the wear-and-tear cost of the generators. This could also lead to large flow variations in the gas network as gas-fired plants ramp up and down, which in return, incurs pressure fluctuation in the gas network that may constrain gas delivery [2].

There has been much debate on the ability of wind energy to provide reliable and

cheap electricity supplies. While Berry [17] and Graves and Litvinova [26] highlighted the significant role of wind energy in hedging and stabilising gas and electricity prices in the short- and long-term, other studies pointed out difficulties of integrating large amounts of wind generation into a power network [2]. The impact of wind generation variability on the operation of power systems has been investigated by many researchers [27; 28; 29; 30; 31], but its effects on the gas network have not been well studied. There have been a number of studies that have analysed the operation of integrated gas and electricity networks [14; 15; 23; 32] but none have considered the varying nature of wind energy.

1.3.3 Wind uncertainty

Uncertainty of wind power forecasts is an important issue in wind farms integration. A large capacity of flexible generators and higher amount of reserves is required to compensate for wind forecast uncertainty. Therefore, as the share of wind power capacity in generation portfolios increases, wind power forecasting becomes essential. An accurate forecast of wind power reduces the reserve requirement and also leads to a better time-ahead unit scheduling.

1.4 Research Objective

The objectives of the research described in this thesis are focused on investigating the three main impacts of large scale integration of wind energy into an electricity network: (a) transmission network reinforcement (b) the effect of wind variability on the gas network and (c) wind uncertainty.

A large amount of wind power generation capacity is expected to be installed in Great Britain by 2020. A considerable amount of this capacity will be located in Scotland. This will require reinforcement of power transmission capacity between Scotland

and England-Wales. Western and Eastern submarine HVDC links are two transmission reinforcement options proposed by Electricity Network Strategy Group (ENSG) [25]. Efficacy of the reinforcement options (Eastern and Western HVDC links) as well as the economic feasibility of each were analysed.

Given the significant role of gas-fired generators in order to compensate for wind variability, gas and electricity networks operation need to be analysed in an integrated manner to take into account the gas supply constraints for power generation. This also helps to investigate the impacts of wind variability on the gas network operation. A hypothesised structure of the GB gas and electricity networks in 2020 was used to study the impacts of wind power variability on the gas and electricity networks.

Wind uncertainty makes it more difficult to optimally schedule the thermal plants. In this research, two-stage and multi-stage stochastic programming approaches are presented as practical and efficient methods for scheduling the power plants and operating the combined gas and electricity networks.

1.5 Thesis Outline

The structure of the thesis and description of each chapter are discussed in this section.

In Chapter 2 the Combined Gas and Electricity Network (CGEN) model is described. This chapter includes a general formulation of the CGEN model, in addition to explanations of the model properties.

In Chapter 3 the electricity part of the CGEN model was used to analyse the performance of the GB power transmission network in the presence of dispersed wind farms' power output. In this chapter three case studies were defined to investigate three possibilities for GB transmission network in 2020. The base case represents the GB transmission network in 2020 with onshore transmission reinforcement. The other two case studies take into account the onshore transmission reinforcement along with

Eastern and Western sub-sea HVDC links.

In Chapter 4 the impacts of wind power variability on the GB gas network is investigated. The CGEN model was used to analyse three case studies representing the existing GB gas and electricity network in 2009, and hypothesised GB networks in 2020 with high and low wind power generation. The capability of the gas network to meet electrical gas demand during low wind periods was analysed and bottlenecks in the gas network were identified. Suitable mitigation measures to compensate for gas network bottlenecks were proposed and modelled.

In Chapter 5 a method is proposed for probabilistic wind power forecast. Monte Carlo simulation was used to generate a large number of forecast scenarios with their probabilities. Then, an algorithm for reducing the number of scenarios was proposed.

In Chapter 6 stochastic models of integrated gas and electricity network are described to take into account the wind forecast uncertainties in the operational optimisation of the integrated network. A simple case study was modelled for the purpose of comparison between different common operational approaches. Four different approaches including perfect foresight, deterministic calculation with high spinning reserve, two-stage stochastic programming and multi-stage stochastic programimg were used for comparison.

In Chapter 7 the stochastic models described in the previous chapter, Chapter 6, were used to model the GB gas and electricity network. The focus of this chapter is to provide policy-making insights on configuring the system in the presence of large capacity of wind generation.

Chapter 2

Combined Gas and Electricity Network model (CGEN)

2.1 Introduction

The Combined Gas and Electricity Network (CGEN) model [15] is a multi-time period optimisation tool to investigate the optimal operation of the gas and electricity networks as an integrated system. The interdependencies between the gas and electricity network can be analysed through CGEN.

CGEN takes into account the varying nature of gas flows, changes in energy demand, and wind generation variability. The time horizon and time step granularity can be defined by users. The optimisation model minimises costs associated with gas and electricity networks [15].

Various elements of gas and electricity networks considered in the CGEN model are depicted in Fig. 2.1. Gas-fired generators including CCGT, OCGT and CHP link the two networks. The gas supply from different sources to Local Distribution Zones (LDZ) and gas-fired generators are modelled in CGEN, including terminals, pipes, storage facilities, and compressors. Centralised generators and high voltage transmission lines

are considered in the electricity network.
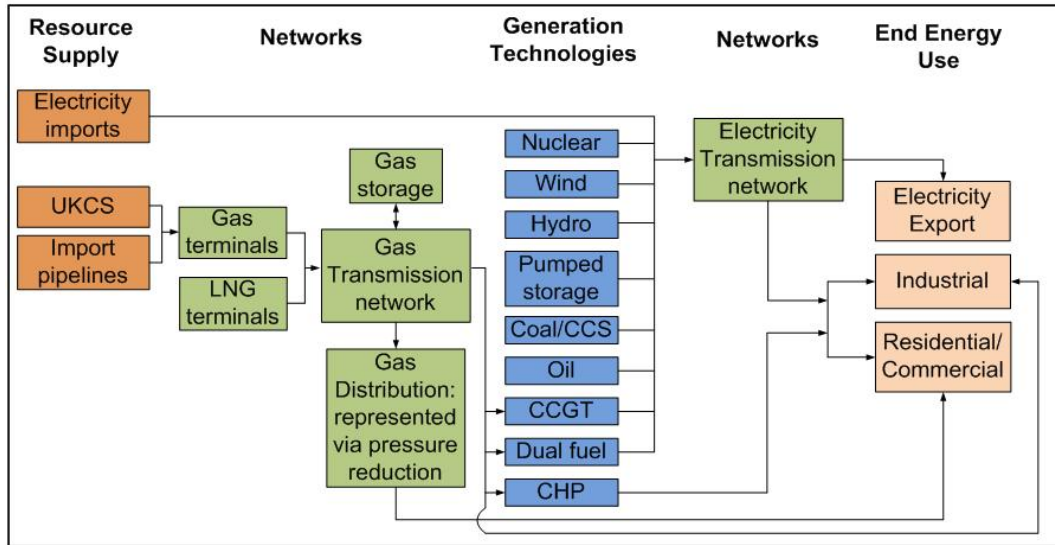
Figure 2.1: CGEN flow diagram

The Fico Xpress Optimisation suite was used to formulate and solve the optimisation problem. The non-linearity of the gas network equations was dealt with through Sequential Linear Programming (SLP) [33].

CGEN is a flexible modelling tool that can handle various case studies. Appropriate control parameters can be implemented to provide computationally efficient algorithms, depending on nature of the problem. The original formulation of CGEN, taken from [15], is described in this chapter. During this research the CGEN model, especially the electricity network model, was improved and additional constraints were implemented in the model (e.g. unit commitment and spinning reserve constraints, start-up and shut-down costs). These equations will be introduced in subsequent chapters.

2.2 CGEN objective function

The aim of the CGEN model is to minimise the total operational costs of the integrated network. The objective function of the CGEN model is presented in Eq. 2.1 which includes costs of gas supply, gas storage, linepack reduction, electricity generation, gas and electricity shedding.

$$
Objective =
$$

$$
\min \sum_t ts \times
\begin{Bmatrix}
\underbrace{\sum_g C_{g,t}^{gas}\, Q_{g,t}}_{cost\ of\ gas\ supply}
+ \underbrace{\sum_u \left(C^\iota\, Q_{u,t}^\iota + C^\omega\, Q_{u,t}^\omega \right)}_{cost\ of\ gas\ storage}
+ \underbrace{\sum_q C_t^{gas,sp}\, \partial LP_{q,t}}_{cost\ of\ linepack\ change} \\[3ex]
+\quad \underbrace{\sum_i C_{i,t}^{gen}\, P_{i,t}}_{cost\ of\ power\ generation}
\quad + \quad \underbrace{\sum_b C^{ue} P_{b,t}^{ue}}_{cost\ of\ unserved\ electricity}
\quad + \quad \underbrace{\sum_m C^{ug} Q_{m,t}^{ug}}_{cost\ of\ unserved\ gas}
\end{Bmatrix}
$$

(2.1)

where $C_{g,t}^{gas}$ is gas price at terminal g and time t, $Q_{g,t}$ is gas flow from terminal g at time t, C^ι is cost of gas injection to a storage facility, $Q_{u,t}^\iota$ is gas injection to storage facility u at time t, C^ω is cost of gas withdrawal from a storage facilty, $Q_{u,t}^\omega$ is gas withdrawal from storage facility u at time t, $C_t^{gas,sp}$ is spot gas prices at time t, $\partial LP_{q,t}$ is changes in linepack of pipe q at time t, $C_{i,t}^{gen}$ is generation cost of generator i at time t, $P_{i,t}$ is power output from generator i at time t, C^{ue} is cost of uncerved electricity, $P_{b,t}^{ue}$ is unserved electricity at bus b and time t, C^{ug} is cost of uncerved gas, and $Q_{m,t}^{ug}$ is unserved gas at node m and time t.

2.3   Gas network

The components of a gas network that are modelled in CGEN are pipelines, compressors, storage facilities and gas terminals.

2.3.1   Gas flow along a pipe

The gas flow rate in a pipe is influenced by the pressure difference between upstream and downstream nodes. Since variation of gas properties along the radius of a pipe is negligible in comparison to the variation along the streamline direction, the gas flow is assumed to be one-dimensional. The assumptions for this one-dimensional flow are [34; 35]:

- the cross-sectional area changes slowly along the path of the gas stream;

- the radius of curvature of the pipe is large compared with its diameter;

- the temperature and velocity profiles are approximately constant along the pipe; and

- the pipe is horizontal.

The gas flow along a pipe (Fig. 2.2) is governed by the *continuity* equation (Eq. 2.2) and *momentum* equation (Eq. 2.3).
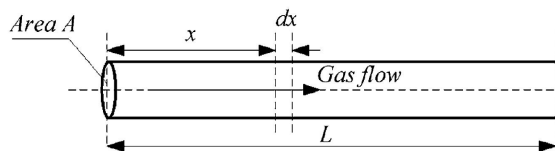
Figure 2.2: Gas flow along a pipe

$$\frac{\partial Q}{\partial x} = -\frac{A}{\rho \; Z \; R \; Temp}\frac{\partial p}{\partial t} \tag{2.2}$$

where $\frac{\partial Q}{\partial x}$ is change flow regarding the distace, A is Pipe cross sectional area, ρ is Gas density, Z is Gas compressibility, R is Gas constant, $Temp$ is temperature, and $\frac{\partial p}{\partial t}$ is chang of pressure over time.

$$\frac{\partial p}{\partial x} = -\frac{\partial\left(\rho\ v\right)}{\partial t} - \frac{\partial\left(\rho\ v^2\right)}{\partial x} - \frac{2\ f\ \rho\ v^2}{D} \tag{2.3}$$

where $\frac{\partial p}{\partial x}$ is change of pressure regarding the distance, v is gas velocity through a pipe, f is friction factor, and D is pipe diameter.

Given the assumptions described above, the change in kinetic energy along a pipe, $\partial\left(\rho\ v^2\right)/\partial x$ in Eq. 2.3, has little effect on the pressure drop and can be neglected [34]. Equation 2.3 can be re-written as:

$$\frac{\partial p}{\partial x} = -\frac{\partial\left(\rho\ v\right)}{\partial t} - \frac{2\ f\ \rho\ v^2}{D} \tag{2.4}$$

Substituting the volumetric flow rate ($Q = v\ A$) into Eq. 2.4 gives the momentum equation (Eq. 2.5).

$$\frac{\partial p}{\partial x} = -\frac{\rho}{A}\frac{\partial Q}{\partial t} - \frac{2\ f\ \rho\ Q\ |Q|}{A^2 D} \tag{2.5}$$

where $\rho\ Q$ is the mass flow rate ($\dot{m}$).

When considering large time steps and slow changes in load, the term $\left(-\frac{\rho}{A}\frac{\partial Q}{\partial t}\right)$ in Eq. 2.5 can be neglected [34], and therefore the momentum equation describing the transient flow of gas through a horizontal pipe is reduced to:

$$\frac{\partial p}{\partial x} = -\frac{2\ f\ \rho^n\ Q^n\ |Q^n|}{A^2 D}. \tag{2.6}$$

where superscript n indicates the standard condition.

The "Panhandle A" implementation of the friction factor (f) for high pressure networks ($p > 7 \times 10^5$ Pa) was used [34]:

$$\sqrt{\frac{1}{f}} = 6.872 \, (Re)^{0.073} \, \eta, \tag{2.7}$$

where Re is the Reynolds number (dimensionless), which is used to characterise gas flow conditions (for fully turbulent flow $Re \gg 4000$ [34]), and η is the efficiency factor that was taken into account for extra friction and drag losses other than losses due to viscous forces.

A finite difference approximation scheme (Fig. 2.3) is used to represent the x (distance along a pipe) and t (time) derivatives for Eqs. 2.2 and 2.6 [36].
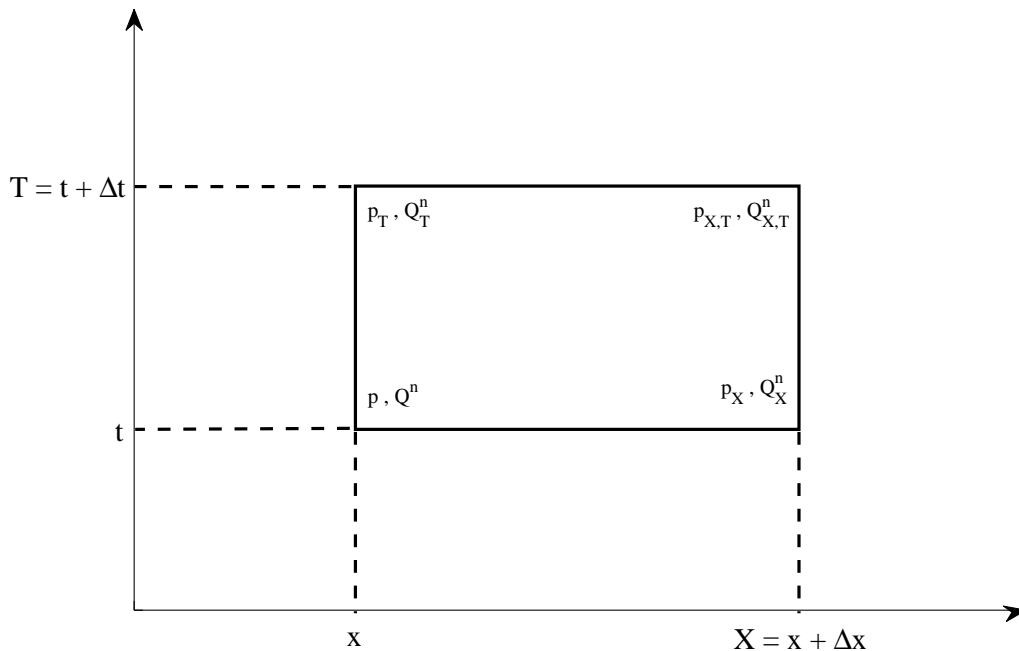
Figure 2.3: Finite difference cell

The steady state average pressure of a pipe at time t and $T = t + \Delta t$ are calculated by using Eqs. 2.8 and 2.9, respectively [34]:

$$p^{av} = \sqrt{\frac{1}{2} \left(p^2 + p_X^2 \right)} \tag{2.8}$$

$$p_T^{av} = \sqrt{\frac{1}{2} \left(p_T^2 + p_{X,T}^2 \right)}. \tag{2.9}$$

The average gas flow in a pipe at time $t + \Delta t$ is:

$$Q_T^{n,av} = \frac{1}{2} \left(Q_T^n + Q_{X,T}^n \right). \tag{2.10}$$

Using Eqs. 2.8, 2.9 and 2.10 with the gas equation of state (Eq. 2.11), transforms the original partial differential Eqs. 2.2 and 2.3 into ordinary differential Eqs. 2.12 and 2.13 used for calculating gas flow through a pipe.

$$Z \ R = \frac{p^n}{\rho^n \ Temp^n} = \frac{p}{\rho \ Temp} \tag{2.11}$$

$$\frac{Q_{X,T}^n - Q_T^n}{\Delta x} = -\frac{A}{\rho^n \ Z \ R \ Temp} \frac{(p_T^{av} - p^{av})}{\Delta t} \tag{2.12}$$

$$\frac{p_{X,T} - p_T}{\Delta x} = -\frac{2 \ Z \ R \ T \ f \ (\rho^n)^2 \left(Q_T^{n,av} \right) \left| Q_T^{n,av} \right|}{A^2 \ D \ p_T^{av}} \tag{2.13}$$

2.3.2 Linepack modelling

The linepack of a pipe is the volume of gas stored in the pipe and is a key factor that affects the ability to supply gas to demand nodes, i.e. a highly packed pipe allows fluctuations in demand be met locally as gas supply from a distant source will take time (typically hours) to reach its intended destination.

The linepack of a pipe (LP) is calculated by combining Eq. 2.11 and Boyle's equation (Eq. 2.14).

$$p^{av} \ V = p^n \ V^n \qquad (2.14)$$

where V is volume of the pipe, V^n is volume of the gas in standard condition, p^{AV} is average presure along a pipe, and p^n is gas pressure in standard condition.

Equation 2.15 is suitable for calculating the volume of gas in a pipe when the gas flow is in steady state. This illustrates that pipe linepack is proportional to the average pressure in the pipe, therefore, increasing the average pressure in the pipe will increase the linepack and vice versa.

$$LP = V^n = \frac{p^{av} \ V}{\rho^n \ Z \ R \ Temp^n} \qquad (2.15)$$

Under dynamic situations, the gas flow into and out of a pipe fluctuates with changing supply and demand. According to the law of conservation of mass, the change of total gas volume is equal to the difference between the flow into and out of the pipe. Thus, Eq. 2.15 is changed to Eq. 2.16:

$$LP_t = LP_0 + \int_0^t \left(Q^n - Q_X^n \right) dt \qquad (2.16)$$

where LP_0 is the initial gas stored in the pipe and is calculated by Eq. 2.15 in the steady state condition.

2.3.3 Gas compressors

Compressors are used in the gas transmission network to maintain gas pressure difference and ensure gas delivery to its intended demand nodes. The power required from the

compressor prime-mover is calculated by Eq. 2.17 [34]:

$$P_c = \frac{Q_c^n\ \alpha}{\eta_c\,(\alpha - 1)}\left[\left(\frac{p^{out}}{p^{in}}\right)^{(\alpha-1)/\alpha} - 1\right].\tag{2.17}$$

where P_c is power consumption by compressor c, Q_c^n is gas flow through compressor c in standard condition, α is Polytropic exponent, η_c is efficiency of compressor c, p^{out} is pressure of gas from a compressor, and p^{in} is pressure of gas into a compressor.

In practice, performance of a compressor is restricted by the following equations:

$$1 \le \frac{p^{out}}{p^{in}} \le CPR^{max} \quad \left(\frac{p^{out}}{p^{in}} = CPR \Rightarrow compressor\ pressure\ ratio\right)\tag{2.18}$$

$$Q_c^n \le Q_c^{n,max}\tag{2.19}$$

$$P_c \le P_c^{max}\tag{2.20}$$

The amount of gas tapped by the compressor as fuel is approximated by Eq. 2.21 [37].

$$\tau_{c,t} = \beta\ P_{c,t}\tag{2.21}$$

where $\tau_{c,t}$ is amount of gas tapped by a compressor, and β is gas turbine fuel rate coefficient of a compressor.

2.3.4   Gas storage

Various types of gas storage are modelled in CGEN such as salt cavern, depleted gas field and LNG, which have different operational characteristics.

Working gas: This is the volume of gas that can be withdrawn from storage. The actual total volume of gas in storage is a summation of the working gas and *cushion* gas. Cushion gas is the volume of gas required in storage to maintain an adequate pressure, and is not normally used. Therefore, the storage capacity of the working gas is constrained by Eq. 2.22.

$$S_u^{cush} + S_{u,t}^{work} \leq S_u^{max} \tag{2.22}$$

Equation 2.23 constrains the amount of gas stored in a storage facility at each time step.

$$S_{u,t}^{work} = S_{u,t-1}^{work} - Q_{u,t}^{\omega} + Q_{u,t}^{\iota} \tag{2.23}$$

where $Q_{u,t}^{\omega}$ and $Q_{u,t}^{\iota}$ are gas withdrawal and injection, and constrained through Eqs. 2.24 and 2.25, respectively.

$$0 < Q_{u,t}^{\omega} \leq Q_{u,t}^{\omega,max} \tag{2.24}$$

$$0 < Q_{u,t}^{\iota} \leq Q_{u,t}^{\iota,max} \tag{2.25}$$

Gas withdrawal: The withdrawal rate is at its highest when a storage facility is close to its maximum capacity and lowest when nearly empty [38]:

$$Q_{u,t}^{\omega,max} = K_u \sqrt{S_{u,t}^{work}} \tag{2.26}$$

Maximum withdrawal occurs at maximum gas capacity S_u^{Max} therefore K_u can be calculated from Eq. 2.26.

Gas injection: The injection rate is at its lowest when a storage facility is at

maximum capacity and at its highest when storage is empty [38].

$$Q_{u,t}^{\iota,max} = K_u' \sqrt{\frac{1}{S_{u,t}^{work} + S_u^{cush}} + K_u''} \qquad (2.27)$$

When a storage facility is at maximum capacity, no more gas injection can take place. Gas injection is therefore zero, $S_{u,t}^{work}$ and S_u^{cush} are known, hence K_u'' from Eq. 2.27 can be calculated. The maximum gas injection rate occurs when $S_{u,t}^{work}$ equals zero, therefore K_u' from Eq. 2.27 can be calculated.

2.3.5 Gas network constraints

At each node in the gas network, gas flow balance and pressure constraints are imposed, Eqs. 2.28 and 2.29 respectively. For each time step, gas inflows at each node (gas supply, gas storage withdrawal) are balanced with gas outflows (gas demand, compressor fuel usage, gas storage injection).

$$M_{m,g}Q_g + M_{m,q}Q_q + M_{m,c}Q_c - M_{m,\tau}\tau_c + M_{m,u}Q_u = M_{m,d}\left(Q^{dem} - Q^{shed}\right) \quad (2.28)$$

where $M_{m,g}$ is node-terminal incidence matrix, $M_{m,q}$ is node-pipe incidence matrix, $M_{m,c}$ is node-compressor incidence matrix, $M_{m,u}$ is node-storage incidence matrix, and $M_{m,d}$ is node-demand centre incidence matrix.

$$p_m^{min} \leq p_{m,t} \leq p_m^{max} \qquad (2.29)$$

2.4 Electricity network

A dc power flow model [39; 40] was used to represent the electricity network. The dc power flow model is a simplification of an ac power flow and is based on the following

assumptions:

- the line resistance in a high voltage transmission system is very much smaller when compared to line reactance, such that resistance and system losses can be neglected

- the phase voltage angle difference of a high voltage line is very small

- the bus voltage per unit is close to nominal value ($\sim$ 1.0 p.u).

2.4.1 Power balance constraints

The power balance equations are satisfied such that total generation is equal to total demand minus load shedding at each time step (Eq. 2.30):

$$\sum_i P_{i,t} = \sum_b P_{b,t}^{demand} - \sum_b P_{b,t}^{ue} \tag{2.30}$$

where $P_{i,t}$ is power output of generator i at time t, $P_{b,t}^{demand}$ is electrical power demand at bus b and time t, and $P_{b,t}^{ue}$ is uncerved electricity at bus b and time t.

2.4.2 Power generation

The generation schedule produced is kept within the physical limitations of the generating units (Eq. 2.31):

$$P_i^{min} \leq P_{i,t} \leq P_i^{max} \tag{2.31}$$

2.4.3 Ramp rate constraints

Since power plants cannot ramp up or ramp down instantaneously, the following constraints were imposed:

$$P_{i,t} - P_{i,t-1} \leq \overline{R}_i \tag{2.32}$$

$$P_{i,t-1} - P_{i,t} \leq \underline{R}_i \tag{2.33}$$

where $\overline{R}_i$ and $\underline{R}_i$ are ramp-up and ramp-down for generator i, respectively.

2.4.4 Power transmission

Power transmission along a line is constrained by maximum transmission capacity of the line (Eq. 2.34).

$$P_{l,t} \leq P_l^{max} \tag{2.34}$$

where $P_{l,t}$ is electrical power transmitted through line l.

2.5 Linkage between gas and electricity network

Gas turbine generators provide the linkage between gas and electricity networks. They are considered as energy converters between these two networks. For the gas network, the gas turbine was looked upon as a gas load. Its value depends on the power flow in the electricity network. In the electricity network, the gas turbine generator is a source. The relationship between the gas fuel flow and the real electrical power generated is expressed as:

$$P_{i,t} = \eta_i \, Q_{i,t} \, H \tag{2.35}$$

where η_i is thermal efficiency of generator i, $Q_{i,t}$ is gas consumption by generator i at time t, and H is Heat value of natural gas.

2.6 Summary

The general formulation of the CGEN model was presented. Additional constraints will be introduced in subsequent chapters when they are used. CGEN is a flexible modelling tool which can be used to optimise either the integrated network or each individual network separately.

Chapter 3

GB Transmission Network Study Using the Power Output of Dispersed Wind Farms

3.1 Introduction

A large amount of wind power generation capacity is expected to be installed in Great Britain by 2020. A considerable amount of this capacity will be located in Scotland. This will require reinforcement of power transmission capacity between Scotland and England-Wales. Western and Eastern HVDC links are two transmission reinforcement options proposed by Electricity Network Strategy Group (ENSG) [25].

The Western subsea HVDC link will provide additional capacity of 1800 MW to the circuit between Hunterston on the west coast of Scotland and Deeside in North Wales at an approximate cost of £800 million [41; 42]. The Eastern subsea HVDC link with capacity of 1800 MW connects Peterhead in north east of Scotland to Hawthorne Pit on the east coast of England. The total cost of reinforcement was estimated to be around £760 million.

3. GB Transmission Network Study Using the Power Output of Dispersed Wind Farms

The CGEN model (only the electricity network) was used to analyse the GB electricity transmission network performance given the presence of significant and geographically dispersed wind power capacity. The main focus was to investigate the role of Eastern and Western HVDC links through three hypothesised case studies. For this purpose, wind generation output from 29.5 GW of dispersed wind turbines, expected to be installed by 2020 in GB, was modelled. A sixteen bus electrical network shown in Fig. 3.1 was used to represent the simplified GB electricity network.

The busbars are connected by 15 transmission circuits and two eastern and western HVDC links. The capacity of different generation technologies at each bus and maximum transmission capacities for the lines are presented in Table 3.1 and 3.2, respectively.

Table 3.1: Expected generation capacity (GW) on different busbars in 2020

Bus	Nuclear	Coal	Gas-fired	Interconnector	Biomass	Wind	Hydro
Bus 1	—	—	—	—	—	3	0.9
Bus 2	—	—	1.64	—	—	3.9	—
Bus 3	—	—	—	—	—	—	0.25
Bus 4	—	—	—	—	—	—	0.23
Bus 5	—	1.3	—	—	0.05	2.25	0.44
Bus 6	1.2	—	0.34	—	0.05	2.25	0.03
Bus 7	1.2	2.93	3.21	—	0.3	2.37	—
Bus 8	—	—	—	—	—	—	—
Bus 9	2.22	1.48	4.26	0.87	—	4.24	2
Bus 10	—	4.7	4.7	—	—	2	—
Bus 11	—	—	—	—	—	—	—
Bus 12	—	2.97	2.85	—	—	0.98	—
Bus 13	—	1.8	3.88	—	—	4.5	—
Bus 14	—	—	2.43	—	—	1	—
Bus 15	—	3.16	5.88	—	0.4	1.5	—
Bus 16	2.28	1.46	5.71	3.33	—	1.46	—
Total	6.9	19.8	34.9	4.2	0.8	29.45	3.85

Table 3.2: Maximum capacity of interconnecting GB transmission circuits

GB transmission boundaries	Maximum capacity (MW)
TB1	1600
TB2	2800
TB3	500
TB4	3300
TB5	5150
TB6	5800
TB7	7500
TB8	649
TB9	3842
TB10	10800
TB11	3908
TB12	5215
TB13	11724
TB14	3381
TB15	2590
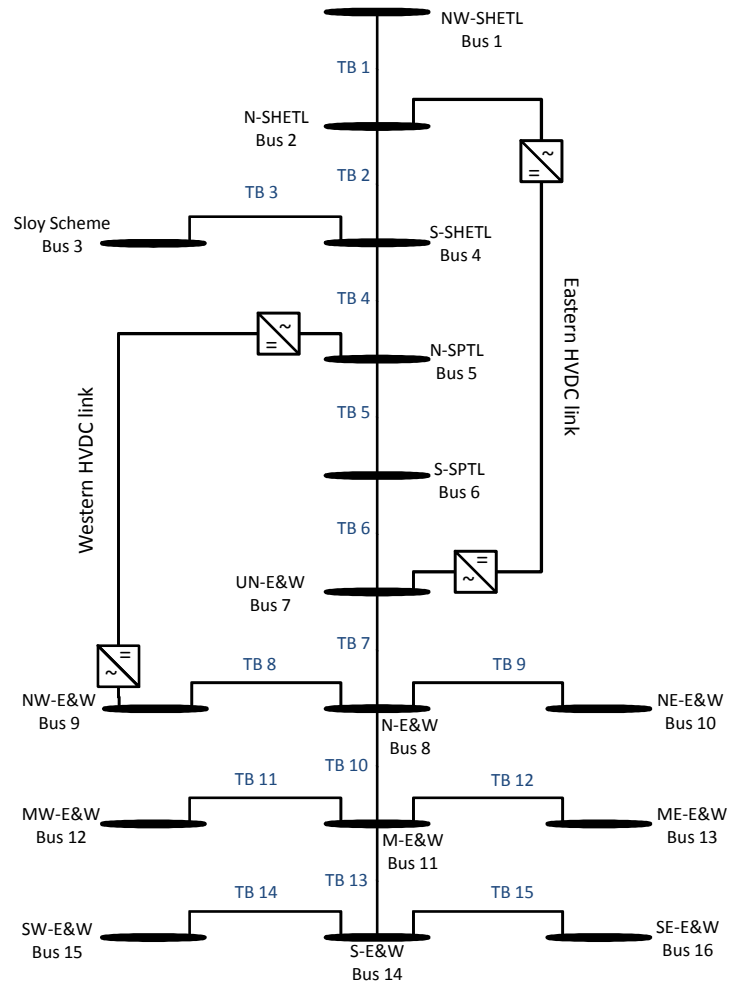
Figure 3.1: Sixteen bus representation of GB electricity network with the proposed HVDC links

3.2 Method for artificial wind power output generation

To obtain a geographically distributed wind power output, wind turbines were assumed to be installed at the 14 onshore and offshore locations shown in Table 3.3. They include

existing wind farm locations as well as prospective onshore [8] and offshore sites [43] chosen in accordance with [41].

Using the information provided in Table 3.3 and average monthly long-term wind speed in different locations, a method for artificially producing wind power output was developed by Gerber et al, [9; 44]. Artificially generated wind power data produced by [9] was used in this study as input to the model (see Fig. 3.2).

Table 3.3: Locations with installed wind power capacity in different buses (13.1 GW onshore and 16.4 GW offshore)

Location	Capacity (GW)	Bus number	Region
North Scotland (onshore)	3	1	NW-SHETL
Northwest Scotland (onshore)	3.9	2	N-SHETL
Firth of Forth (offshore)	2	5	N-SPTL
South Scotland (onshore)	2.5	6	S-SPTL
Dogger Bank (offshore)	2.4	7	UN-E&W
Rhyl (onshore)	0.7	9	NW-E&W
North West (offshore)	3.5	9	NW-E&W
Hornsea (offshore)	2	10	NE-E&W
West Wales (onshore)	1	12	MW-E&W
Norfolk and Triton (offshore)	4.5	13	ME-E&W
Isle of Wight (offshore)	1	14	S-E&W
South West England (onshore)	0.5	15	SW-E&W
Bristol Channel (offshore)	1	15	SW-E&W
Thames (offshore)	1.5	16	SE-E&W

Monthly long-term wind speed averages from the Met Office were used for onshore sites. For offshore locations monthly wind speed averages from the nearest buoys or vessels were used [45]. Where these measurements were not available, linear regression was used to calculate estimates based on the nearest suitable onshore site [46; 47].

Figure 3.2 shows the artificially generated wind power data at each electrical bus over the modelling horizon.
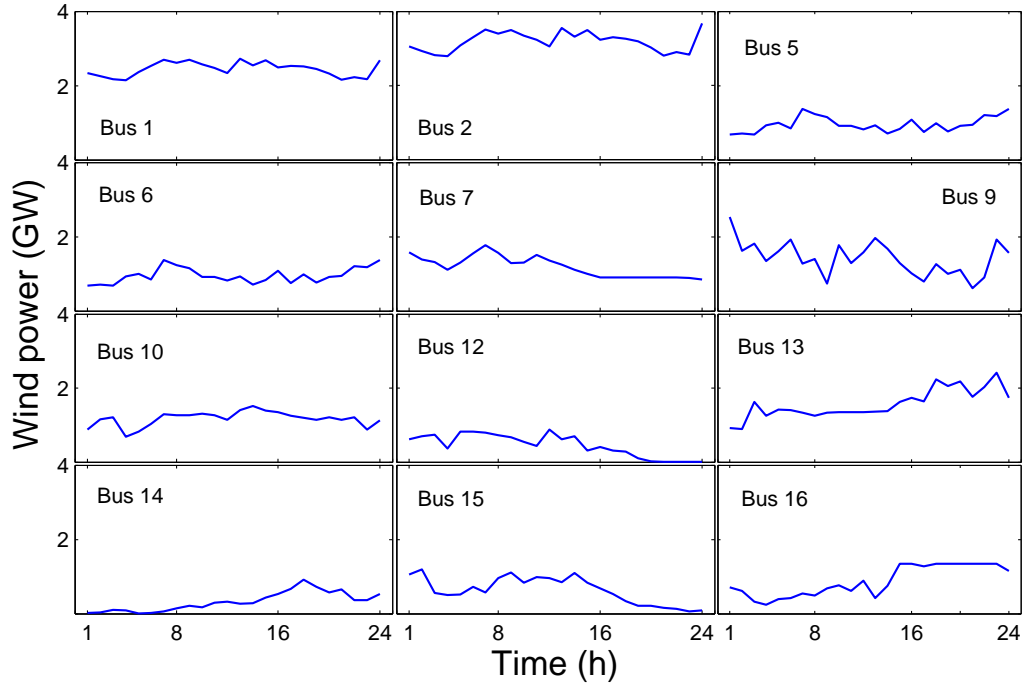
Figure 3.2: Artificially generated wind data at different electrical busbars, over a 24 hour time horizon

3.3 Case studies

Three hypothesised case studies were defined to analyse the performance of the Western and Eastern HVDC links in the GB electricity network. The Base case includes the expected onshore transmission reinforcement by 2020 (with none of the HVDC links). This includes reinforcement in North of Scotland and the Beauly-Denny transmission lines [41]. The Western HVDC case represents enhancement of the Base case network with the 1800 MW Western HVDC link. The Eastern HVDC case includes the Base case network with the 1800 MW Eastern HVDC link.

The proposed location of the Western and Eastern HVDC lines (busbar linkages) are illustrated in Fig. 3.1.

The electricity winter peak demand data for 7th January 2009 is used in this study to represent the 2020 demand [48]. No annual increase in demand was assumed. This implicitly takes into account any demand side management that may be expected in 2020. Electricity generation costs for different technologies are shown in Table 3.4.

Table 3.4: Cost of power generation [5]

Generation technology	Marginal operating cost (£/MWh)
Coal	12.6
Nuclear	11.3
CCGT	24.7
Pumped storage	20
Interconnector	60
OCGT	44.6
Oil	47.3
Biomass	35.7

3.4 Results

3.4.1 Base case

The shares of different electricity generation technologies for the Base case over the time horizon are shown in Fig. 3.3. It can be seen that coal-fired plants are used extensively due to their low operating and fuel costs. Nuclear power generation is fairly constant over the time horizon. Gas-fired plants have relatively low operating and high fuel (gas) costs, so therefore they are operated as marginal plants to ensure power generation meets demand.

Figure 3.4 shows wind power curtailment occurs in the Base case. This is mainly caused by the lack of transmission capacity between Scotland and England-Wales to accommodate the 11.4 GW of wind generation capacity installed in Scotland. During hours 10 to 21, when the electricity demand is high, roughly 2 GW wind generation

is curtailed. This leads to greater generation from marginal power plants and higher operating costs.
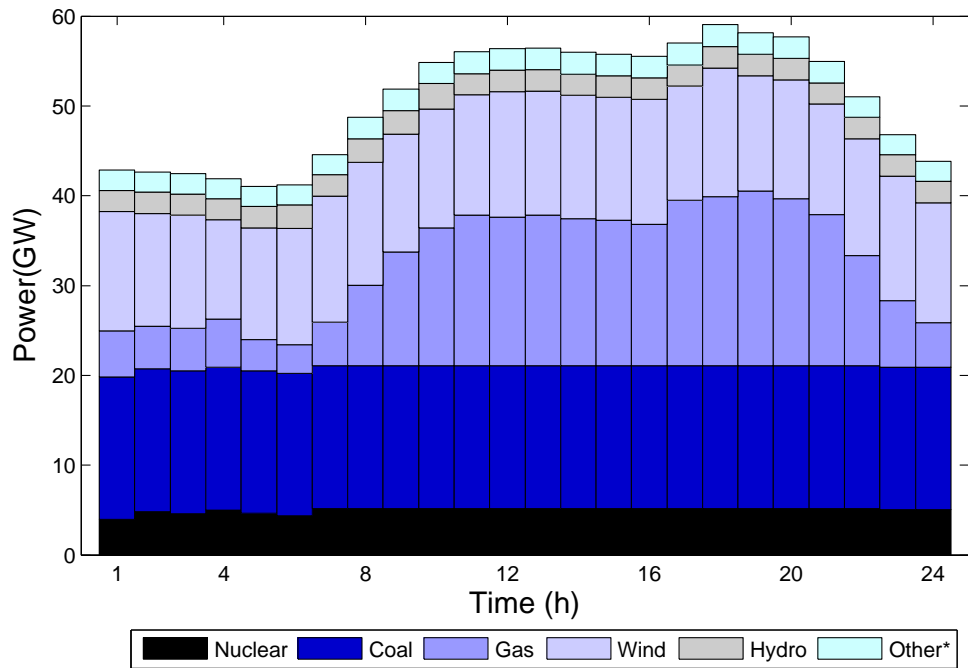
Figure 3.3: Power generation mix for the Base case (* other generation includes biomass, waste and interconnector)
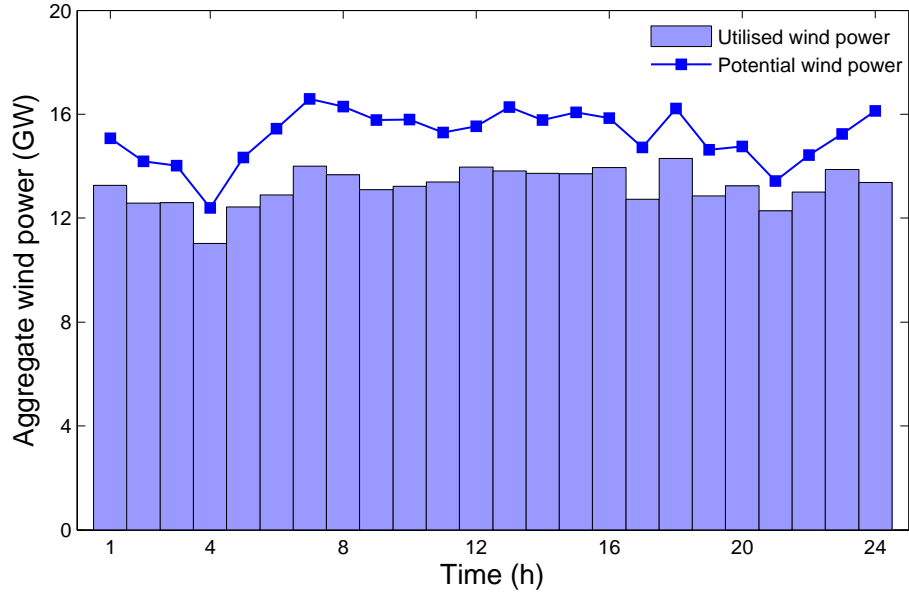
Figure 3.4: Potential and utilised wind power for the Base case

3.4.2 Eastern and Western HVDC cases

Figure 3.5 shows that the 1800 MW Eastern HVDC link results in less gas-fired genera-tion than the Base case as more wind generation is used to meet demand. The addition of the 1800 MW Western HVDC link shows that gas-fired generation is marginally lower than the Eastern HVDC case during periods of high electricity demand (hours 10 to 22).
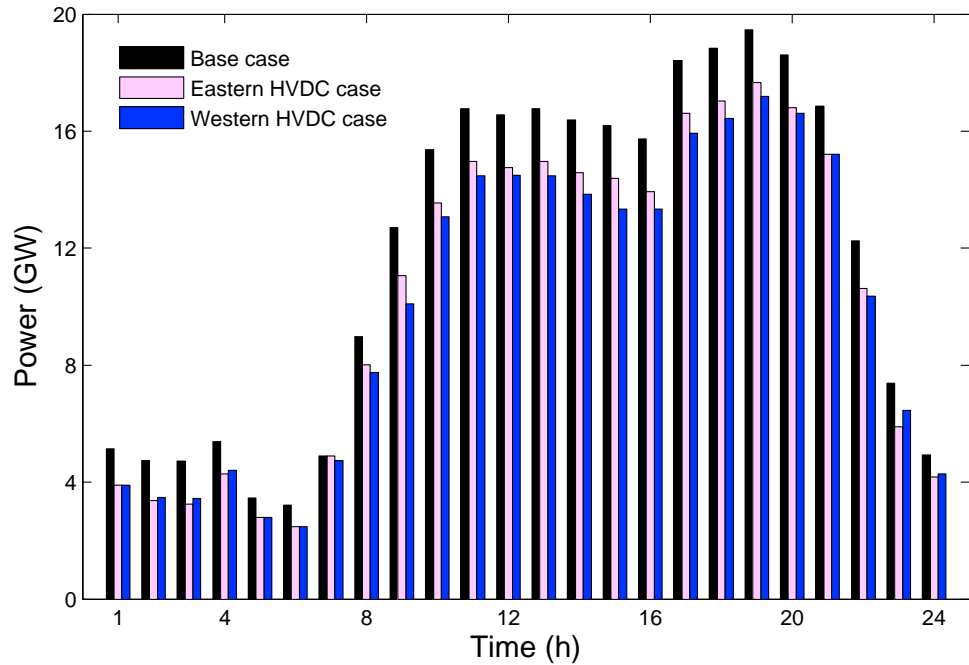
Figure 3.5: Gas-fired generation for all case studies

Figure 3.6 shows that less wind is curtailed due to the Eastern HVDC link compared to the Base case. There is no wind curtailment during peak hours (hours 17 to 20), when otherwise the most expensive generators would be used to meet demand. Therefore by reducing wind curtailment by 1000 MW during peak hours, 1000 MW of expensive electricity generation is avoided. This results in a decrease in operating costs.
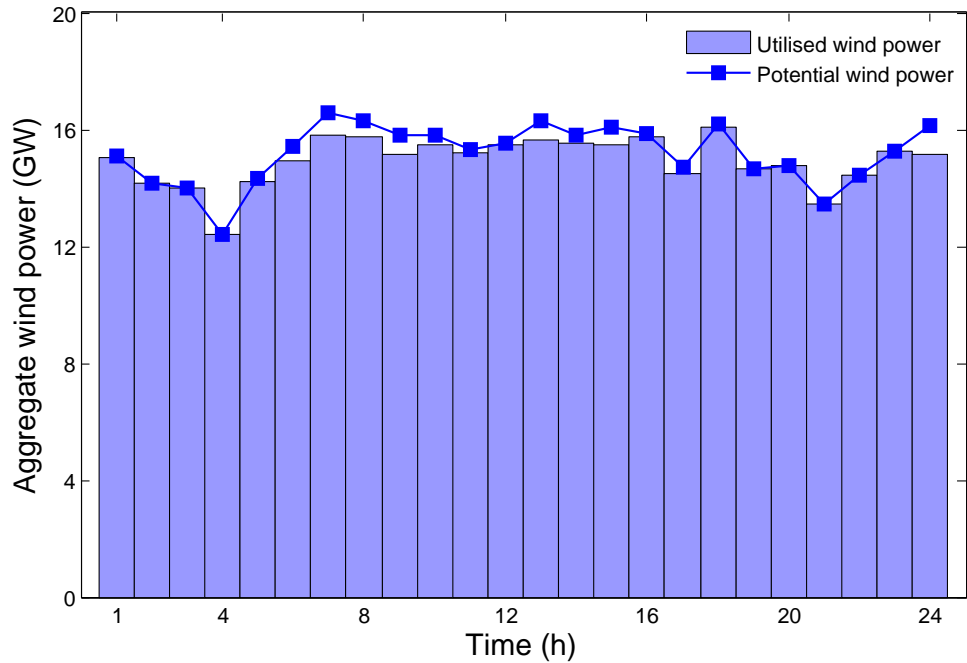
Figure 3.6: Potential and utilised wind power for the Eastern HVDC case

The addition of the Western HVDC link results in no wind curtailments (Fig. 3.7). The wind generation from Scotland is fully utilised and there are no north-south power flow constraints.

Power flow through Eastern and Western HVDC links, over the time horizon, are depicted in Fig. 3.8.
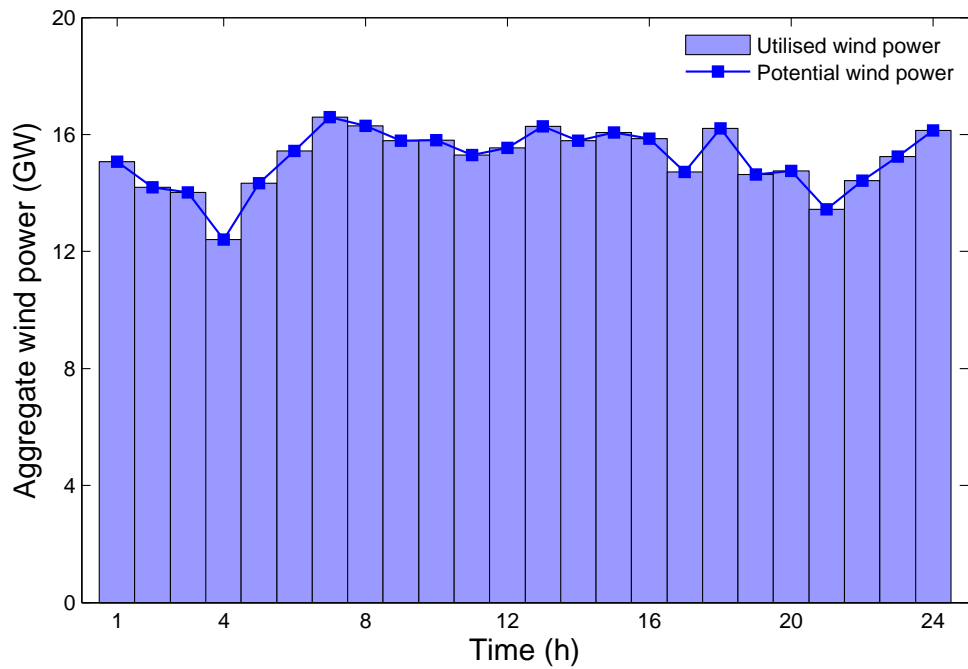
Figure 3.7: Potential and utilised wind power for the Western HVDC case
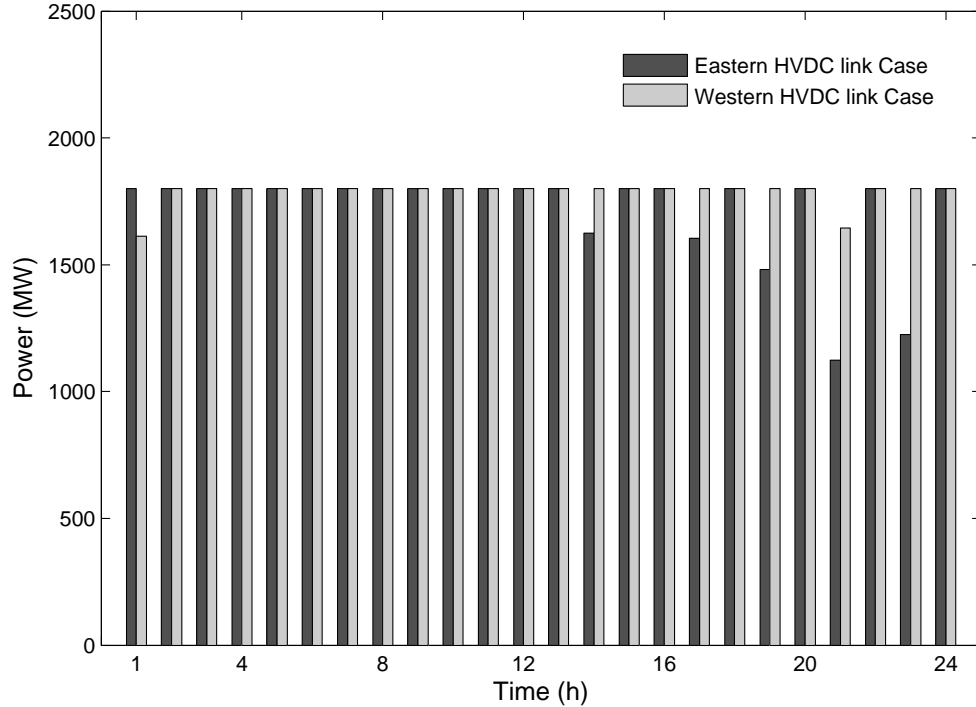
Figure 3.8: Power flow through Eastern and Western HVDC links in the case studies

Table 3.5 shows the operational costs for the three cases. Both HVDC links result in lower operational costs mainly due to the increased use of wind generation (zero operational costs). The Western link was shown to eliminate wind curtailments for the case studied. If it is assumed that similar results occur during 10% of the year (with a conservative assumption of 50% wind output performance for the remaining 90% of the year) for the western HVDC case this would result in roughly £250 million in operational cost savings. This translates into a payback period of approximately 4 years for the HVDC development.

Table 3.5: Operational costs of the case studies

Case studies	Operational costs (£million)
Base case	14.3
Eastern HVDC case	13.3
Western HVDC case	13.1

3.5 Conclusion

The artificially generated wind power data was used to analyse performance of the GB electricity network for three case studies. It was shown that both HVDC links connecting Scotland to England-Wales resulted in greater use of available wind generation (curtailment reduction), lower gas use for electricity generation and reduced operating costs. Therefore investment in either HVDC link results in favourable pay back periods. This conclusion is supported by National Grid current initiatives to develop the HVDC submarine links.

The geographical wind generation data and electricity network power flow were shown to be useful for investigating transmission network bottlenecks and provide insight into investments that enable greater use of renewable power generation.

Chapter 4

Impact of Significant Wind Capacity on the GB Gas Network

4.1 Introduction

The UK government has ambitious plans to increase the share of electrical energy generated from renewables to more than 30% by 2020 [11]. Wind generation capacity is expected to contribute the majority of new renewable generation and be around 30 GW by 2020 [4; 11].

Although there are many advantages of wind energy, especially its environmental benefits, integrating large capacity of wind generation into a power network is challenging. Wind is an intermittent source of energy hence the amount of electricity generated by wind farms is variable. Such intermittency requires other generators to ramp up and down, as wind power varies, to balance the electricity demand. Due to ramping constraints, rapid electric power swings caused by wind cannot be compensated by base load generation plants. Hydro and pumped storage plants are capable of rapid ramping, but the total capacity of these technologies is small in GB (around 3.7 GW, see Table 1.2 in Chapter 1). The total capacity of coal-fired power plants in the GB system is

also expected to decline due to the Large Combustion Plant Directive (LCPD) [12]. Combined Cycle Gas Turbines (CCGT) with their large generating capacity in GB are potential candidates to compensate for wind variability. However, this would lead to large flow variations in the gas network as CCGT plants ramp up and down. The costs associated with these gas swings have not been included in many wind generation cost calculations [2].

The CCGTs would be required to ramp up and down more often and operate more frequently at a reduced output thereby increasing maintenance, lowering average capacity factors and operating efficiencies. This would result in higher generation costs and emissions [2; 49].

The volume of gas stored in a pipe is known as linepack and is a key factor that affects the ability to supply gas to demand nodes. During low wind periods, when CCGTs are operating close to their maximum capacity to meet peak electricity demand, large amounts of gas are delivered which increases the risk of linepack depletion. A gas network with low linepack is not capable of meeting abrupt demand changes since it typically takes hours for gas to reach demand nodes from a terminal.

4.2   Wind generation variability

A typical wind turbine power curve is shown in Fig. 4.1. Wind turbines start generating electricity at wind speeds of around 3.5 m/s. Between 3.5 and 12 m/s the output rapidly climbs to full wind turbine rating, and remains constant at the maximum level between 12 and 25 m/s. Above 25 m/s the turbine is shut down. Typically, after shut down a wind turbine restarts after 3 minutes of wind speed being below 20 m/s (these thresholds are likely to be higher in turbines designed for offshore applications).

At wind speeds of 3.5 to 12 m/s and also around 25 m/s, small variations in wind speed result in large changes in output which leads to difficulties in predicting the power

output of a wind turbine.
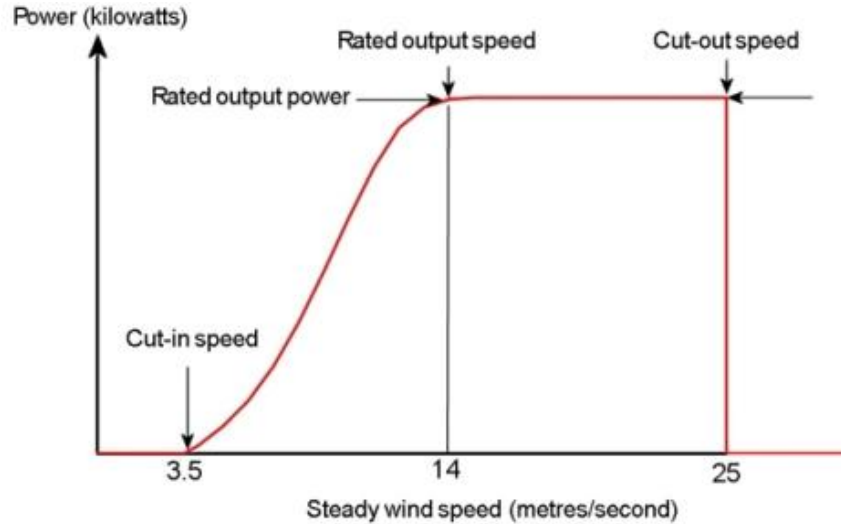
Figure 4.1: Typical wind turbine power curve [1]

With many turbines connected in a wind farm, the aggregate power output of the farm is smoother than the output from a single turbine shown in Fig. 4.1. Furthermore, because of geographical dispersion, the variability of wind output over the GB as a whole is smoother than the output from any individual site and region.

Oswald, et al. [2] used hourly wind speed data in January 2005 and modelled the aggregate electricity output of 25 GW wind farms which could be installed across GB by 2020. The wind generation was subtracted from electricity demand for the same period to calculate the residual electricity demand which must be met by other generation plants. As shown in Fig. 4.2, residual electricity demand varied between 5.5 and 56 GW over the month, and there are many power cycles with larger fluctuations than is currently seen in the GB network. For example, around the 300th hour an 18 GW fall within 22 hours is closely followed by a 14 GW rise within 16 hours [2].

The residual electricity demand from Oswald et al. [2] that represents relatively high and low wind generation levels were used to define two case studies for 2020.
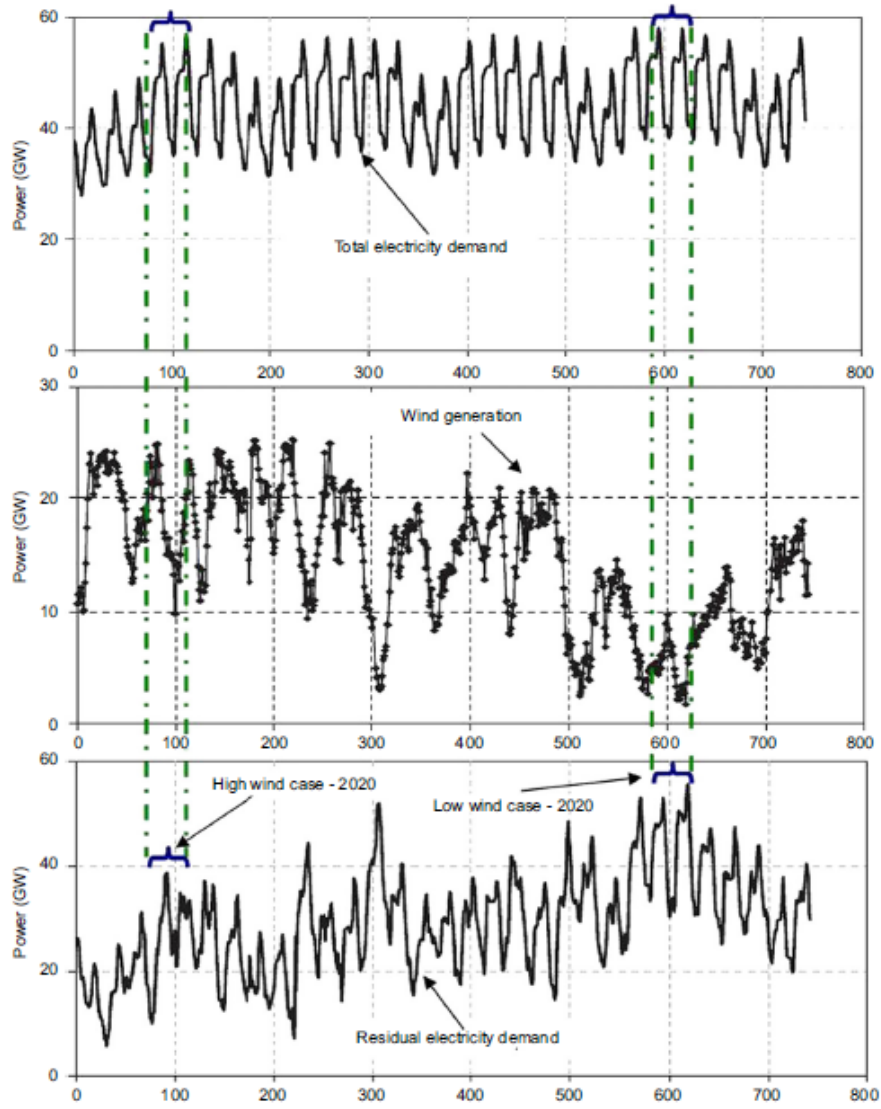
Figure 4.2: Electricity demand, wind generation and residual electricity demand data for low and high wind cases [2]

4.3   System modelling

4.3.1   Simplified GB gas network

The National Transmission System (NTS) [50] was simplified and used to represent the GB gas network [51]. The simplification of the NTS reduces network complexity and simulation runtime. The major difference between the NTS and the simplified network is the number of pipes and nodes. Gas terminals and storage facilities are kept the same for both networks.

The simplified network is shown in Fig. 4.3 was applied to the CGEN model. The results for gas supplied from different terminals together with pressures at specific nodes were compared with the complete gas network (NTS). The reduced model was shown to imitate the complete gas model (validation results are provided in Appendix A).

Figure 4.3: GB simplified gas network

4.3.2   Simplified GB electricity network

A sixteen bus power system was used to represent the GB electricity network (Fig. 4.4). The busbars are connected by 15 transmission circuits. The capacity of different generation technologies at each bus and maximum transmission capacities for the lines are presented in Table 3.1 and 3.2, Chapter 3.
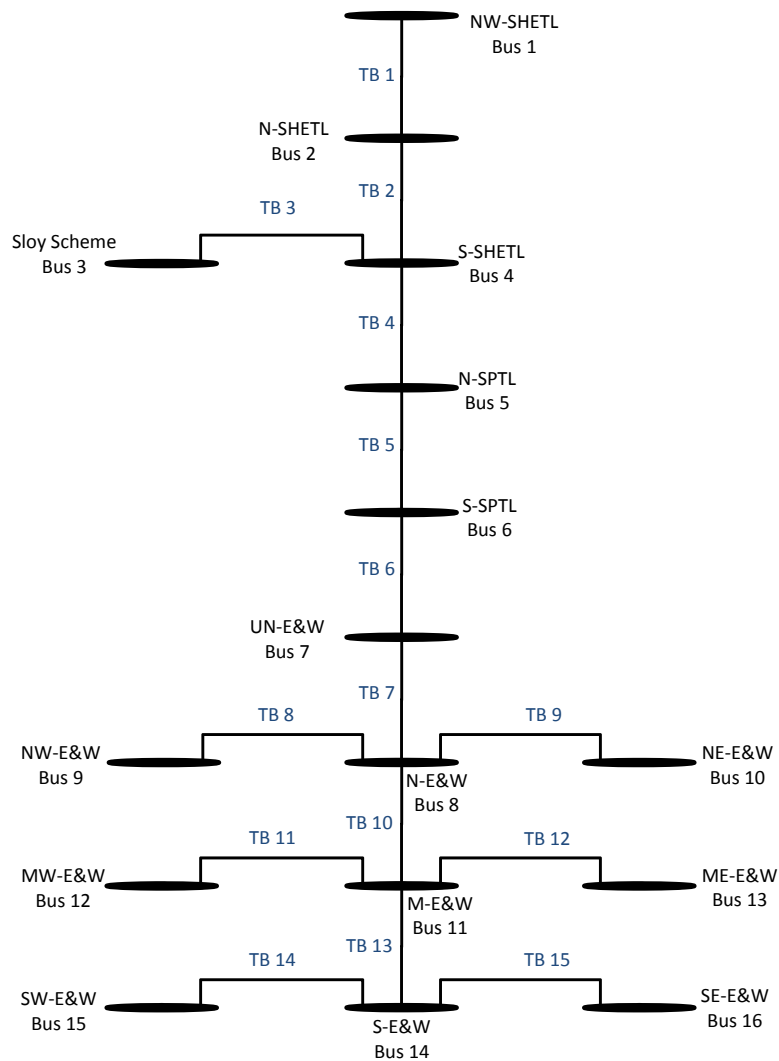
Figure 4.4: GB simplified electricity network

4.4 Case studies

Three case studies were defined. The Base case represents the existing GB network (2009), and the other two represent the GB network in 2020 with two distinct levels of wind generation corresponding to low and high wind periods. The main characteristics of the case studies are shown in Table 4.1.

Table 4.1: The main characteristics of the case studies

Case studies	Year	Non-electrical gas demand (mcm)	Installed wind capacity (GW)	Wind generation (GWh)
Base	2009	550	2.4	46.1
High Wind	2020	550	25	820.2
Low Wind	2020	550	25	190.3

The impact of gas prices are neglected in this study (a constant price of £0.15/m^3 is assumed for all terminals). The operational costs (fuel and maintenance) of electricity generation from various technologies are shown in Table 4.2. Due to low operating costs, nuclear and wind are considered as must run units in all the cases.

Table 4.2: Cost of power generation [6]

Generation technology	Marginal operating cost (£/MWh)
Coal	16
Nuclear	9.4
CCGT	25
Pumped storage	20
Interconnector	60
OCGT	34
Oil	40
Biomass	41

The annual increase rate of total gas demand is forecast to be 1.5% over the next decade which is mostly due to electrical gas demand [50]. Hence, average non-electrical gas demand (residential, commercial and industrial) for each winter day in January 2009 and 2020 was assumed to remain constant at 275 mcm (Fig. 4.5). The non-electrical gas demand of 275 mcm/day was distributed over a day using an hourly gas demand profile.
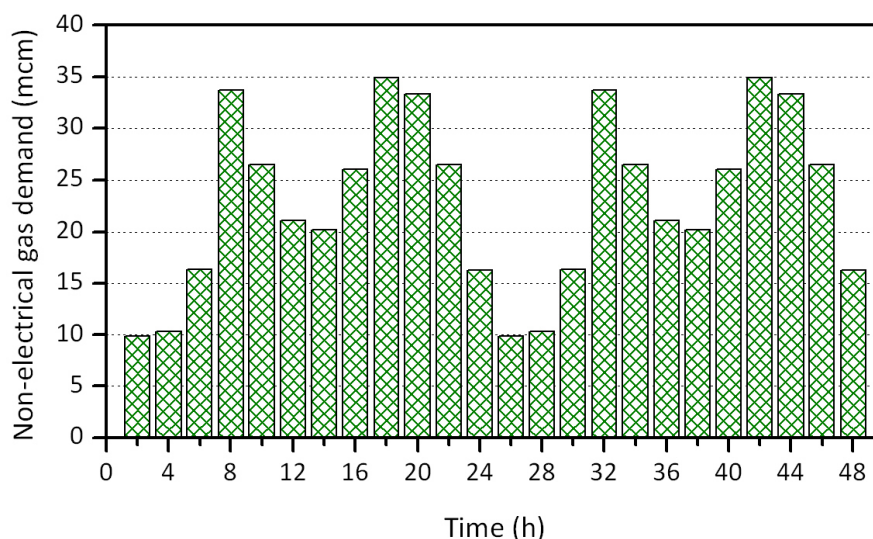
Figure 4.5: Non-electrical gas demand in all three cases

4.4.1 Base case - existing gas and electricity network

The Base case was represented by the GB gas and electricity network (and generation capacity mix) in 2009. Electricity demand for this case is shown in Fig. 4.6 which is derived from the actual data of two typical winter days (8th and 9th January 2009) [48].

The wind generation capacity in 2009 is fairly low (the capacity is 2.4 GW, around 3% of the total generation capacity) and its fluctuation does not have any noticeable effect on network operation. Therefore in the Base case a capacity factor of 40% [4] and constant injection of wind power over the two days were assumed.
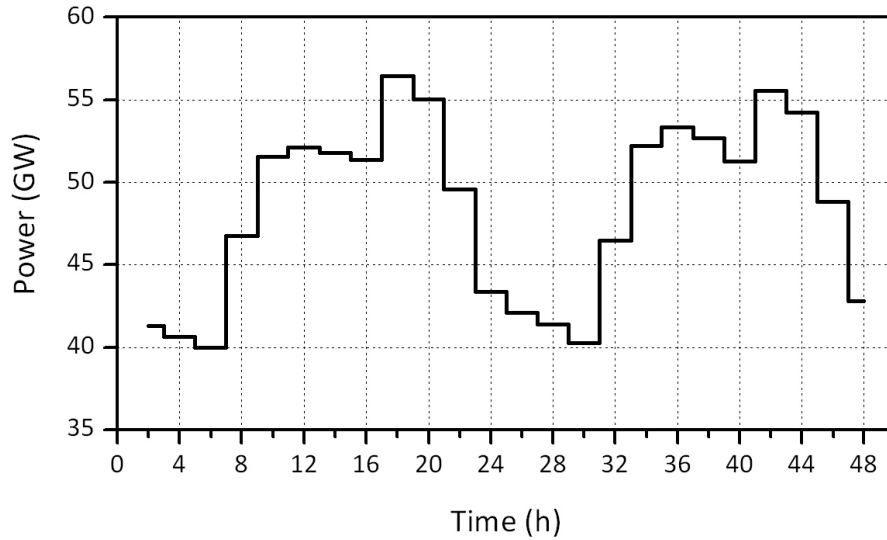
Figure 4.6: Electricity demand in the Base case

4.4.2 Case studies in 2020 - High Wind vs. Low Wind

The residual electricity demand acquired from Oswald et al.'s paper [2] was used in these cases, after applying an annual increase rate of 0.7% [52]. The escalated residual electricity demand for High Wind and Low Wind cases are shown in Figs. 4.7 and 4.8.

For both 2020 case studies the CGEN model uses nuclear as must run units, and then determines the optimal amounts of electricity generation from other technologies (excluding wind) to satisfy the difference between the residual electricity demand and electricity generation of the must run plants. Non-electrical gas demands for these cases are the same as the Base case (Fig. 4.5).
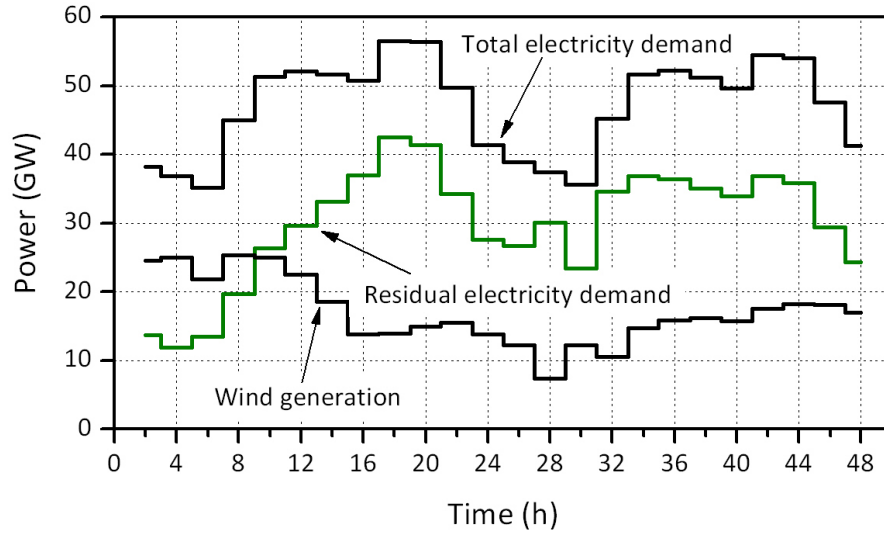
Figure 4.7: Residual electricity demand in the High Wind case 2020
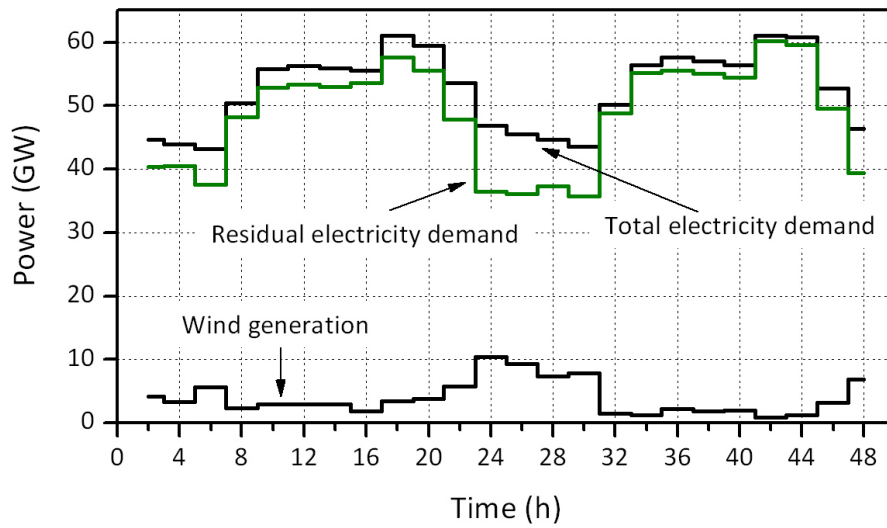
Figure 4.8: Residual electricity demand in the Low Wind case 2020

4.5   Results

4.5.1   Impacts on electricity generation

The shares of different electricity generation technologies, calculated by CGEN, are shown in Fig. 4.9. In the Base case, coal-fired power plants are used extensively. A number of these plants will be decommissioned within the next decade under the LCPD, as shown in Table 6.9. Therefore, the share of coal-fired generation in the two 2020 network cases is lower.
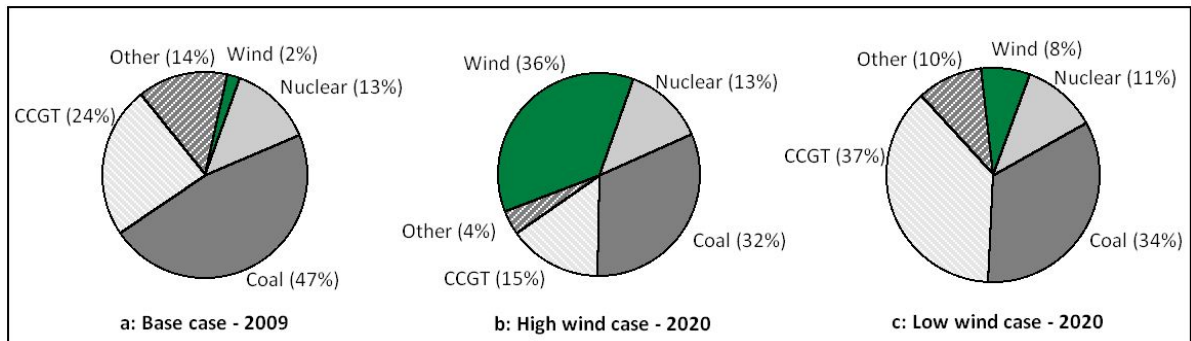
Figure 4.9: Share of different technologies for electricity generation

As shown in Fig. 4.10, in the High Wind case, the remaining coal-fired generators supply electricity near their maximum capacity except during the first six hours, when high wind generation coincides with low electricity demand resulting in less electricity generation from coal-fired power plants. In the Low Wind case, coal-fired plants generate electricity at their maximum capacity during the entire time horizon.

Electricity generation by CCGTs varies considerably from the High Wind to Low Wind cases. CCGTs are used primarily to compensate for wind generation variability. In the High Wind case, CCGTs operate with reduced capacity and undergo more fluctuations in their output of large magnitudes (Fig. 4.11) over a short time period. For example CCGTs ramp up 15 GW from hour 6 to 18, and immediately ramp down 13 GW within the following 6 hours. In the Low Wind case, CCGTs are the major

contributor to electricity production over the entire time horizon.
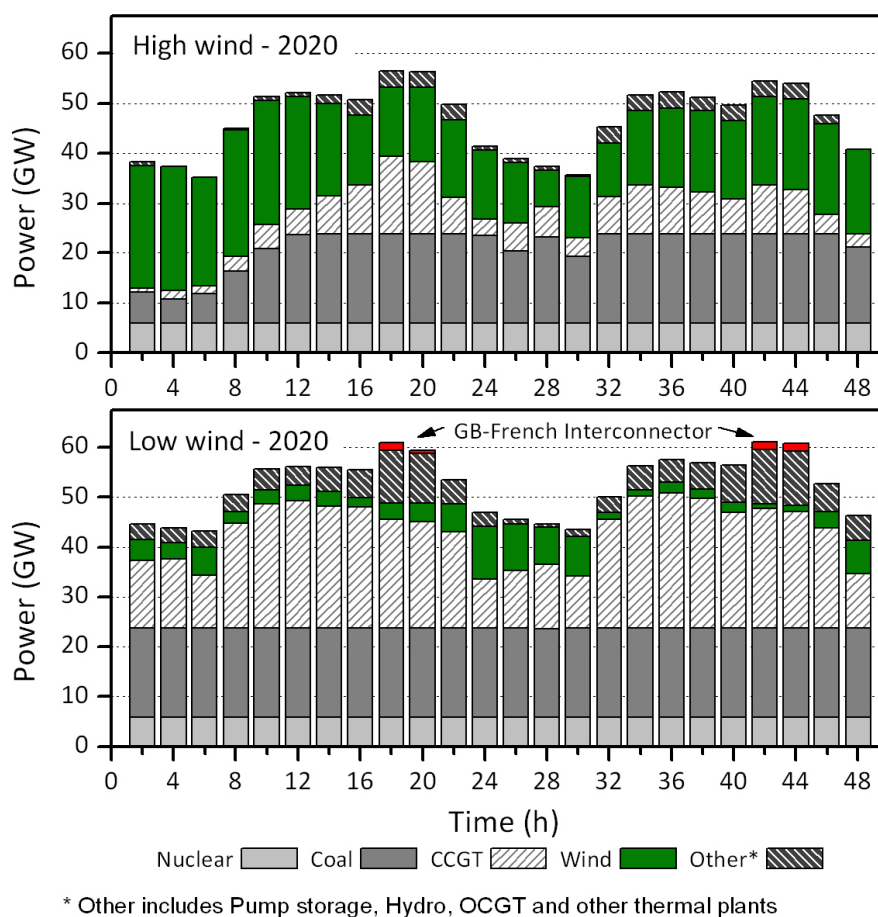
Figure 4.10: Electricity generation mix for the High Wind and Low Wind cases

At hours 18-20 and 42-44 in the Low Wind case, peak residual electricity demand coincides with peak non-electrical gas demand and leads to rapid and large increase of total gas consumption. Given this situation, the gas network cannot fully supply gas to CCGTs. Consequently, power output from CCGTs decreases by 3.1 GW at hours 42-44 (see Fig. 4.11) and more expensive electricity supply from the GB-France interconnector is used to avoid electricity load shedding.
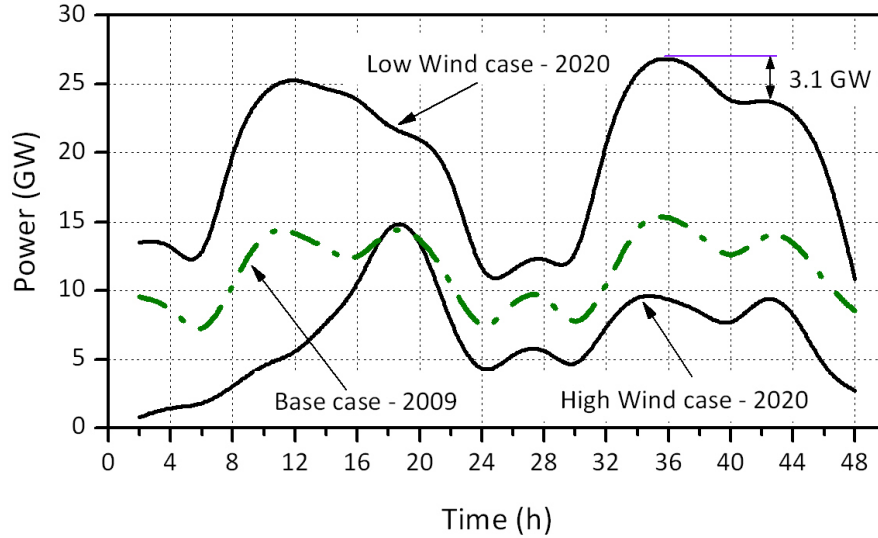
Figure 4.11: CCGT power output in the three cases

4.5.2 Impacts on the gas network operation

The amounts of gas supplied from various terminals at each time step for the Base case are shown in Fig. 4.12. In the High Wind case, due to lower electrical gas demand, total gas supplies from terminals decrease. This reduction mainly takes place at the St Fergus gas terminal in order to minimise compressor power consumption and gas network operating costs (gas transmission from the St Fergus terminal to the rest of the network requires extensive compressor use in order to maintain the north to south flow).
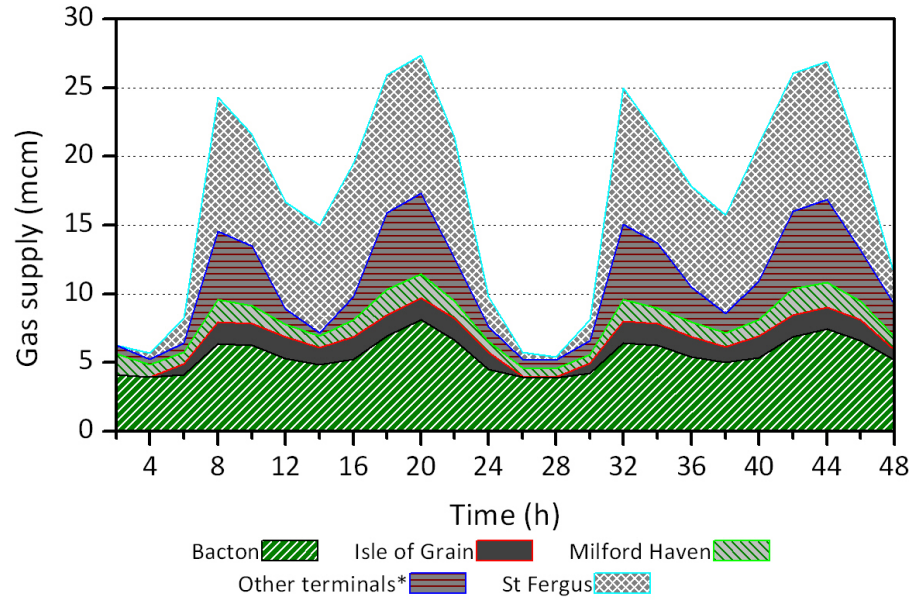
Figure 4.12: Gas supply from different terminals in the Base case

As a result of higher total gas demand in the Low Wind case, gas supply and total compressor power (Fig. 4.13) in this case are higher in comparison to the other cases.
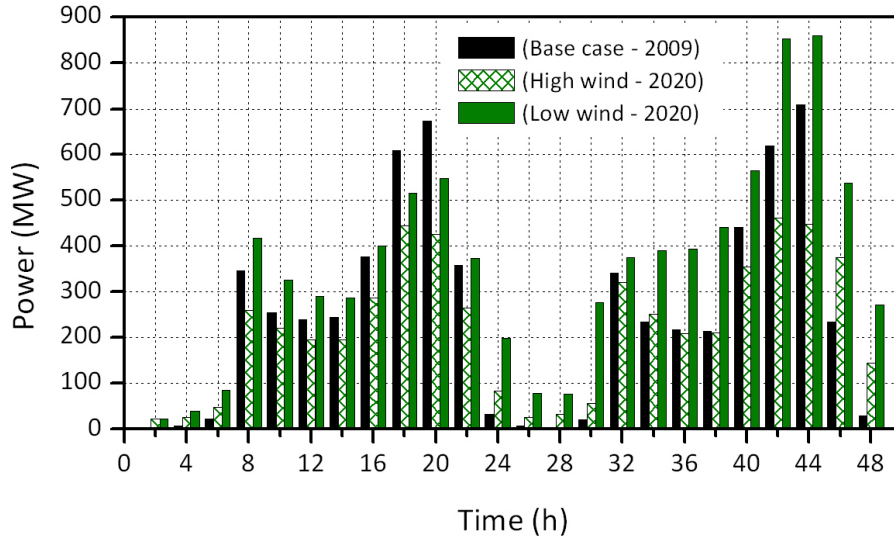
Figure 4.13: Compressor power consumption

Gas storage facilities are used extensively. Storage facilities typically store gas during the spring and summer when gas prices are low and withdraw gas during the winter. It was assumed that gas from storage facilities is cheaper than gas at the supply terminals. These assumptions cause all the storage facilities to supply gas near to their maximum flow rates over the two days (Fig. 4.14). Gas supplied from storage facilities are similar for all three cases.
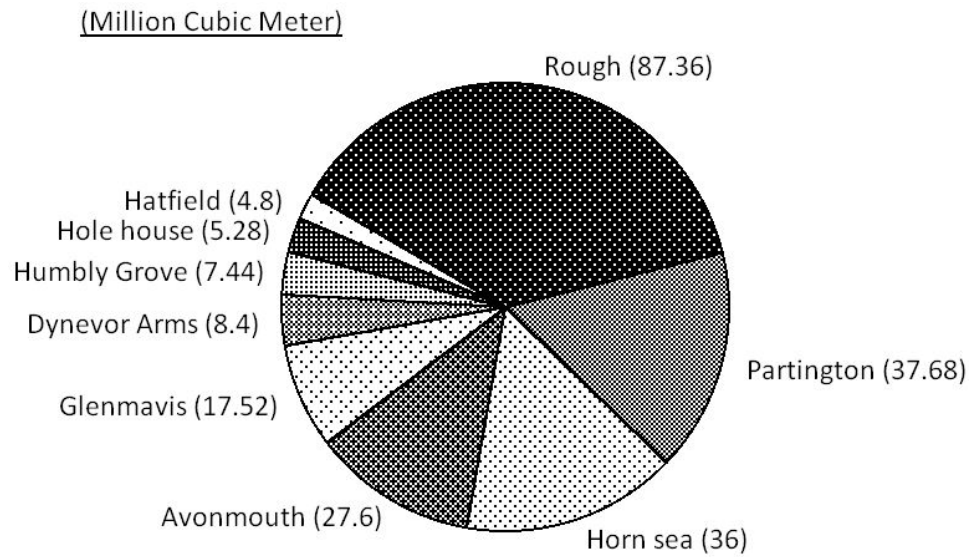
Figure 4.14: Gas supply from various storage facilities over the time horizon (similar for all cases)

Fig. 4.15 shows the aggregate gas network linepack for the different cases. The linepack in the High Wind case shows reduced fluctuations even during rapid changes in wind generation.
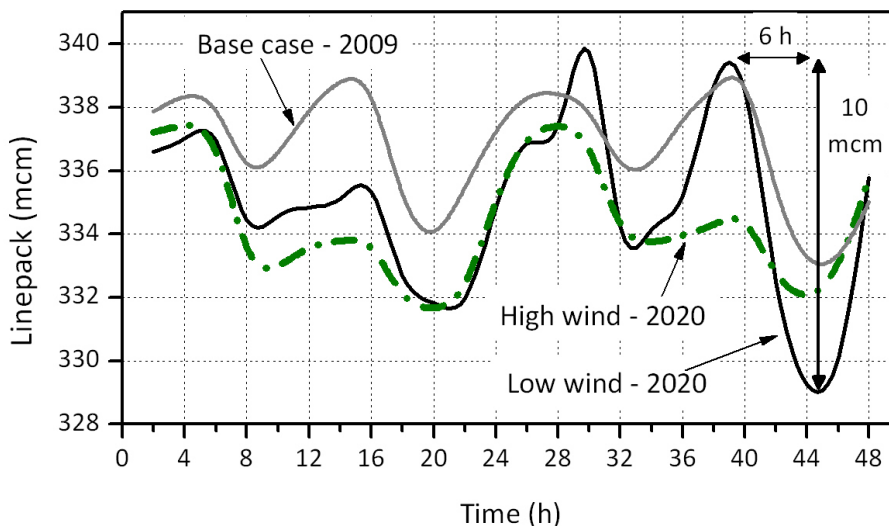
Figure 4.15: Comparison of the gas network linepack for the case studies

In the Low Wind case, despite high compressor power during hours 42-44 (Fig. 4.13), the network linepack abruptly decreases by 10 mcm. This is due to the peak non-electrical and electrical gas demand occurring at roughly the same time. The resulting pressure drop in the gas network limits its ability to meet rapid changes in gas demand and causes interruption of gas supplies to CCGTs (see Fig. 4.11).

Examination of the power output of individual CCGTs shows the plants close to Burton point gas terminal generate far less than their maximum capacity during peak hours. This is due to the limited gas supply capacity of Burton point terminal (around 1 mcm/day) as well as low network linepack during these hours.

A sensitivity analysis was performed on the withdrawal rate of the Partington gas storage facility (close to Burton point). It showed that a 50% increase in the withdrawal rate results in higher power output from the local CCGTs and a reduction of electricity supplied through the GB-France interconnector at peak hours (Table 4.3). This illustrates the requirement for new storage facilities with high withdrawal rates in

this region.

Table 4.3: Comparison of CCGT output for the Low Wind case (* CCGTs in the vicinity of Burton Point gas terminal; **Electricity from GB-France Interconnector)

	CCGT output (MW)*				Electricity importation (MW)**			
	18 h	20 h	42 h	44 h	18 h	20 h	42 h	44 h
With existing withdrawal rate of gas storage facility	606.2	165.7	649.6	572.7	1530.8	718.9	1530.8	1530.8
50% increase in withdrawal rate of Partington gas storage facility	1469.1	1471.1	1313	1122.5	370.5	0	985.1	1024.8

4.5.3   Impacts of gas supply on the electricity network

Figure 4.16 shows the share of different sources for supplying gas. Interconnectors and LNG terminals play a crucial role in supplying gas to GB in 2020. GB electricity generation will be dependant on the gas network during low wind generation periods when large amounts of gas must be delivered to CCGTs in order to meet residual electricity demand.
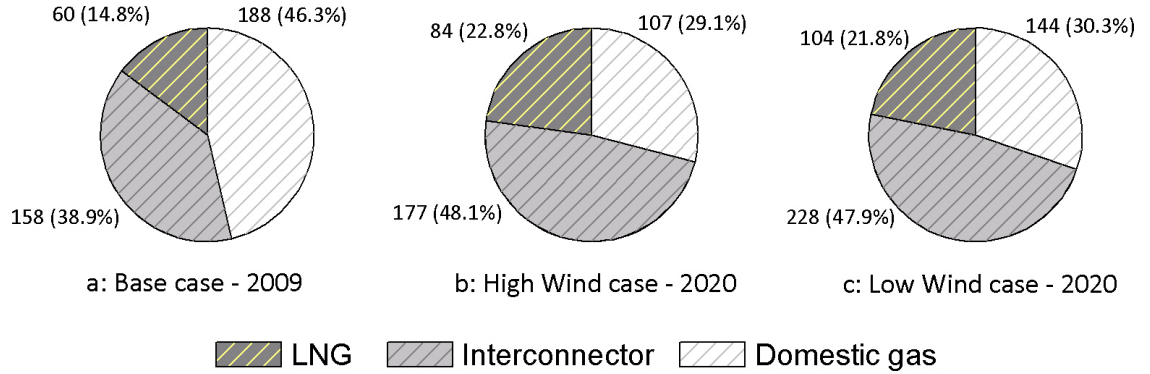
Figure 4.16: Gas supply in all case studies (mcm)

The simulation results indicated that in some areas with large amounts of CCGT capacity the existing gas infrastructure is not capable of handling abrupt changes in demand for gas in 2020. For instance, Burton point gas terminal cannot fully supply gas to CCGTs located at Bus 9 (GB electricity network) at peak hours (18-20 hrs and 40-42 hrs) of electricity demand in the Low Wind case. This will affect the ability of the electricity network to meet demand at low cost.

4.5.4 System operating costs

The operating costs of the integrated network for the different case studies are shown in Table 4.4.

Table 4.4: Optimal objective value (operating cost) for different case studies

Case studies	Optimal objective value (£million)
Base case	135.04
High Wind case	111.39
Low Wind case	137.94

The operating cost of the High Wind case decreases 17% over the two days compared to the Base case. Such a large decrease in operating costs is mainly due to wind generation (with very low operating costs) which supplies the bulk of electricity demand.

Although wind generation in the Low Wind case is not very large, it is still four times greater than wind generation in the Base case. Therefore, despite extensive compressor usage and greater gas supplies, the total operating cost of the Low Wind case over the two days is fractionally higher than the Base case (increase of 2%). This is mainly due to low operating cost of wind generation.

4.5.5 CCGT operation and maintenance

Power from wind generation is non-dispatchable, and as such is accepted into the grid whenever it is available. As a result, gas-fired generators must be ready to dispatch power to the grid in the event of a decline in wind availability.

Figure 4.17 shows the number of times the CCGTs in the GB network stop/starts over the two days for all cases. The high wind (2020) case shows an increase in the number of times CCGTs in GB network stops/starts over the two days. The increase of stopping and starting of CCGTs leads to increased operating and maintenance (O&M) costs. Lefton and Besuner [53] estimated that for each single CCGT stop/start cycle O&M costs ranged from $300 to $80,000. The costs represent the increased damage to plant equipment, lower fuel efficiencies and potentially shortened plant life. However, the Low Wind case results in reduced frequency of CCGTs stop/starts over the two days when compared with the Base case. The analysis did not consider specific start-up costs for generation plants.
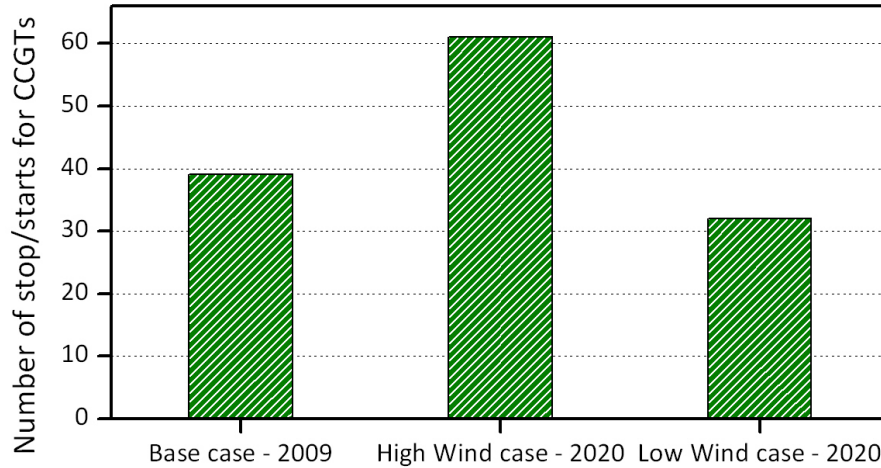
Figure 4.17: Number of stop/starts for CCGTs during the time horizon for different case studies

4.6 Conclusion

Given the large amount of wind generation and low coal-fired generation capacity anticipated in the UK by 2020, CCGTs will be used to compensate for wind power variability due to their fast ramping rates and sizable generation capacity. However, this could lead to significant power swings on the gas network as CCGT plants ramp up and down.

The simulation results showed that the simultaneous occurrence of low wind generation and peak electricity demand in 2020 will result in rapid and large increases in gas consumption, mainly due to the demand from gas-fired generation. The insufficiency of local linepack in the gas network will constrain gas supply to some CCGTs. Consequently these plants will operate with reduced output and more expensive sources of electricity such as the GB-France interconnector will be employed to meet shortfalls in generation. The gas interconnectors and LNG terminals will have a crucial role in supplying gas to GB in 2020.

The operating costs of the combined gas and electricity network during low wind periods were shown to be high. This is due to increase of gas supplies, extensive compressor use, and balancing electricity demand through more expensive generation technologies. This is in contrast to high wind periods when the low cost of wind generation results in considerably lower operating costs.

The results illustrated a high degree of within day (intraday) linepack fluctuations during periods of low wind generation in the hypothesized 2020 network. Gas pipe pressure variation (proportional to linepack) results in additional costs (gas supplies and compressor use) in order to stay within operational pressure margins.

Given the unpredictable and variable use of gas-fired generators in future networks with large amounts of wind generation capacity, intra-day linepack balancing requirements may be required. This will expose all participants (shippers/suppliers and gas-fired generators) to the cost of linepack imbalances within a day (hourly balancing). This will reflect the true cost of using gas for electricity generation during periods of limited network capacity and gas supplies.

It was shown that additional gas storage facilities could enhance gas availability and linepack during periods of high gas demand for electricity generation due to variability of wind generation.

Chapter 5

Probabilistic Wind Power Forecast

5.1 Background

The large increase in wind turbine installations in many countries has led to a greater focus on the importance of wind power forecasts. A number of forecasting models have been proposed and studied [54; 55; 56; 57]. For a detailed review of wind power forecasting models refer to [58].

The models use either physical or statistical approach to forecasting wind power [55; 57]. The models that use a physical approach take into account the physical relationship between wind speed, atmospheric conditions, and local topography. In contrast, the models that use a statistical approach estimate a statistical relationship between relevant input data (weather and wind farms) and wind power generation. However, more advanced models are often based on a combination of both approaches [57].

Although, in general, the error from wind power forecasting increases as the forecast horizon increases, the errors differ from model to model. For longer forecasting horizons, physical models introduce smaller errors compared to statistical models, while statistical models work better for shorter horizons [55]. The main drawbacks of physical models are the requirement for high volume of meteorological data and computing power.

The vast majority of wind power forecasting models developed so far produce single-valued point forecast (SVPF) which is an estimate of the wind power's conditional mean [58]. Such models do not take into account the error distribution of the forecasted values to provide several possible forecast scenarios, therefore, cannot be used for stochastic decision making such as wind-thermal unit commitment [59; 60]. The probabilistic approach, which produces more than one forecast, results in a more complete characterisation of the conditional distribution of wind power forecast.

Juban et.al. [60] proposed a method based on Kernel density estimation technique to produce a complete predictive probability density function (PDF) for the wind power forecast. A probabilistic algorithm based on histogram analysis is also presented in [59] to assess the capacity and ramping requirement of a power system in order to compensate for wind uncertainty. Pinson et. al. [61] presented a method for the generation of probabilistic wind power scenarios using forecasted density/cumulative probability functions for the time horizon. A Monte Carlo simulation is used for the generation of equiprobable scenarios. Bremnes [62] used a local quantile regression to compute quantiles of wind power generation.

5.2 Singular Spectrum Analysis (SSA)

Singular Spectrum Analysis (SSA) was used for short term single-valued point forecast of wind power. A description of the SSA technique is provided below [63].

"Singular Spectrum Analysis (SSA) is a novel forecasting technique which decomposes the original time series into the sum of a small number of interpretable components such as slowly varying trend, oscillatory components, and noise. The basic concept of the SSA method consists of two complementary stages: (a) *decomposition* and (b) *reconstruction*. At the first stage the series is decomposed and at the second stage the noise-free series is re-

constructed and used for forecasting new data points. A short description of the SSA technique is provided below (for more information see [64]).

5.2.1   Time series decomposition

Step 1: Embedding

Embedding is a mapping that transfers a one-dimensional time series $Y_T = (y_1, \ldots, y_N)$ into a multi-dimensional series $X_1, \ldots, X_K$ with vectors $X_i = (y_i, \ldots, y_{i+(L-1)})^T \in \mathbf{R}^L$, where L $(2 \leq L \leq N-1)$ is the *window length* and $K = N - L + 1$. The result of this step is the trajectory matrix

$$\mathbf{X} = [X_1, \ldots, X_K] = (x_{ij})_{i,j=1}^{L,K} . \tag{5.1}$$

Note that the trajectory matrix $\mathbf{X}$ is a Hankel matrix, i.e., all the elements along the diagonal $i + j = const$ are equal.

Step 2: Singular Value Decomposition (SVD)

In this step the SVD of $\mathbf{X}$ is performed. Denote by $\lambda_1, \ldots, \lambda_L$ the eigenvalues of $\mathbf{X}\mathbf{X}^T$ arranged in the decreasing order $(\lambda_1 \geq \ldots \lambda_L \geq 0)$ and by $U_1, \ldots, U_L$ the corresponding eigenvectors. The SVD of $\mathbf{X}$ can be written as $\mathbf{X} = \mathbf{X}_1 + \cdots + \mathbf{X}_L$, where $\mathbf{X}_i = \sqrt{\lambda_i} U_i V_i^T$ and $V_i = \mathbf{X}^T U_i / \sqrt{\lambda_i}$ (if $\lambda_i = 0$ then $\mathbf{X}_i = 0$ is set).

5.2.2   Noise-free time series reconstruction

Step 1: Grouping

The grouping step corresponds to splitting the elementary matrices into several groups and summing the matrices within each group. Let $I = \{i_1, \ldots, i_p\}$ be a group of indices $i_1, \ldots, i_p$. Then the matrix $\mathbf{X}_I$ corre-

sponding to the group I is defined as $\mathbf{X}_I = \mathbf{X}_{i_1} + \cdots + \mathbf{X}_{i_p}$. The split of the set of indices $\{1, \ldots, L\}$ into disjoint subsets $I_1, \ldots, I_m$ corresponds to the representation $\mathbf{X} = \mathbf{X}_{I_1} + \cdots + \mathbf{X}_{I_m}$. The procedure of choosing the sets $I_1, \ldots, I_m$ is called *grouping*. For a given group I, the contribution of the component $\mathbf{X}_I$ is measured by the share of the corresponding eigenvalues $\sum_{i \in I} \lambda_i / \sum_{i=1}^d \lambda_i$, where d is the rank of $\mathbf{X}$.

Step 2: Diagonal averaging

The purpose of diagonal averaging is to transform a matrix to the form of a Hankel matrix, which can be subsequently converted to a time series. If z_{ij} stands for an element of a matrix $\mathbf{Z}$, then the kth term of the resulting series is obtained by averaging z_{ij} over all i, j such that $i + j = k + 1$. By performing the diagonal averaging of all matrix components of $\mathbf{X}_{I_j}$ in the expansion of $\mathbf{X}$ above, we obtain another expansion: $\mathbf{X} = \widetilde{\mathbf{X}}_{I_1} + \ldots + \widetilde{\mathbf{X}}_{I_m}$, where $\widetilde{\mathbf{X}}_{I_j}$ is the diagonalized version of the matrix $\mathbf{X}_{I_j}$. This is equivalent to the decomposition of the initial series $Y_N = (y_1, \ldots, y_N)$ into a sum of m series; $y_t = \sum_{j=1}^m \widetilde{y}_t^{(j)}$, where $\widetilde{Y}_N^{(j)} = (\widetilde{y}_1^{(j)}, \ldots, \widetilde{y}_N^{(j)})$ corresponds to the matrix $\widetilde{\mathbf{X}}_{I_j}$.

In what follows, two groups of indices, $I_1 = \{1, \ldots, r\}$ and $I_2 = \{r + 1, \ldots, L\}$ were used which are associated with a signal component and with noise, respectively. It is worth mentioning, if $\widetilde{x}_{ij}$ is the ij^{th} entry of the matrix $\widetilde{\mathbf{X}}$, then applying diagonal averaging formula follows that:

$$\widetilde{y}_j = \frac{1}{s_2 - s_1 + 1} \sum_{i=s_1}^{s_2} \widetilde{x}_{i, j+1-i} \tag{5.2}$$

where, $s_1 = \max\{1, j + 1 - K\}$, $s_2 = \min\{L, j\}$, and $\widetilde{y}_j$ is the jth element of the reconstructed series $\widetilde{Y}_N$.

5.2.3 Forecasting procedure

The SSA technique can be applied to the time series that approximately satisfies linear recurrent formulae[1]. The class of time series governed by linear recurrent formulae is rather wide; it includes harmonics, polynomial, and exponential time series. The SSA recurrent forecasting algorithm is briefly described here (for more information see [64]).

Define the original series $Y_N = (y_1, \ldots, y_N)$ and the reconstructed series $\widetilde{Y}_N = (\widetilde{y}_1, \ldots, \widetilde{y}_N)$. For an eigenvector $U \in \mathbb{R}^L$, the vector of the first $L-1$ components of the vector U is denoted as $U^\triangledown \in \mathbb{R}^{L-1}$. Set $v^2 = \pi_1^2 + \ldots + \pi_r^2 < 1$, where π_i is the last component of the eigenvector U_i $(i = 1, \ldots, r)$. It can be proved that the last component y_L of any vector $Y = (y_1, \ldots, y_L)^T$ is a linear combination of the earlier components $(y_1, \ldots, y_{L-1})$; that is, $y_L = a_1 y_{L-1} + \ldots + a_{L-1} y_1$ where the vector of coefficients $A = (a_1, \ldots, a_{L-1})$ can be expressed as $A = \sum_{i=1}^r \pi_i U_i^\triangledown / (1 - v^2)$. The forecasts $\hat{y}_{T+1}, \ldots, \hat{y}_{N+h}$ are then obtained as

$$
\hat{y}_i = \begin{cases} \widetilde{y}_i & \text{for } i = 1, \ldots, N \\ \sum_{j=1}^{L-1} a_j \hat{y}_{i-j} & \text{for } i = N+1, \ldots, N+h. \end{cases}
$$

"

5.3 Wind power single-valued point forecast

Aggregate hourly power output from wind farms across the GB over two months were used as the historical time series to forecast wind power for the following two days. Real

---

[1]Time series Y_N satisfies linear recurrent formulae of order $L-1$ if there are numbers $a_1, \ldots, a_{L-1}$ such that

$$
y_{N-i} = \sum_{k=1}^{L-1} a_k y_{N-i-k}, \qquad 0 \le i \le N - L.
$$

wind power data were taken from [65] and is shown in Fig. 5.1.
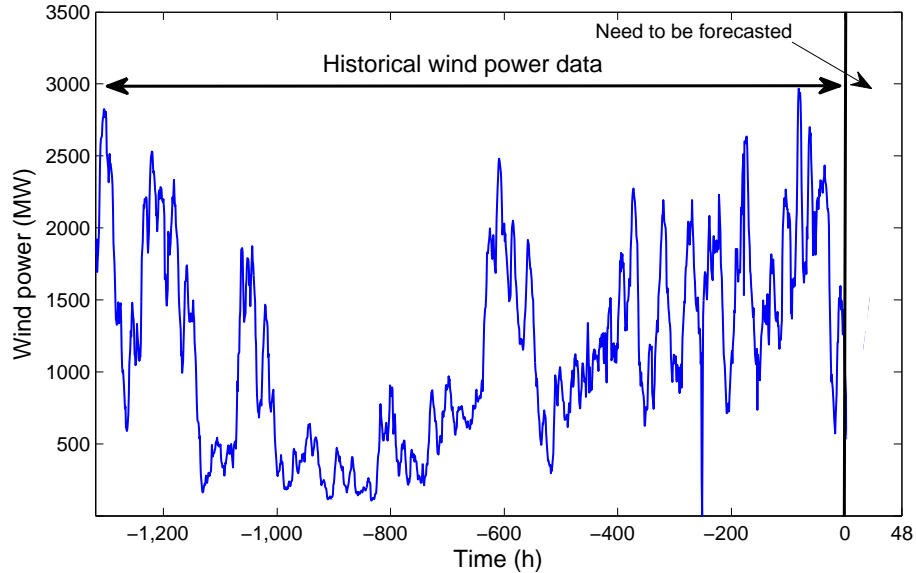
Figure 5.1: Aggregate real wind power output from wind farms across GB, used to forecast wind power

After forecasting wind power over the two days using SSA, the forecast wind power is compared to the real wind power output (Fig. 5.2)[1]. Wind power forecast was performed in an iterative manner. Therefore the historical time series of wind was updated for every time step. Root Mean Square Error (RMSE) of forecast performed by SSA is 116 MW.

---

[1]It is acknowledged that SVPF data was calculated by Dr Hossein Hassani (hhassani@bournemouth.ac.uk) from Bournemouth University.
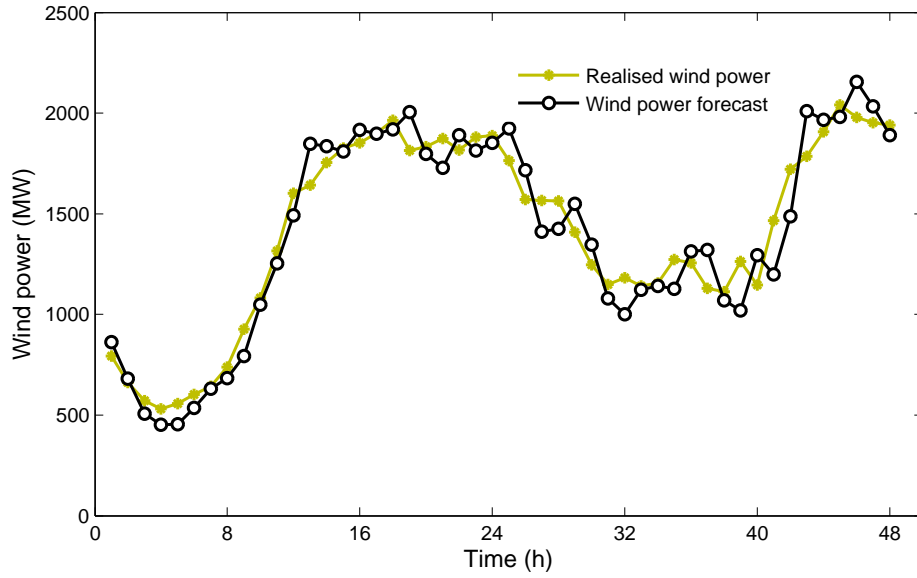
Figure 5.2: Comparison of the single-valued point forecast produced by the SSA technique and real wind power.

5.4 Probabilistic wind power forecast from the SVPF

A method was proposed to generate probabilistic wind power forecast scenarios using the SVPF. Different steps of the method are presented in Fig. 5.3.
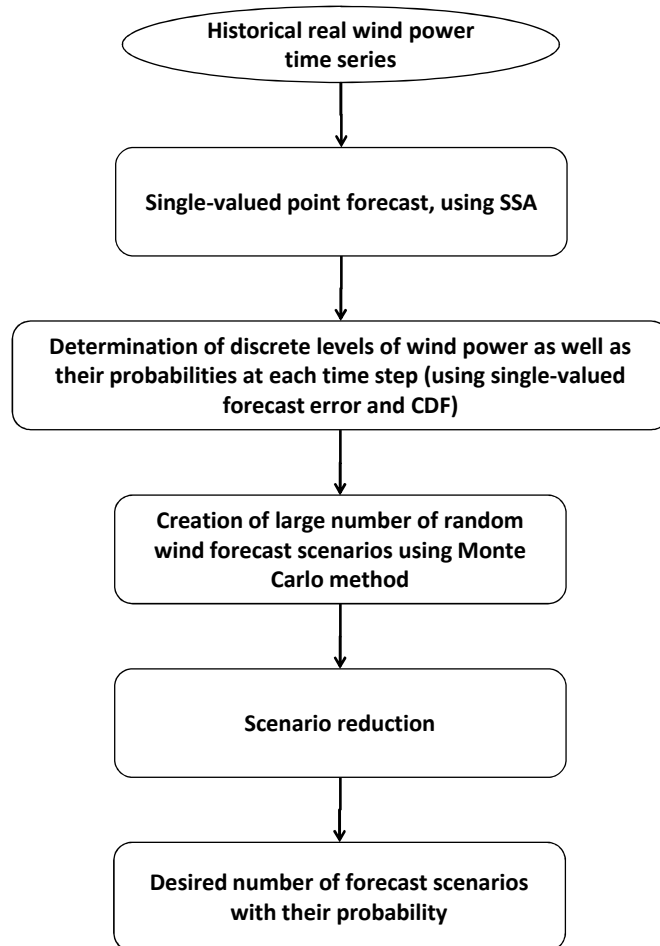
Figure 5.3: An algorithm for producing probabilistic wind power forecast scenarios

5.4.1 Discretisation of possible levels of wind power at each time step

SVPF data and forecast errors provided by SSA were used to determine lower and upper bounds for wind power at each time step which wind power outcomes fall within this range with probability higher than a specified value (*confidence interval*).

A normal probability density function ($\mathbf{N}(\mu, \sigma)$) was used to model the distribution of forecast errors. Since, forecast errors differ from one time step to another, (i.e., increase in forecast time spans results in greater errors), therefore normal PDFs, representing the forecast error distribution, at different time steps have different characteristics (Fig. 5.4). The mean value of the normal PDF at time t, μ_t, is the single-valued wind forecast at that time step, and the standard deviation, σ_t, derived from forecast errors, has the form of $\sigma_1 < \sigma_t < \sigma_T$.
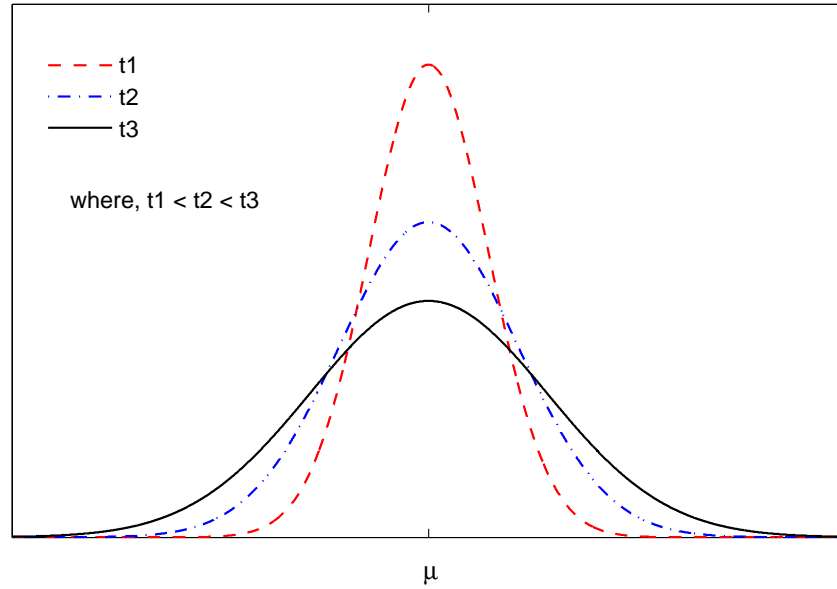
Figure 5.4: Schematic of wind forecast errors distribution over time (t1, t2 and t3)

The normal PDFs at all time steps were then discretised into several regions as shown in Fig. 5.5. Any possible wind power outcomes that fall into a region are rounded to the mean value of that region. This avoids having too many close scenarios that do not provide different information. The length of steps, Δw, are equal for all the distributions at all the time steps, therefore, in the earlier time steps there are lower number of possible levels of wind power compared to far-ahead time steps, because the

distance between lower and upper bounds are smaller. In other words, the number of possible levels of wind power at time step t, N_t^w, has the form of $N_1^w \leq N_t^w \leq N_T^w$. The length of steps should be chosen such that it is large enough to divide the distribution distance into a reasonable number of regions therefore avoiding complexity, and similar WPF scenarios.
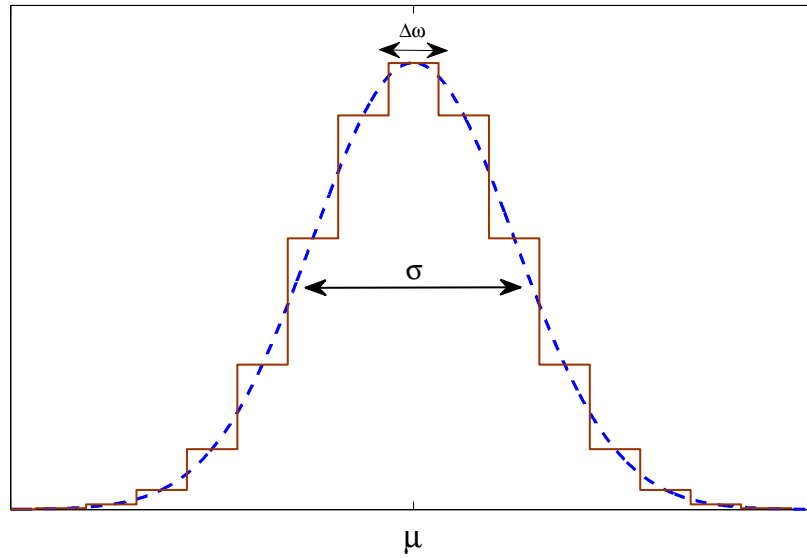
Figure 5.5: Discretised normal PDF at each time step used to model wind power forecast distribution

The probability of different levels of wind power at each time step was calculated using a normal cumulative density function as presented in Eq. 5.3.

$$\mathbf{Pr}\left(\widetilde{P}_{z,t}^w\right) = F_t\left(\widetilde{P}_{z,t}^w + \frac{\Delta w}{2}\right) - F_t\left(\widetilde{P}_{z,t}^w - \frac{\Delta w}{2}\right) \tag{5.3}$$

where Pr is probability, F_t is cumulative density function for wind power distribution at time t, $\widetilde{P}_{z,t}^\omega$ is possible wind power at level z and time t, and $\Delta w/2$ is the distance between $\widetilde{P}_{z,t}^\omega$ with the begining and end of the level.

Figure 5.6 shows all the possibilities for wind power level at various time steps. Darker colours in the interior parts of the distribution at each time step shows the higher probability of these levels. While moving toward the lighter colours at the edges of the distributions, the probability associated with the wind power levels decrease (the probability distribution has the form of a normal PDF). The length of step (Δw) (distance between every two adjacent levels of wind power) was assumed to be 100 MW for producing discretised wind power levels shown in Fig. 5.6.
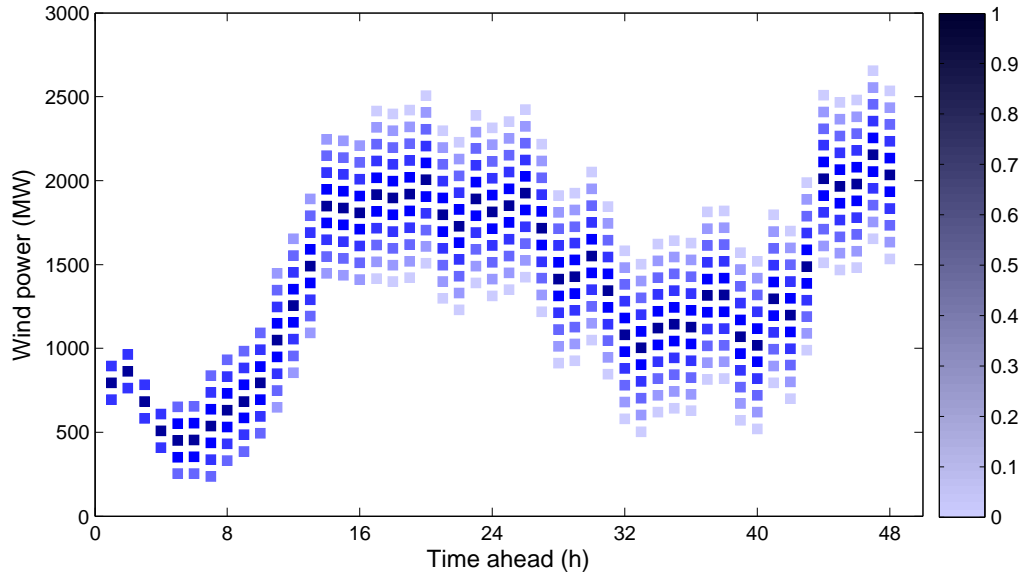
Figure 5.6: Possible levels of wind power outcome at each time step

5.4.2 Random WPF scenario generation

Given the possible levels of wind power calculated above and presented in Fig. 5.6, a Monte Carlo simulation was used to create a large number of random WPF scenarios.

As illustrated in Algorithm 1, at every run of Monte Carlo simulation one scenario is constructed. For constructing every scenario, the wind power forecast level at the

first time step is chosen based on a uniform random distribution. In the latter time steps a level of wind power is randomly selected using a normal distribution function with a mean value equal to a selected level of wind power at the previous time step, and standard deviation equal to the distance between upper and lower bounds of wind power levels at that time step.

Algorithm 1: Algorithm for random scenario generation

Large number of forecast scenarios N^{rs} are generated.

for $s = 1 : N^{rs}$ **do**

    At each time step of a scenario a level of wind is randomly selected.

    for $t = 1 : T$ **do**

        if $t == 1$ **then**

            For the first time step a level of wind is randomly selected using a uniform probability distribution.

$$P_1^{w,s} = \mathbf{U}\left(\underline{P}_1^w, \overline{P}_1^w\right)$$

        else

            For the other time steps a level of wind is randomly selected using a normal probability distribution.

$$P_t^{w,s} = \mathbf{N}\left(P_{t-1}^{w,s}, \left(\overline{P}_t^w - \underline{P}_t^w\right)\right)$$

        $\phi^s += \left(P_t^{w,s}\right)$

    Probability of a scenario is calculated by multiplying the probability of the selected level of wind power.

    $\pi^s = \displaystyle\prod_{t=1}^{T} \pi_{z,t}^s$

---

where $\mathbf{U}(a, b)$ is uniform probability distribution function with lower and upper bounds

of a and b, respectively, $\mathbf{N}\left(\mu, \sigma\right)$ is normal probability distribution function with mean value of μ and standard deviation of σ, $\overline{P}^w$ is upper bound of possible wind power outcome at each time step, $\underline{P}^w$ is lower bound of possible wind power outcome at each time step, $\widetilde{P}^w$ is possible wind power outcome at every time step, ϕ is wind power forecast scenario, π^s is probability of scenario s, and $\pi_{z,t}$ is probability of wind power level z at time t.

The top plot in Fig. 5.7 shows 1000 randomly generated WPF scenarios ($N^{rs} =$ 1000). These scenarios are most likely to occur, because the probability of transition between wind power levels at two successive time steps was taken into account.

5.4.3 Scenario reduction

It is very difficult to numerically obtain a solution for a stochastic optimisation problem using the large number of random wind forecast scenarios initially generated [66]. It is also not practical to apply the resultant solutions on a power system to achieve optimal operation. Generating a small number of scenarios through the Monte Carlo simulation, as explained above, is not favourable because a lower number of scenarios provides less information about the possible forecasts. An alternative solution is to generate a very large number of scenarios by using the Monte Carlo simulation, and then apply a scenario reduction algorithm to remove scenarios that have similar information, but lower probabilities. The resultant set of scenarios has only lost a minimum amount of information compared to the original set [66; 67].

In Algorithm 2, hierarchical steps for reducing the number of scenarios are illustrated in detail. Figure 5.7 shows how 1000 randomly generated WPF scenarios was reduced

to a desired number of scenarios (from top to down).

Algorithm 2: Scenario reduction algorithm

---

begin

Calculate distances between scenario pairs

$$\Delta\left(\phi^s, \phi^{s'}\right) = \sqrt{\sum_{t=1}^{T}\left(P_t^{w,i} - P_t^{w,j}\right)^2}, \quad \text{i,j} \in \{1 : S\}$$

$k = N^{rs}$

repeat

Find the two closest scenarios

$$\Delta\left(\phi^s, \phi^{s^*}\right) = \min_{i \neq j} \Delta\left(\phi^i, \phi^j\right),$$

Determine the scenario to be deleted

$$\pi^{s^*} \min_{s \neq s^*} \Delta\left(\phi^s, \phi^{s^*}\right) = \min_{m \in \{1:k\}}\left\{\pi^m \min_{n \neq m} \Delta(\phi^n, \phi^{m^*})\right\},$$

Delete the selected scenario (m) from the scenarios set ($\mathbf{\Phi}$), and update the probability of the closest scenario (n)

$\mathbf{\Phi}- = \phi^m$

$$\pi^n = \pi^n + \pi^m,$$

$k = k - 1$

until $k = N^{ds}$;

---

where N^{rs} is number of random scenarios that initially generated, N^{ds} is desired num-

ber of scenarios, $\Delta\left(\phi^s, \phi^{s'}\right)$ is distance between scenarios s and s', and $\boldsymbol{\Phi}$ is set of wind power forecast scenarios.
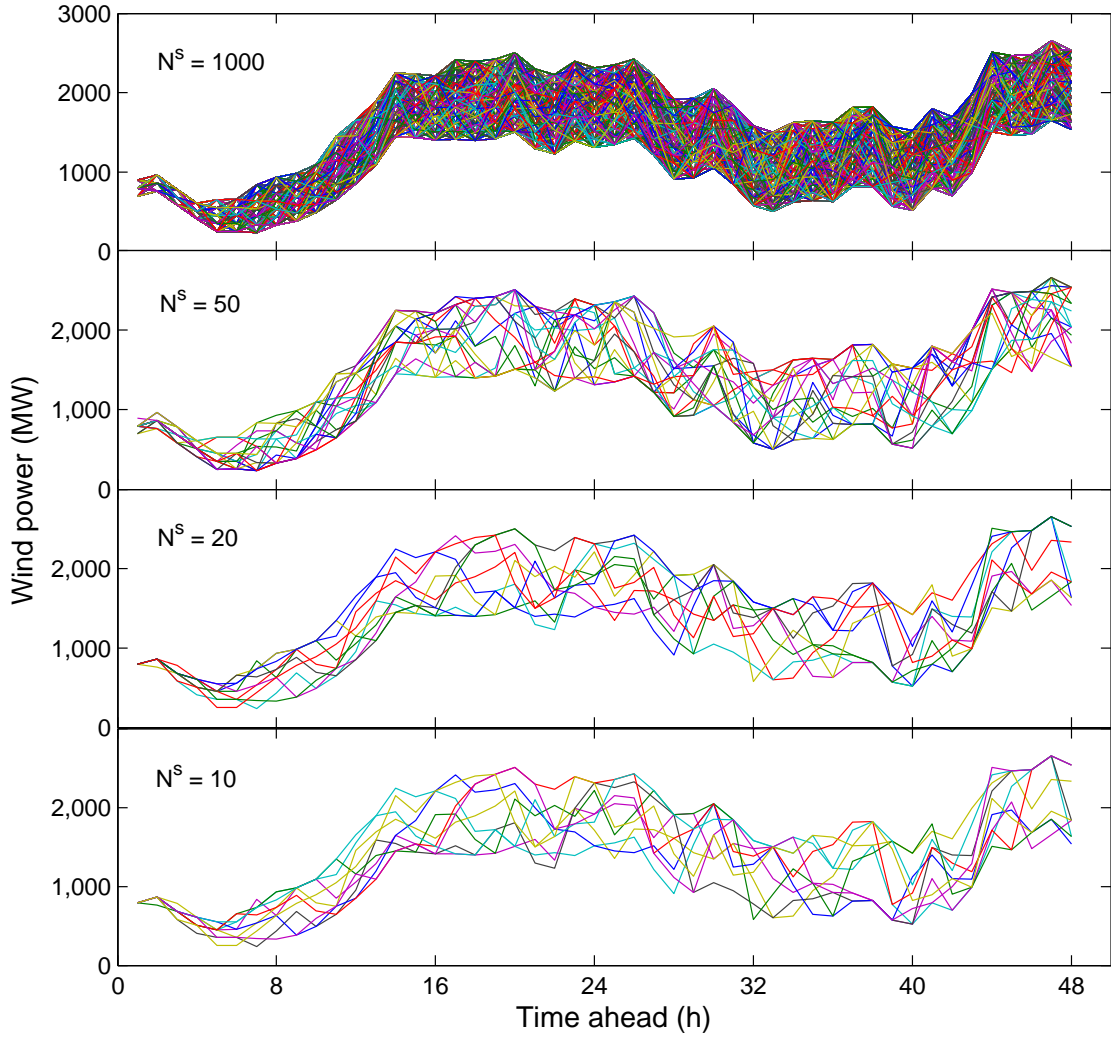
Figure 5.7: Different number of scenarios derived by applying the scenario reduction algorithm on 1000 randomly generated WPF scenarios.

In Fig. 5.8, five selected scenarios with their probabilities are presented. These scenarios are used for the purpose of stochastic optimisation of integrated gas and

electricity network in the following chapters.
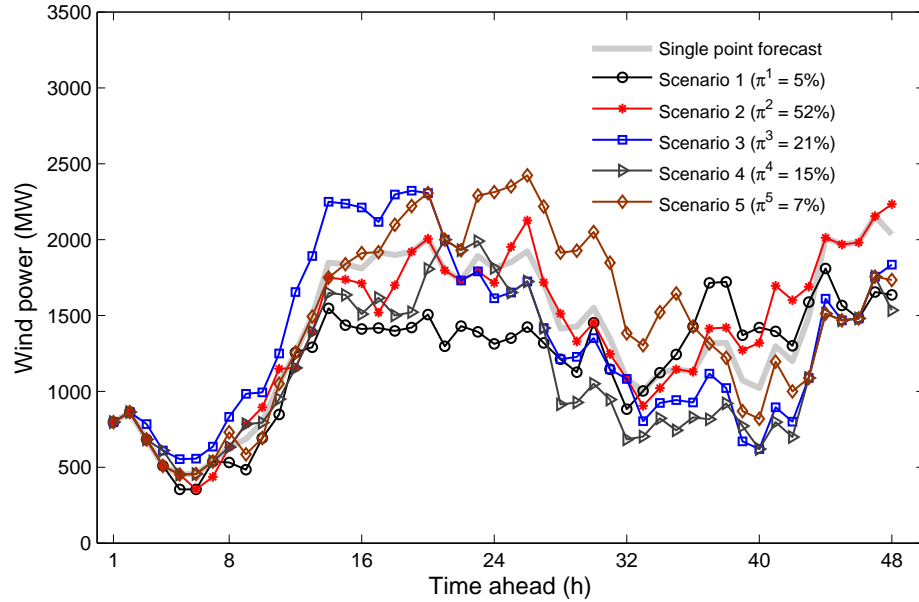
Figure 5.8: Five WPF scenarios obtained from 1000 randomly generated scenarios.

5.5 Summary

An algorithm was proposed to construct a large number of probabilistic wind power forecast scenarios using a single-valued point forecast. After applying a scenario reduction algorithm on the large number of randomly generated WPF scenarios, a desired number of scenarios were obtained to be used in a stochastic optimisation of the integrated gas and electricity network in the following chapters.

Chapter 6

Stochastic Optimisation of Integrated Gas and Electricity Network

6.1 Introduction

In a conventional power system, unit commitment decisions are usually made in advance by using a single forecast for electricity demand and wind power generation. But, as the share of wind power capacity in generation portfolios increases, taking account of wind power uncertainty in unit commitment scheduling becomes important. Therefore, it is essential that power utilities should determine an optimal unit commitment schedule by taking account of spinning reserve levels under wind power uncertainty [68].

Several models have been proposed in recent literature to address wind generation uncertainty in the unit commitment problem (e.g. [68; 69; 70; 71; 72; 73; 74; 75]). In [68], the particle swarm optimisation technique is used to solve a stochastic cost model considering load and wind power uncertainties. In [69] a two-stage stochastic integer programming model is proposed for the integrated optimisation of power production and

trading which includes a specific measure accounting for risk management. Wu et. al. [70] presented a model for calculating the cost of power system reliability based on the stochastic optimisation of long-term security-constrained unit commitment. Random outages of generating units and transmission lines as well as load forecasting inaccuracies are also modelled as scenario trees using Monte Carlo simulation. In [54] uncertain wind power forecast based on an artificial neural network is developed and integrated into a unit commitment scheduling problem.

Preliminary results in the literature indicate that a stochastic approach can reduce operational costs while maintaining system security under increased uncertainty. However, interaction between operating reserve requirements and unit commitment scheduling under uncertainty is an area that needs further investigation [57].

Given the strong linkage between gas and electricity networks, wind uncertainty not only affects the operation of electricity network but also impacts on gas network operation through uncertainty of gas demand for gas-fired generators. Although the high inertia of the gas transmission network provides a buffer to partly compensate for wind forecast errors, gas supply and pressure in the network will be affected. In addition, modelling the integrated network through a stochastic programming approach, provides the optimal unit commitment scheduling and operation subject to the constraints that govern gas supply to gas-fired generators such as transmission capacity and pressure constraints. In the literature, the impact of wind uncertainty on the operation of the gas network, and gas supply constraints on generation units has, so far, been neglected.

Due to the lower uncertainties in energy demand forecasts (in terms of magnitude and probability) compared to those of wind generation, in this research only uncertainty associated with wind power generation was taken into account.

6.2 Stochastic programming approaches

In stochastic programming there is no unique way of formulating an optimisation problem [76]. The approach taken will depend on the purpose of the modelling and of the behaviour of random parameters. A brief description on the most widely used approaches in stochastic programming (probabilistic constraints, two-stage and multi-stage recourse) are provided in the following subsections. The two-stage and multi-stage recourse methods were used in this research, therefore, they are described in greater details. For further reading about these approaches refer to [76; 77; 78; 79; 80].

6.2.1 Optimisation with probabilistic constraints

In optimisation with probabilistic constraints (also called chance constraints), a probability level $(1 - \pi^*)$ is defined for violation of a set of constraints [81]. The general representation for this type of problem can be shown as Eq. 6.1:

$$\textbf{min } f(x)$$
$$\textbf{s.t. } \textbf{Pr} \{g_i(x, \xi) \leq 0\} \geq \pi^*, \quad i \in I, \ x \in X \tag{6.1}$$

where $f(x)$ is the objective function, $\textbf{Pr}\{\cdot\}$ is the probability of meeting a constraint, and $g_i(x, \xi)$ is the left-hand-side of the constraint set which includes variable set x and the uncertainty parameter ξ.

The chance constrained problem in Eq. 6.1 needs to be re-formulated into a deterministic form in order to be solved [82]. Some sophisticated solution techniques have been developed especially in the case that the random parameter follows a multivariate normal distribution [83]. The chance constrained approach has been applied in power system planning and operation to model random parameters for wide range of problems such as optimal scheduling of generation mix and capacity expansion [84; 85; 86; 87; 88; 89].

6.2.2 Two-stage stochastic programming

In two-stage recourse problems, decisions are made in two stages[1] and uncertain parameters are observed in between. Therefore, the first decision must be made before observation of uncertain parameters, and then at the second stage when the uncertainties are known, the second stage decision is made.

The optimal decision for the first stage can be obtain by minimising the objective function of the problem, which consists of costs of the first stage and the expected costs of the second stage (Eq. 6.2), taking into account all the possibilities for the uncertain parameters (scenarios). The first stage decision can be applied at the time the decision is made (current time). For the second stage, there are as many decision variable sets as the number of scenarios. Every decision variable set can be considered as a strategy for the appropriate scenario. In practice, when time proceeds and uncertainties are observed at the second stage, the appropriate decision set for this stage will be applied given the observed uncertainties, this is called a *recourse decision*.

$$f = \min_{x \in X} f_1\left(x_1\right) + \mathbb{E}\left[f_2\left(x_2, \xi_2\right)\right] \tag{6.2}$$

The objective function for a two-stage recourse problem consists of two parts, cost of the first stage, $f_1(x_1)$ (which is certain), and the expected cost of the second stage, $\mathbb{E}\left[f_2(x_2, \xi_2)\right]$. Where the expected cost of the second stage is a summation of the cost multiplied by the probability of every scenario:

$$\mathbb{E}\left[f_2\left(x_2, \xi_2\right)\right] \equiv \sum_{s=1}^{N^s} \left[\pi^1 f_2\left(x_2^1, \xi_2^1\right) + \cdots + \pi^S f_2\left(x_2^{N^s}, \xi_2^{N^s}\right)\right], \tag{6.3}$$

where, N^s is the number of scenarios.

---

[1] In general, the term *stages* represents the sequence that uncertain parameters are observed. In multi-period models when independent uncertain parameters are involved with every time step, the terms *stage* and *time step* can be used interchangeably. In two-stage models, stage does not represent time step.

6.2.3 Multi-stage stochastic programming

The multi-stage problem is an extended form of the two-stage recourse. In the multi-stage problems there are uncertainties associated with all stages from the second to the last. Similar to the two-stage, in multi-stage problems decisions variables for all future scenarios are made at the first stage ($t = 1$). Then, in practice, as time proceeds and the uncertain parameters at different stages ($\xi_2 \cdots \xi_t$) are gradually observed, appropriate decisions are applied. The decision process in a multi-stage stochastic programming has the form of:

$decision(X_1, \ldots, X_T) \rightsquigarrow realisation(\xi_2) \rightsquigarrow recourse(X_2, \ldots, X_T) \rightsquigarrow \quad \cdots \quad \rightsquigarrow$

$realisation(\xi_T) \rightsquigarrow recourse(X_T),$

where $X_t, \ldots, X_T$ are sets of decisions for stages t to the end of the horizon, T.

The objective function of a generic T-stage stochastic programming problem can be presented in nested form

$$f = \min_{x \in X} f_1 \left(x_1 \right) + \mathbb{E} \left[f_2 \left(x_2, \xi_2 \right) + \mathbb{E} \left[\cdots + \mathbb{E} \left[f_T \left(x_T, \xi_T \right) \right] \right] \right], \tag{6.4}$$

where all the data at the first stage, i.e. function f_1, and the set X_1 are deterministic.

In order to proceed with numerical calculations of a stochastic problem, the random parameters needs to be discretised and therefore should have a finite number of realisations. The possible sequences of realisations can be demonstrated in the form of a *scenario tree* [76]. A schematic representation of a scenario tree is provided in Fig. 6.1. At the first stage ($t = 1$) of the tree there is only one node called *root node*, there are no uncertainties associated with this stage (the time when an initial decision has to be made).
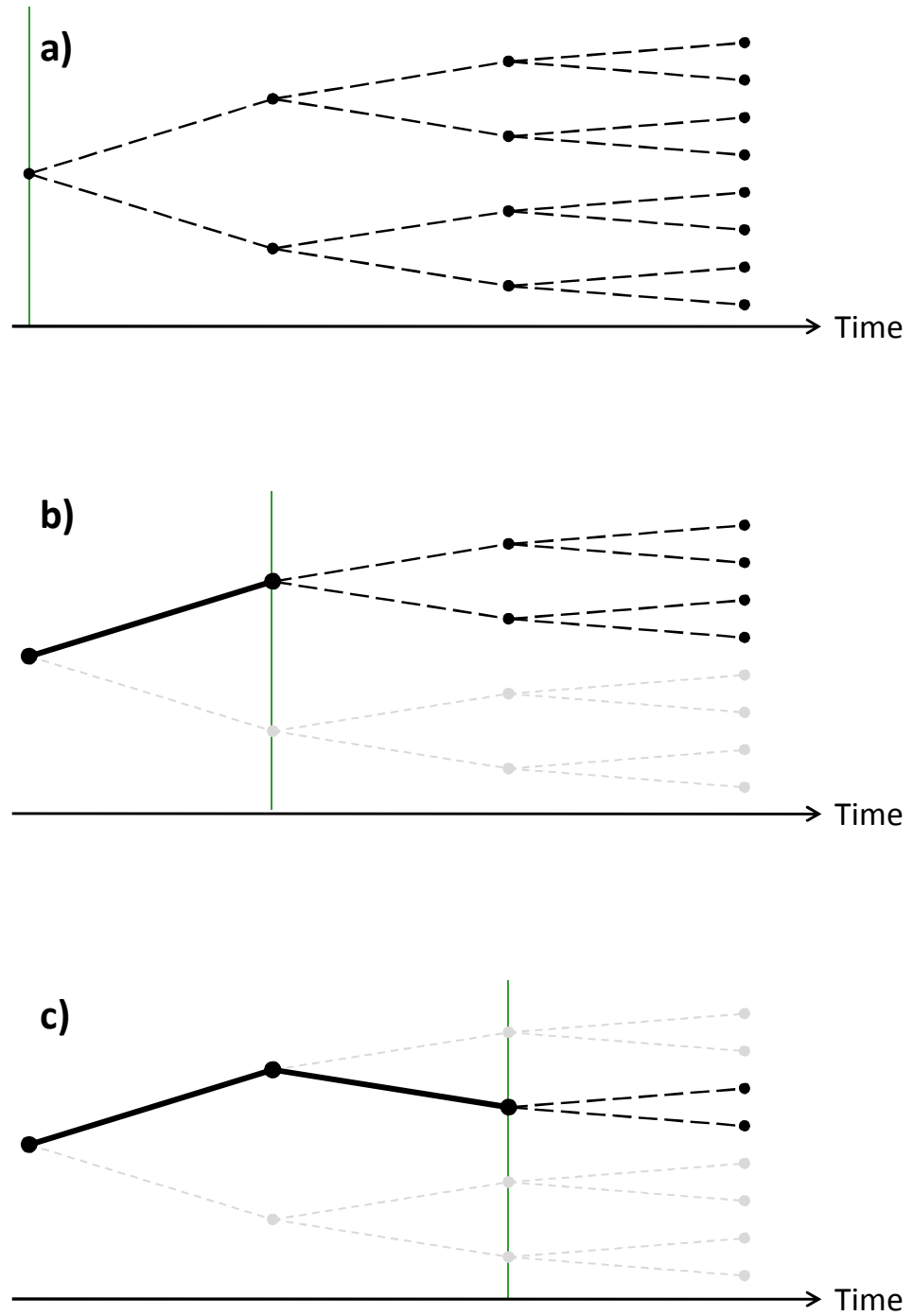
Figure 6.1: Scenario tree in a multi-stage stochastic problem

Figure 6.1 shows how solution of a recourse-based multi-stage stochastic problem is used in practice when uncertainties associated with each time step are gradually observed over time. In this representation, it was assumed that there are uncertainties associated with every time step, therefore, time steps can be considered as different stages of the stochastic problem.

Scenario tree (a) shows the condition at the first time step when the problem is solved for the whole time horizon taking into account future uncertainties. The dashed lines in the scenario tree represent uncertain future scenarios.

Scenario tree (b) shows the conditions at the second time step. The bold black lines represents the observed uncertain parameter associated with the second time step, and the light dashed lines represent the scenarios that are not valid anymore. At this time step the appropriate decision set for time step t_2 is applied (recourse action). This procedure repeated for all remaining time steps.

At different nodes in a particular time step, different decisions are determined. These decisions are linked to decisions in previous and future stages of the same scenario by constraints such as ramping rate or minimum up/down time, therefore, all the previous decisions should be optimally matched to different future decisions for the various scenarios.

After solving the stochastic problem, optimal decisions for all the scenarios are quantified. Only the first stage's decisions are applied in practice, all future stages' decisions for possible scenarios would only apply if a scenario is realised (as shown in Fig. 6.1). In short, the value of stochastic programming approach is providing decision strategies for different scenarios, which have the same history.

The values of the decision variables at time t, X_t, depend on observed information of uncertain parameters available up to time t, $\xi_{[t]}$, and on possible outcomes for future uncertainties (not future observations). The fact that in multi-stage stochastic problems future observations cannot be seen, is modelled using *non-anticipativity* constraints.

These constraints ensure that the solutions obtained by the model for time t, do not depend on future information that is not yet observed. In other words, decision variables for different scenarios must not be distinguished before the scenarios branch out. For example, all decision variables associated with the two scenarios that are left in the bottom plot of Fig. 6.1 should belong to a common ancestry up to the third time step (before they branch out).

Example: A simple stochastic unit commitment (UC) and economic dispatch (ED) problem

In order to explain the two- and multi-stage stochastic programming problems, a simple example including three thermal units and a wind farm is presented. The aim is to minimise the objective function (including generation cost at $t = 1$ and expected generation costs at $t = 2$ and 3) while meeting operational constraints of the thermal units. Shedding costs of £1000/MWh is assumed for unserved electrical energy demand.

Figure 6.2 shows a hypothesised electricity demand and four wind power forecast scenarios. Figure 6.3 shows four scenarios for the net electricity demand that are derived from subtracting the wind forecast scenarios from the total electricity demand. Operational characteristics of the thermal units are presented in Table 6.1.
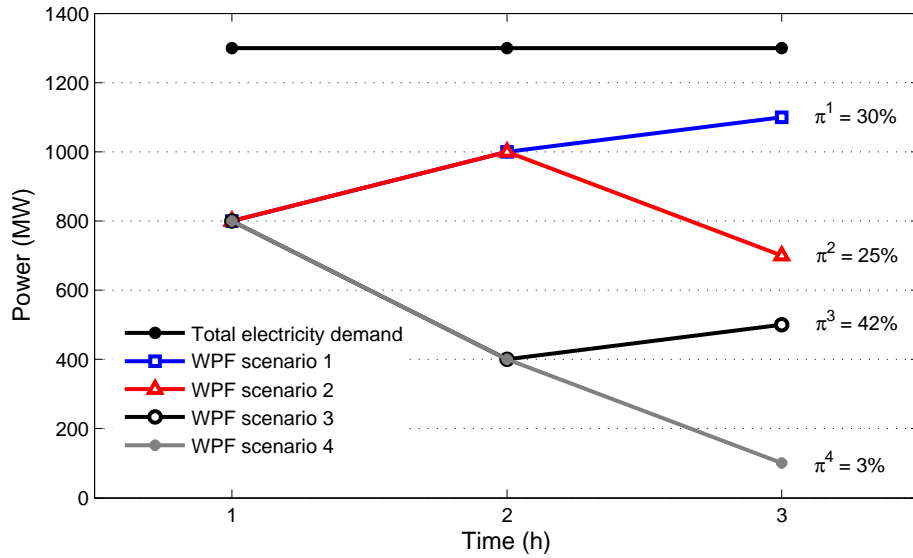
Figure 6.2: Total electricity demand and wind power forecast scenarios
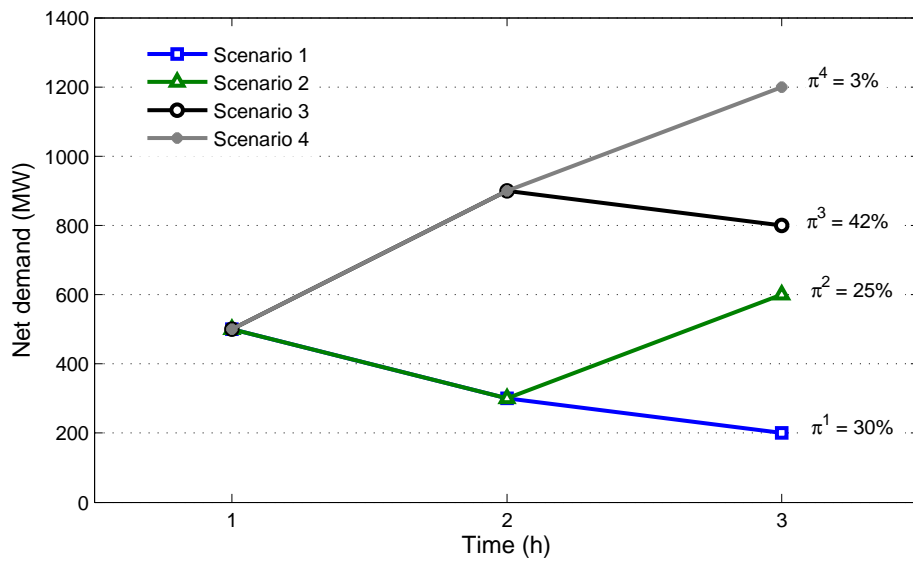
Figure 6.3: Net electricity demand scenarios

Table 6.1: Operational characteristics of thermal units. Minimum up-time and ramp-down rate for each unit is equal to its minimum down-time and ramp-up rate, respectively.

Units	$\underline{P}_i$ (MW)	$\overline{P}_i$ (MW)	C_i (£/MWh)	DT_i (h)	$\overline{R}_i$ (MW/h)
A	200	500	40	4	200
B	200	500	60	4	200
C	100	300	100	4	100

It is assumed that up to the first time step, units **A** and **B** have been online for a period longer than their minimum up-time, and unit **C** has been offline for period longer than its minimum down-time. This means that at $t = 1$ all the units can be set to be either ON or OFF. For the sake of simplicity, in this example, start-up/shut-down cost and reserve requirement is not considered.

a) Two-stage stochastic programming

For solving the above stochastic problem through the two-stage recourse approach, the UC problem needs to be solved for the whole horizon, at $t = 1$ (first stage decision), taking into account future uncertainties. It should be noted that only one unique solution is possible for the UC problem. The UC solution is optimal with respect to all the possible scenarios. After solving the UC problem, the ED problem will be solved for different scenarios (second stage or recourse decision). The ED solutions have to fall in the feasible space already defined by the UC solution. In case that any of the expected scenarios occur, the appropriate ED solution will be applied in practice. Table 6.2 and 6.3 contain results of UC and ED, respectively, using the two-stage stochastic approach.

Table 6.2: Unit commitment solution using the two-stage stochastic approach

	t = 1	t = 2	t = 3
unit **A**	1	1	1
unit **B**	1	1	1
unit **C**	0	0	0

ED solutions for scenario 1 shows 100 and 200 MWh of excess electrical energy is generated at $t = 2$ and 3, respectively. Scenario 2 has 100 MWh of excess electrical energy at $t = 2$. On the other hand, in scenario 4, at $t = 3$, 200 MWh electrical energy demand remained unserved. The excess energy generation as well as unserved energy demand incur additional costs to the system. This illustrates that in the stochastic programming approach the first stage decision is not optimal for individual scenarios, but is optimal with respect to all the future scenarios (taking into account the probability of the scenarios).

Table 6.3: Economic dispatch solution for the two-stage stochastic approach

		t = 1	t = 2	t = 3
Scenario 1	unit **A**	300	200	200
	unit **B**	200	200	200
	unit **C**	0	0	0
Scenario 2	unit **A**	300	200	400
	unit **B**	200	200	200
	unit **C**	0	0	0
Scenario 3	unit **A**	300	500	500
	unit **B**	200	400	300
	unit **C**	0	0	0
Scenario 4	unit **A**	300	500	500
	unit **B**	200	400	500
	unit **C**	0	0	0

The objective value of the problem obtained from the two-stage stochastic approach is calculated by Eq. 6.5:

$$\min \sum_s \pi^s \times \sum_t \left(C^{ue} P_s^{ue,s} + \sum_i C_i P_{i,t}^s \right) =$$

$$10^3 \times \left\{ \underbrace{(0.3 \times 64)}_{\text{scenario 1}} + \underbrace{(0.25 \times 72)}_{\text{scenario 2}} + \underbrace{(0.42 \times 106)}_{\text{scenario 3}} + \underbrace{(0.03 \times 318)}_{\text{scenario 4}} \right\} = 91.26 \text{ (£k)} \tag{6.5}$$

where π^s is probability of scenario s, C^{ue} is cost of unserved electricity, $P_s^{ue,s}$ is unserved electricity in scenario s, C_i is cost of electricity generation by generator i, and $P_{i,t}^s$ is power output from generator i at time t in scenario s.

b) Using multi-stage stochastic programming approach with recourse

At $t = 1$, UC and ED problems are solved for the first stage taking into account future uncertainties. In case that any of the expected scenarios is realised, feasible optimal decisions on UC and ED are made, considering all the remaining possibilities for wind power forecast scenarios and constraints that link the status of the units from a time step to another time step such as ramp rate and minimum up/down -time.

At the first time step, although unit **A** has enough capacity to meet the net demand by itself and minimise the operational cost at $t = 1$, unit **B** still cannot be shut down because in the following time step ($t = 2$) there is a possibility of having 900 MW net demand (with probability of 45%), and given the minimum down-time constraint, if unit **B** goes offline it cannot come online again after an hour at time $t = 2$ which could result in using a more expensive generation option (unit **C**) in addition to load shedding. Therefore, optimal power outputs at $t = 1$ for units **A**, **B** and **C**, taking into account the wind uncertainty, are 300, 200 and 0 MW, respectively. The result of UC and ED over the time horizon for all the scenarios are presented in Table 6.4 and 6.5,

respectively.

The optimal power outputs from different units at $t = 2$ for scenario 3 and 4, given the uncertainty at $t = 3$, were calculated to be 500, 400 and 0 MW for units **A**, **B** and **C**, respectively (*decision I*). This decision will cause 100 MW load shedding at $t = 3$ in scenario 4, because unit **C** cannot supply the 200 MW difference between total demand and total generation by units **A** and **B**, due to it's maximum 100 MW ramp-up limit. This will, consequently, incur shedding costs of £1000/MWh. Compared to the alternative decision (500, 300 and 100 MW power output from units **A**, **B** and **C**, respectively), *decision I* results in lower operational costs for scenario 3 and higher cost for scenario 4. Given the quite low probability of scenario 4 (only 3%), the expected cost of the scenarios 3 and 4 is minimised by applying *decision I*.

Table 6.4: Unit commitment solution for the multi-stage stochastic approach

		$t = 1$	$t = 2$	$t = 3$
	unit **A**	1	1	1
Scenario 1	unit **B**	1	0	0
	unit **C**	0	0	0
	unit **A**	1	1	1
Scenario 2	unit **B**	1	0	0
	unit **C**	0	0	1
	unit **A**	1	1	1
Scenario 3	unit **B**	1	1	1
	unit **C**	0	0	0
	unit **A**	1	1	1
Scenario 4	unit **B**	1	1	1
	unit **C**	0	0	1

Table 6.5: Economic dispatch for the multi-stage stochastic approach

		t = 1	t = 2	t = 3
	unit **A**	300	300	200
Scenario 1	unit **B**	200	0	0
	unit **C**	0	0	0
	unit **A**	300	300	500
Scenario 2	unit **B**	200	0	0
	unit **C**	0	0	100
	unit **A**	300	500	500
Scenario 3	unit **B**	200	400	300
	unit **C**	0	0	0
	unit **A**	300	500	500
Scenario 4	unit **B**	200	400	500
	unit **C**	0	0	100

The non-anticipativity constraints result in the same solution for different scenarios before they branch out, to model the fact that the system operator does not know which scenario will happen, and at the same time has to make a decision that is optimal regarding the future scenarios. For example, a unique solution is proposed for scenario 3 and 4 over the first two time steps.

The objective value of the problem is calculated in Eq. 6.6:

$$
\min \sum_s \pi^s \times \sum_t \left(C^{ue} P_t^{ue,s} + \sum_i C_i P_{i,t}^s \right) =
$$

$$
10^3 \times \left\{ \underbrace{(0.3 \times 40)}_{\text{scenario 1}} + \underbrace{(0.25 \times 62)}_{\text{scenario 2}} + \underbrace{(0.42 \times 106)}_{\text{scenario 3}} + \underbrace{(0.03 \times 228)}_{\text{scenario 4}} \right\} = 78.86 \ (\pounds k) \tag{6.6}
$$

The objective value obtained from the multi-stage stochastic problem is lower than two-stage stochastic problem, due to updating the UC decision when uncertainty associated with each stage is observed.

6.3 Formulation of the stochastic model of the integrated gas and electricity network

In the original formulation of the CGEN model, unit commitment constraints are not taken into account. In order to analyse the impacts of wind power uncertainty on the power system using a stochastic programming approach, unit commitment constraints were modelled. In this section the stochastic formulation of unit commitment are presented as part of the stochastic model of the integrated gas and electricity network, developed in this research.

The uncertainty of wind power is transfered to the gas network through gas demand for electricity generation in different scenarios. There are no significant changes in the formulation of the gas network apart from adding an index to every variable to represent different scenarios.

The stochastic optimisation model of the gas and electricity network was developed in Fico Xpress suite. After adding unit commitment constraints to the original CGEN model the nonlinear optimisation problem becomes a nonlinear mixed integer problem which is computationally difficult to solve. Therefore, the stochastic model was decomposed into two separate models: mixed integer linear programming (MILP) model for the electricity network and a nonlinear model for the gas network. The electricity network is run first and then results for gas demand for electricity generation for different scenarios are imported into the gas network model. The solution of the gas network model is checked to make sure there is no gas shedding due to operation of gas-fired generators. In the case that the gas shedding occurs, power output from the appropriate gas-fired plants will be constrained to avoid gas shedding, and then the electricity and gas models will be run repeatedly until a feasible solution is determined. The decom-

position of gas and electricity models was done to reduce mathematical complexity of the problem and also roughly imitate what happens in practice, since gas and electricity networks are usually not operated by the same ISO. Practically both networks are optimised separately with the gas network supplying gas to gas-fired plants until it is not feasible to do so.
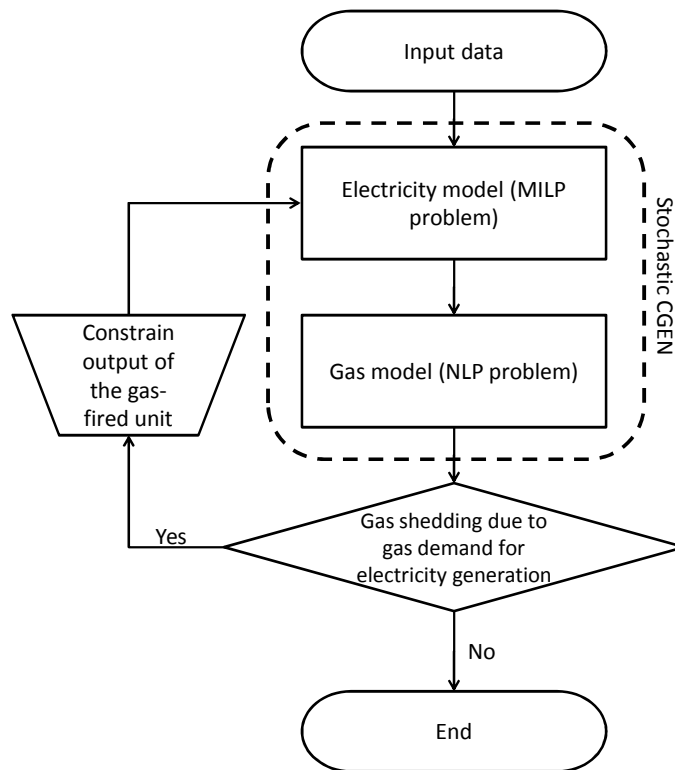
Figure 6.4: Structure of the stochastic model of the integrated gas and electricity network

6.3.1 Objective function

In the stochastic CGEN model, the complete set of unit commitment constraints were formulated for thermal plants, therefore, associated cost items such as start-up and shut-

down costs were added to the original objective function. Also, part-load efficiency of the thermal plants was taken into account.

The cost function of every scenario for electricity and gas networks are shown in Eqs. 6.7 and 6.8, respectively. The objective function of the stochastic problem consists of summation of the costs of all the scenarios multiplied by their probabilities (Eq. 6.9).

$$
f^{elec}(s) = \sum_t \left(\underbrace{\sum_i \left(C_i^f + C_i^{var} \right) P_{i,t}^s}_{cost\ of\ power\ generation} + \underbrace{\sum_b C^{ue} P_{b,t}^{ue,s}}_{cost\ of\ unserved\ electricity} + \underbrace{\sum_k C_{k,t}^{su,s}}_{start-up\ cost} + \underbrace{\sum_k C_{k,t}^{sd,s}}_{shut-down\ cost} \right)
$$

(6.7)

where C_i^f is fuel cost for generator i, C_i^{var} is variable cost for generator i, $P_{i,t}^s$ is power output from generator i at time t in scenario s, C^{ue} is cost of unserved electricity, $P_{b,t}^{ue,s}$ is electricity unserved at bus b and time t in scenario s, $C_{k,t}^{su,s}$ is start-up cost for thermal plant k at time t in scenario s, and $C_{k,t}^{sd,s}$ is shut-down cost for thermal plant k at time t in scenario s.

$$
f^{gas}(s) = \sum_t \left(\underbrace{\sum_g C_{g,t}^{gas} Q_{g,t}^s}_{cost\ of\ gas\ supply} + \underbrace{\sum_u \left(C^\iota Q_{u,t}^{\iota,s} + C^\omega Q_{u,t}^{\omega,s} \right)}_{cost\ of\ gas\ storage} + \underbrace{\sum_l C_t^{gas,sp} \partial LP_{q,t}^s}_{cost\ of\ linepack\ management} + \right.
$$
$$
\left. \underbrace{\sum_m C^{ug} Q_{m,t}^{ug,s}}_{cost\ of\ unserved\ gas} \right.
$$

(6.8)

where $C_{g,t}^{gas}$ is gas price at terminal g and time t, $Q_{g,t}^s$ is gas supply from terminal g at time t in scenario s, C^ι is cost of gas injection to storage facilities, $Q_{u,t}^{\iota,s}$ is gas injection to storage facility u at time t in scenario s, C^ω is cost of gas withdrawal from storage facilities, $Q_{u,t}^{\omega,s}$ is gas withdrawal from storage facility u at time t in scenario s, $C_t^{gas,sp}$

is spot price of gas at time t, $\partial LP_{q,t}^s$ is change of gas linepack in pipe q at time t in scenario s, C^{ug} is cost of unserved gas, and $Q_{m,t}^{ug,s}$ is unserved gas at node m and time t in scenario s.

$$f = \mathbf{min} \sum_s \pi^s \left(f^{elec}(s) + f^{gas}(s) \right) \tag{6.9}$$

In the following, the unit commitment constraints added to the stochastic CGEN are described.

6.3.2 Start-up cost

The start-up cost of a thermal plant depends on its down-time; it may vary from a maximum cold start value to a much smaller value when the plant is still relatively close to its operating temperature. A typical start-up cost function for a thermal plant has an exponential form [90]. Because the time step in this optimisation problem is discrete the exponential start-up cost was approximated into a discrete function using a stepwise form depicted in Fig. 6.5.
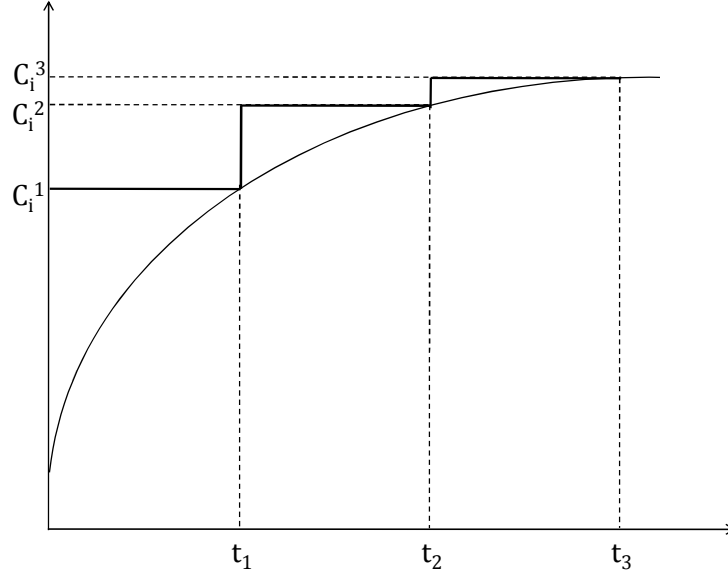
Figure 6.5: Discretised start-up cost for thermal units. The horizontal axes shows time length in which a thermal plant remained off, before starting up. The vertical axes represents start-up cost.

The start-up cost of thermal plants was implemented through Eq. 6.10 [91]:

$$C_{k,t}^{su} \geq C_{k,T'} \times \left(\nu_{k,t} - \sum_{t'=1}^{T'} \nu_{k,t-t'} \right), \tag{6.10}$$

where $C_{k,t}^{su}$ is start-up cost for thermal plant k at time t, $0 = C_{k,0} < \cdots < C_{k,TC}$ are fixed cost coefficients derived from the stepwise form of start-up cost, and ν is ON/OFF state of thermal unit (1/0).

Discretised start-up costs for thermal plants are presented in Table 6.6, and they were assumed to be the same for different technologies.

Table 6.6: Discretised start-up costs for thermal plants [7]

Time (h)	1	2	3	4	5	6	7	8	9	10
Cost (£)	1334	2748	3868	4598	5167	5475	5575	5644	5738	5820

6.3.3 Shut-down cost

A constant shut-down cost of £1000 [7] was implemented for thermal plants (Eq. 6.11), to model the waste of fuel when a unit is brought offline [39].

$$
\begin{aligned}
C_t^{sd} &\geq C^{sd} \left[\nu_{k,t-1} - \nu_{k,t} \right], \\
C_t^{sd} &\geq 0
\end{aligned}
$$
(6.11)

where C_t^{sd} is shut-down cost for thermal plant k at time t, and C^{sd} is constant shut-down cost assumed for thermal plants.

6.3.4 Part-load efficiency

The impact of part-load efficiency on the variable generation cost of thermal units was taken into account. For the sake of simplicity, the part-load efficiency was modelled using a linear approximation depicted in Fig. 6.6 [9].
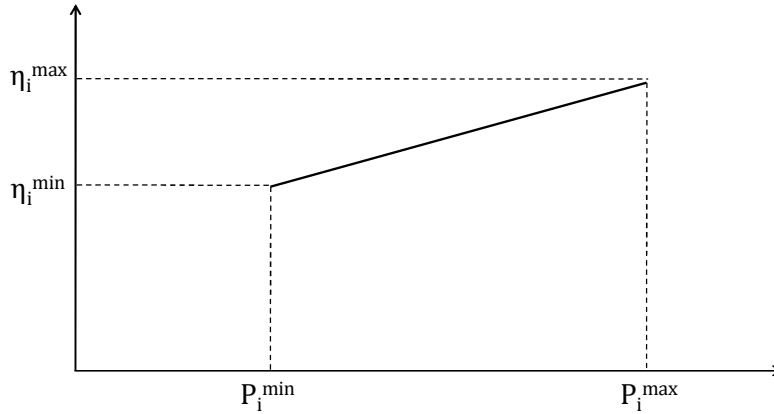
Figure 6.6: Linear approximation of part-load efficiency for thermal units. The horizontal axes shows range of power output. The vertical axes represents range of efficiency.

Minimum and maximum efficiency of different thermal plants are presented in Table 6.7.

Table 6.7: Efficiencies for different thermal plants [8].

Technology	$\eta^{\mathbf{min}}$	η^{max}
Coal	35%	45%
CCGT	50%	60%
OCGT	30%	40%

6.3.5 Spinning reserve

Spinning reserve is used to control the frequency and maintain the balance between power demand and supply at all times. The amount of available spinning reserve is equal to the unused capacity of synchronised generators which can be used immediately on the decision of the system operator [92]. Minimum spinning reserve requirement ($\underline{r}$)

97

varies in different systems. In conventional systems, the required amount of spinning reserve is usually equal to the capacity of the largest generator, or a certain percentage of the peak load. In [92], methods used to calculate the required spinning reserve for some actual power systems are provided.

Due to the significant penetration of wind capacity, a higher level of reserve is required to deal with uncertainties in wind power forecast. In the stochastic approach, the uncertainties of wind forecasts are implicitly taken into account through different representative wind forecast scenarios. Therefore, in the stochastic programming models reserve requirement is considered only for contingencies and outages.

In a deterministic approach, the up spinning reserve (r^{up}) supports any outages in addition to a sudden fall in wind power. The reserve requirements in the deterministic model was implemented using Eq. 6.12. In the stochastic models, reserve requirement was only considered to cope with any outages, therefore, reserve requirement modelled in the stochastic approach is $r_t^{up} = \sum_k r_{k,t}^{up} \geq \underline{r}^{up}$ (equal to the first part of Eq. 6.12).

$$r_t^{up} = \sum_k r_{k,t}^{up} \geq (\underline{r}^{up} + wu\% \times P_t^w) \tag{6.12}$$

where $r_{k,t}^{up} = \nu_{k,t} \times \left(\overline{P}_k - P_{k,t}\right)$, r_t^{up} is total spinning reserve provided at time t, $r_{k,t}^{up}$ is spinning reserve provided by thermal plant k at time t, $wu\%$ is percentage of wind generation contributing to up spinning reserve requirements, and P_t^w is wind power generation.

6.3.6   Minimum up- and down-time

When a thermal plant is up/down it must remain up/down for at least UT/DT periods. Minimum up/down constraints were implemented using Eqs. 6.13 and 6.14 [91].

$$\nu_{k,t'} - \nu_{k,t'-1} \leq \nu_{k,t}, \qquad t' = [t - UT_k + 1,\ t - 1] \tag{6.13}$$

$$\nu_{k,t'-1} - \nu_{k,t'} \leq 1 - \nu_{k,t}, \qquad t' = [t - DT_k + 1, \ t - 1] \tag{6.14}$$

where UT_k and DT_k are minimum up and down time for thermal plant k, respectively.

Minimum up/down time as well as ramp up/down data for different thermal plants are presented in Table 6.8.

Table 6.8: Minimum up/down time, cool-down time and ramp up/down data for different thermal plants [9].

Technology	$\mathbf{UT}(h)$	$\mathbf{DT}(h)$	$\mathbf{CDT}(h)$	$\overline{\mathbf{R}}$ (MW/h)	$\underline{\mathbf{R}}$ (MW/h)
Coal	8	4	8	200	200
CCGT	4	4	4	250	250
OCGT	1	1	2	300	300

where UT and DT are minimum up and down time, respectively, CDT is cool-down time, $\overline{R}$ and $\underline{R}$ are maximum ramp-up and -down rates.

6.3.7 Pumped storage plant

The dynamic behaviour of pumped storage plants was formulated in this study. The storage level or the equivalent stored electrical energy was implemented by Eq. 6.15. Power generation from a pumped storage is constrained by Eq. 6.16.

$$E_{i,t} = E_{i,t-1} + ts \times \left(\eta^{pump} \times P_{i,t}^{pump} - P_{i,t} \right), \quad i \in \{\text{pumped storage plants}\} \tag{6.15}$$

where $E_{i,t}$ is stored electrical energy in a pumped storage plant i at time t, η^{pump} is pumping efficiency (70% in this study [9]), $P_{i,t}^{pump}$ is pumping power for plant i at time

t, and $P_{i,t}$ is power output from plant i at time t.

$$P_{i,t} \leq \min\left(\overline{P}_i, E_{i,t-1}\right) \tag{6.16}$$

6.4 Case study

6.4.1 Integrated gas and electricity network

A simple integrated system of gas and electricity shown in Fig. 6.7 was modelled. The electricity network consists of two busbars with generation mix representing Scotland and England-Wales. The gas network, has a gas terminal, a gas storage facility, a compressor and four pipelines. The networks are linked together through gas-fired generators at both busbars.
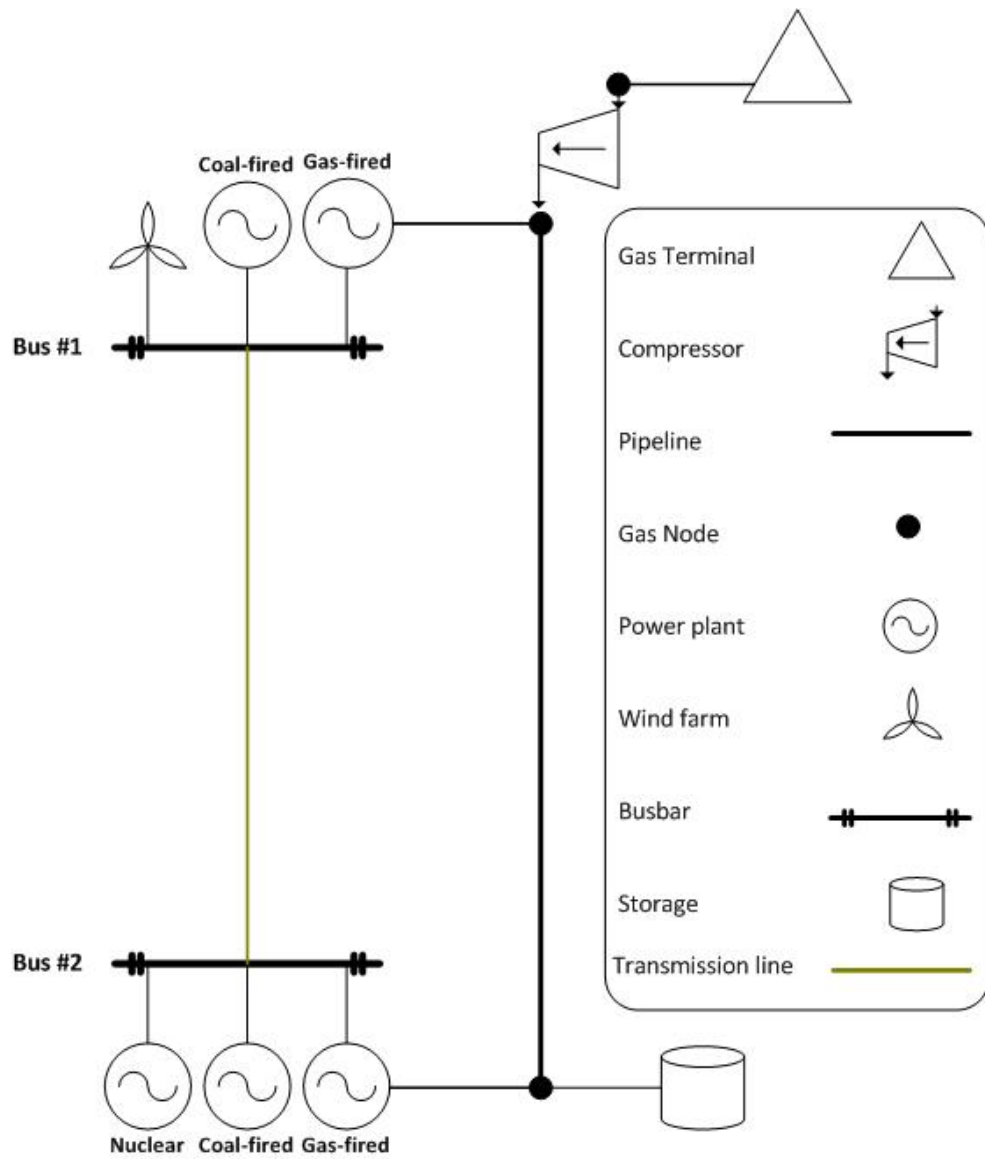
Figure 6.7: Case study

Table 6.9: Capacity of power plants at different locations

	Bus 1		Bus 2	
	Number of plants	Capacity (MW)	Number of plants	Capacity (MW)
Coal	2	800	6	3000
CCGT	2	1100	9	4500
OCGT			2	1100
Nuclear			1	1150
Wind	1	2900	1	2000
Total		**4800**		**11750**

Variable operating cost as well as fuel cost for different technologies are presented in Table 6.10. For the thermal plants, the data for fuel cost is based on their maximum efficiency.

Table 6.10: Fuel and variable operating costs for different generation technologies [10].

Technology	$\mathbf{C^f}(£/MWh)$	$\mathbf{C^{var}}(£/MWh)$
Coal	19.9	2.2
CCGT	50.9	2.3
OCGT	66.3	1.5
Nuclear	5.2	1.8

6.4.2 Probabilistic wind power forecast scenarios

The wind power forecasts which were described in Chapter 5, are used here as input to the stochastic optimisation model of integrated gas and electricity networks. In Fig. 6.8 wind power forecasts with their probability are shown and compared to the single wind forecast.
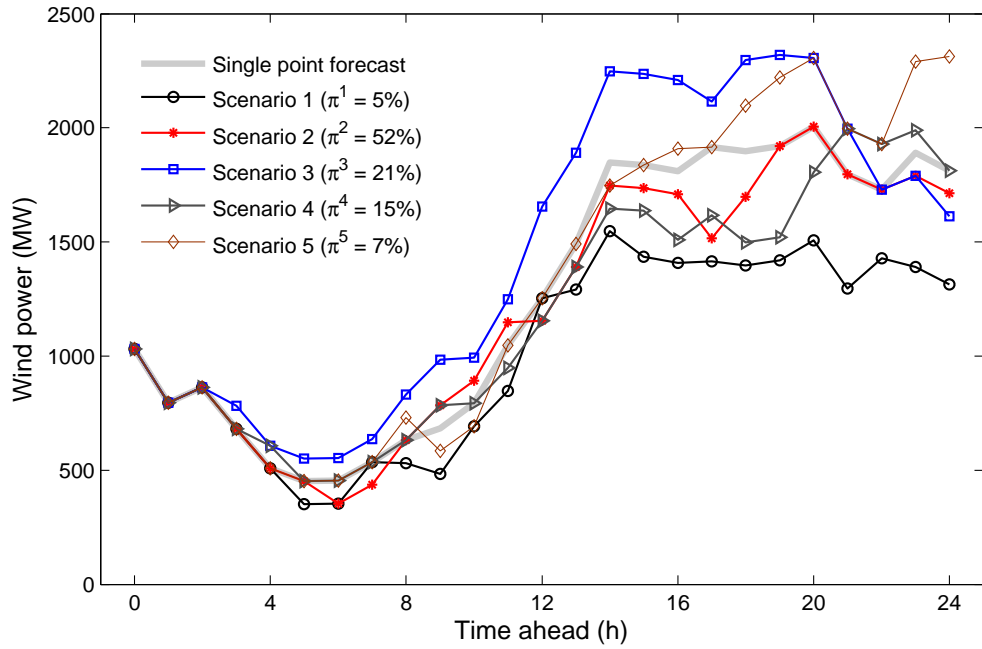
Figure 6.8: Day-ahead wind power forecasts

The stability of the scenario reduction algorithm described in Chapter 5 was tested using the two-stage stochastic model. The model was run several times with different number of scenarios and then the operational costs of the electricity network were compared (Fig. 6.9).
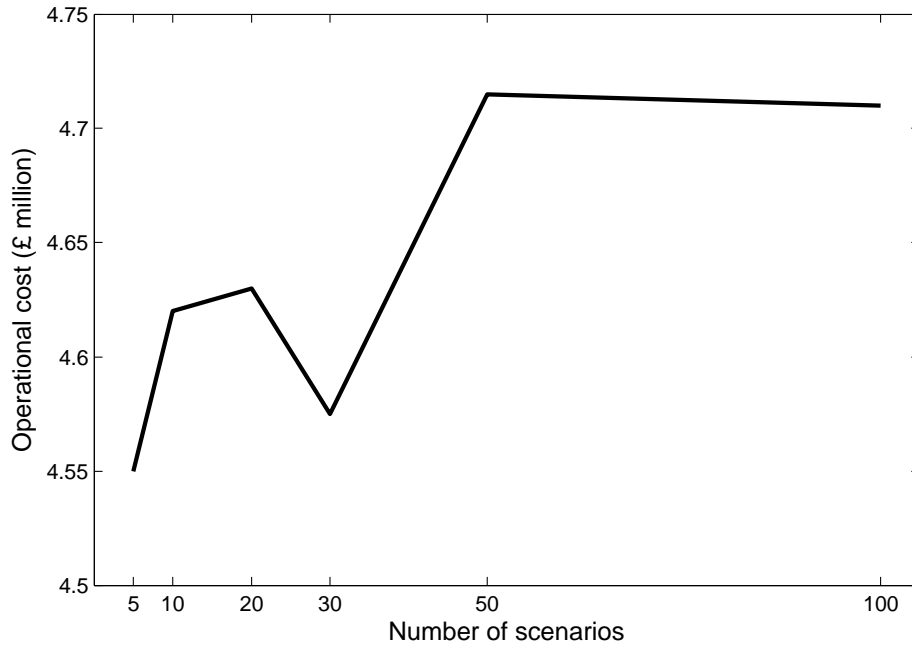
Figure 6.9: Comparison between operational cost of electricity network for different number of scenarios. This comparison is done to test the stability of the scenario reduction algorithm.

6.5 Results

The impact of wind uncertainty on the integrated gas and electricity network was investigated using three models: deterministic, two-stage and multi-stage stochastic. Results from these models were then compared to a perfect foresight model (PFM) that uses single valued wind power forecast and considers no uncertainty in the wind power forecast.

Deterministic Model (DM): In the deterministic model, the single valued point forecast for wind generation was used, but at the same time it was assumed that there is no perfect foresight. Therefore, a level of spinning reserve was maintained to deal with wind uncertainty.

Two-stage Stochastic Programming Model (TSM): In the two-stage stochastic model, probabilistic wind power forecast scenarios (Fig. 6.8) were used. In the first stage, the UC problem was solved in advance for the whole horizon (day-ahead scheduling), and then in the second stage, optimal ED decisions were made for different scenarios.

Multi-stage Stochastic Programming Model (MSM): In the multi-stage stochastic model, a probabilistic wind power forecast (Fig. 6.8) was used. At the first stage, the UC and ED problem was solved taking account of future possibilities. When the uncertainties associated with wind forecast are gradually observed at future stages, new sets of UC and ED decisions were made that are feasible regarding the decision made at the previous stage, and are optimal with respect to the uncertainties in the remaining stages.

6.5.1   Level of spinning reserve used in Deterministic Model

Dealing with the wind forecast uncertainty in the DM necessitates the allocation of extra spinning reserve. Spinning reserve requirement for the single valued wind forecast (Fig. 6.8) for different values of $wu\%$ (see Eq. 6.12) are shown in Fig. 6.10. Impacts of applying different levels of spinning reserve on the operational cost of the electricity network are depicted in Fig. 6.11.

In this research, 20% was considered to be an acceptable value for $wu\%$, due to providing reliable levels of reserve [93] at reasonable operational costs. Therefore, results from the DM with $wu\% = 20\%$ was compared to the results from the other models.
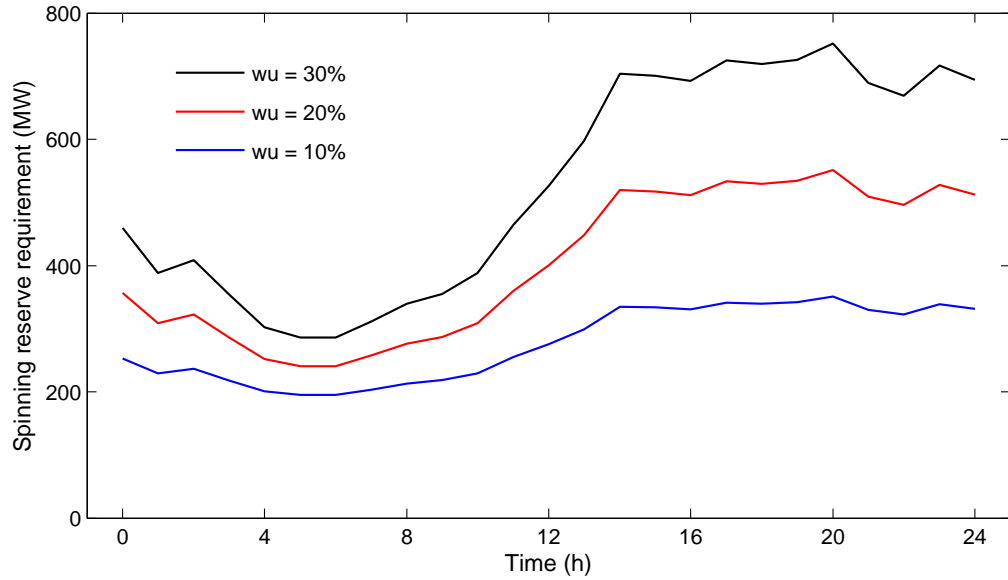
Figure 6.10: Spinning reserve requirement over the time horizon for $wu\% = 10\%$, 20% and 30%.
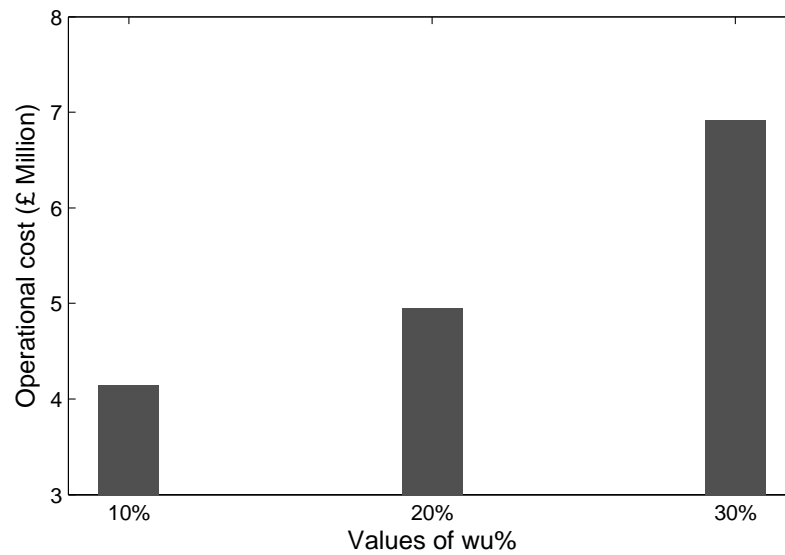
Figure 6.11: Operational cost of electricity network for different levels of reserve requirement ($wu\% = 10\%$, 20% and 30%).

6.5.2 Power generation

Changes of energy generation from different technologies with respect to the results from the PFM are presented in Fig. 6.12 for different models. Comparison of the solutions obtained from different models up to $t = 2$ is of interest, because the probabilistic scenarios match the single point forecast, and therefore, the situations up to this point are the same for all the models (in terms of wind generation). Also there is no uncertainty parameter involved with the first three hours (first stage in the MSM).

The data provided in Fig. 6.12 is the total energy generated over time duration from $t = 0$ to $t = 2$. Energy production from the nuclear plant was shown to be the same for all the models. This reflects the common statement that nuclear plants are not technologically and economically suitable to compensate for wind power uncertainty.

In DM, energy production from a number of CCGTs decrease, compared to PFM. This shows that a number of CCGT plants are operating at reduced output to provide reserve requirement explicitly defined in DM. In response to the decrease in energy production from CCGT plants, the energy generated from OCGT plants (more expensive option) increase to meet the demand.

In comparison to the PFM, coal generation in the stochastic models decreases to provide sufficient spinning reserve to deal with different possible wind forecast scenarios, and therefore energy generation from CCGTs increases to meet the demand.

The stochastic models show similar energy generation outputs, and smaller differences with respect to the PFM, compared to the DM.
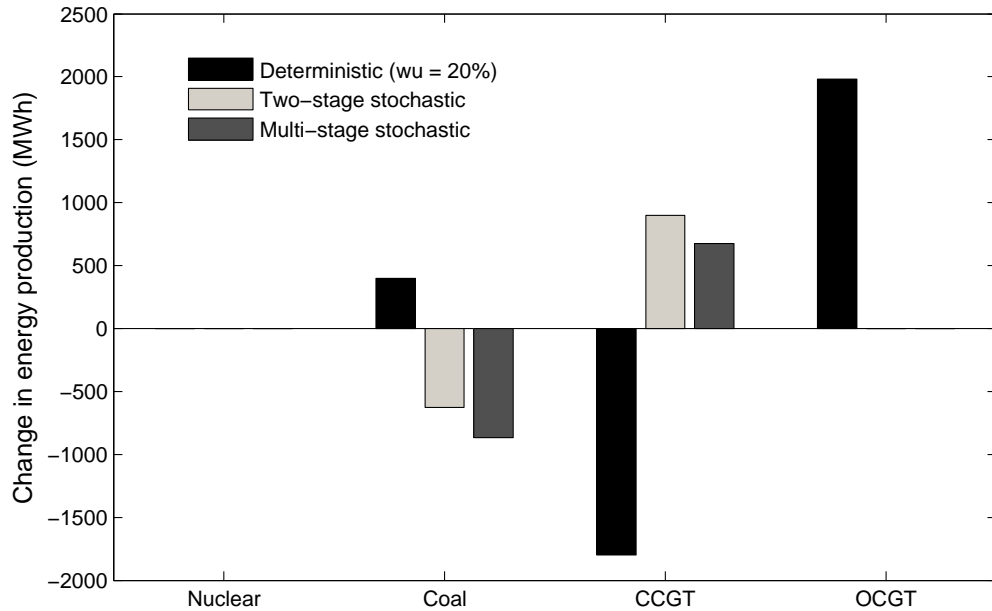
Figure 6.12: Changes of total energy generation during the first 3 hours, for different models with respect to the Perfect Foresight Model (PFM)

Figure 6.13 shows the wind curtailed over the time horizon, for different models. Higher wind curtailment in DM is due to the greater cost of providing sufficient spinning reserve, compared to the marginal cost of power generation. Therefore, it is more economical to use other generators in order to balance supply and demand, rather than using the available wind energy along with providing reserve requirement.

In the Two-stage Stochastic Model (TSM), the unit commitment schedule is determined in advance given possible wind forecast scenarios. The unit commitment solution provides a feasible space for the economic dispatch solution. Therefore, wind energy which leads to infeasible economic dispatch solutions is curtailed.

Lower wind curtailment in the stochastic models compared to the DM shows better utilisation of the available wind energy. Given that successive decisions can be made in the Multi-stage Stochastic Model (MSM) using updated information, better use of

available wind energy occurred.
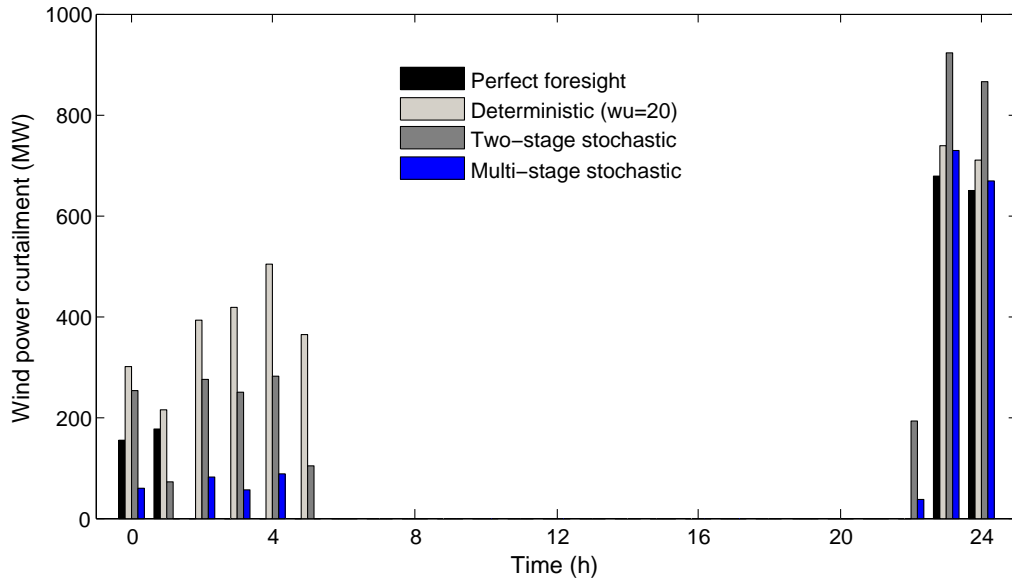
Figure 6.13: Wind curtailment for different models. Data provided for TSM and MSM are expected value, i.e. summation of wind curtailment in the scenarios already multiplied by the probability of the scenarios.

A large amount of wind energy is curtailed during the later hours of the time horizon, when low electricity demand coincides with high wind generation. Wind energy curtailment, especially in the PFM, is due to lack of flexible generation plants with low Start-up/Shut-down costs.

6.5.3 Impact of wind uncertainty on the gas supply

The impacts of wind uncertainty on gas-fired generators is transfered to the gas network. Since the gas network is more flexible compared to electricity network in terms of handling sudden changes, the difference between gas network performance for the different cases is not very significant. Compressor power consumption can be considered as an indicator of gas network performance, i.e. the more power that is consumed by

the compressor, the greater the stress on the gas network.

To show how different amounts of wind generation affects compressor power consumption, total wind energy used in every forecast scenarios of TSM and MSM along with compressor's power consumption for every associated scenarios are presented in Figs. 6.14 to 6.17. There is an inverse relation between utilised wind energy and compressor power consumption. A greater amount of gas is required to compensate for lower level of wind energy. Therefore, compressors consume greater power to deliver gas to gas-fired generators.
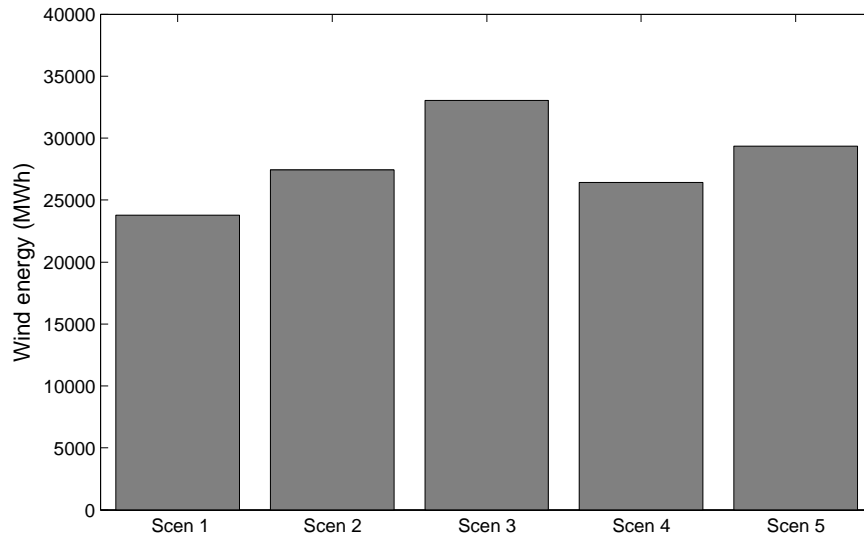
Figure 6.14: Total wind energy used in different scenarios for TSM
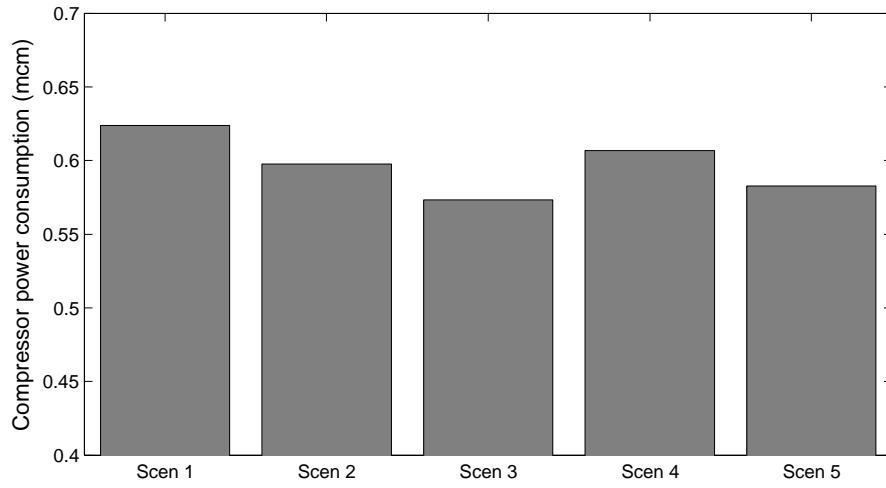
Figure 6.15: Total compressor power consumption in different scenarios for TSM
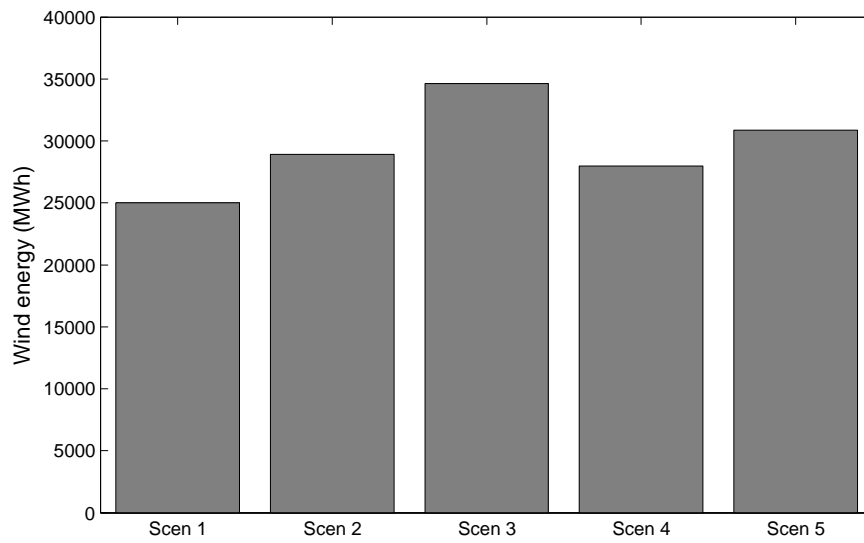
Figure 6.16: Total wind energy used in different scenarios for MSM

Figure 6.17: Total compressor power consumption in different scenarios for MSM

6.5.4 Operational costs of the integrated network

The changes in operational costs obtained from different models with respect to the PFM are shown in Fig. 6.18 and 6.19, for the electricity network and the integrated network, respectively.
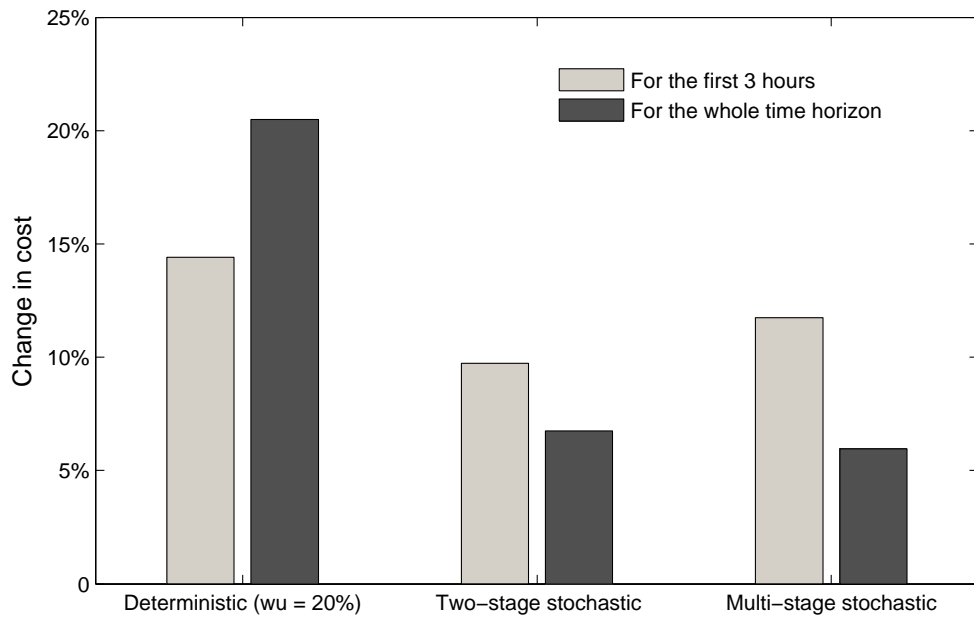
Figure 6.18: Changes of the operational costs of the electricity network for different models with respect to the PFM

Figure 6.19: Changes of the total operational costs for different models with respect to the PFM

6.6   Discussion

Stochastic optimisation models of the gas and electricity network were developed in Fico Xpress suite. Formulation of the stochastic problem as well as simple examples to illustrate two- and multi-stage stochastic models were described. The models were then applied on a simple case study to investigate how different stochastic programming approaches deal with wind power forecast uncertainty.

Comparison between the results obtained from different models shows better performance of the integrated networks occurs when the stochastic models were used.

The Multi-stage Stochastic Model (MSM) allows a system operator to improve the UC and ED decisions, that already were made, at every time step given that constraints link the current state of the systems to the previous and also take into account the remaining future uncertainties. This characteristic makes this approach a powerful tool

for scheduling thermal plants and operating the system in a day-ahead and intra-day electricity markets.

The Multi-stage Stochastic, Two-stage Stochastic and Deterministic Models proposed the least expensive operational strategies for the integrated gas and electricity networks, respectively.

The results of implementing the models introduced here, on the GB gas and electricity networks are presented in Chapter 7.

Chapter 7

Stochastic evaluation of the GB gas and electricity network

7.1   Introduction

The stochastic model of gas and electricity networks, described in Chapter 6, was used to analyse the operation of the GB gas and electricity network in the presence of significant wind generation capacity. Results obtained from different modelling approaches including Perfect Foresight Model (PFM), Deterministic Model with explicit reserve capacity (DM), Two-stage Stochastic Model (TSM) and Multi-stage Stochastic Model (MSM) were compared. Detailed description of these models are provided in Chapter 6.

7.2   Specifications of the case study

Simplified networks, shown in Figs. 4.3 and 4.4 in Chapter 4, were used to represent the GB gas and electricity networks. The capacity of different generation technologies at each electrical busbar are shown in Table 3.1, Chapter 3.

Gas and electricity demand over the time horizon (0-24 hours) are shown in Figs. 7.1 and 7.2.
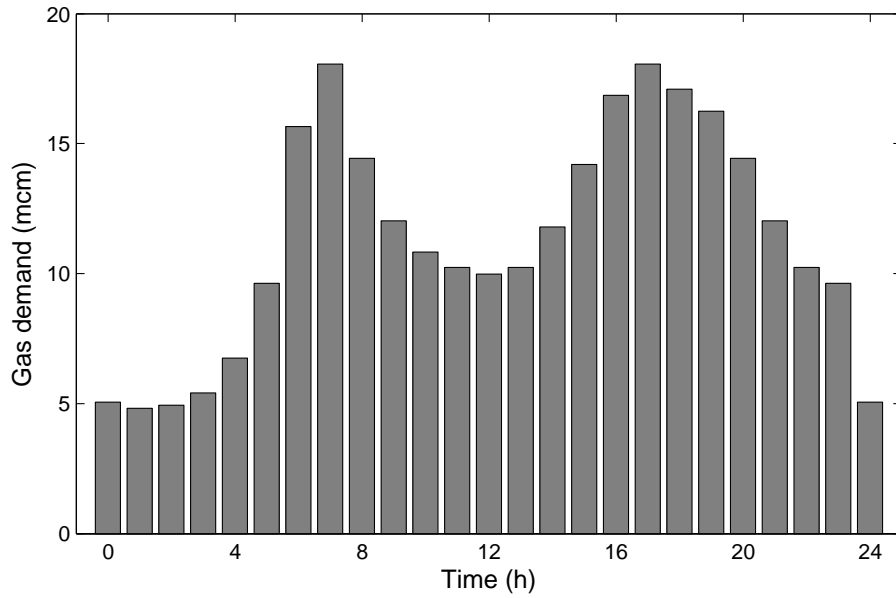
Figure 7.1: Gas demand for the GB case study
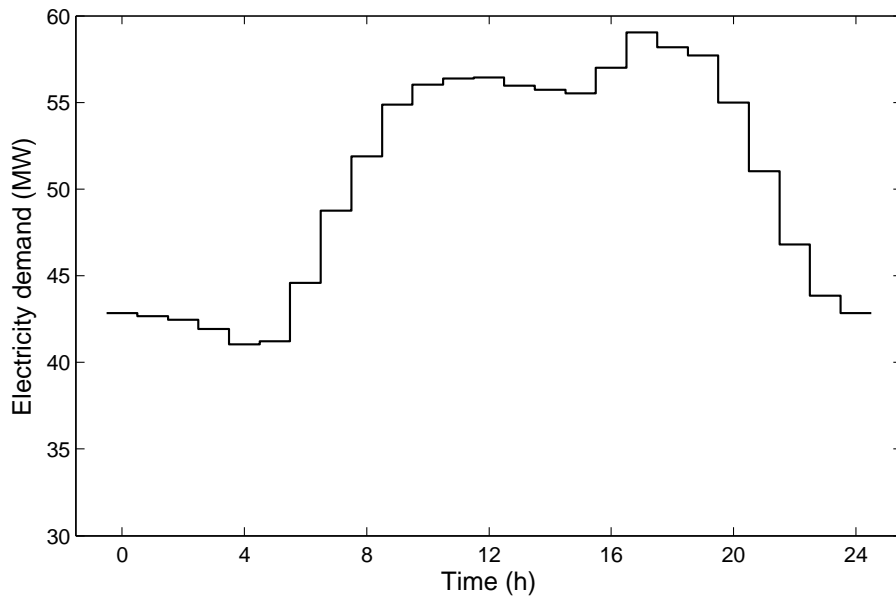
Figure 7.2: Electricity demand for the GB case study

A Single Valued Point Forecast (SVPF) and probabilistic forecast of wind power for GB system over the time horizon are presented in Fig. 7.3. The wind power forecast data for the GB case study in 2020 was obtained through upscaling the wind forecast data calculated in 2011 (refer to Chapter 5).
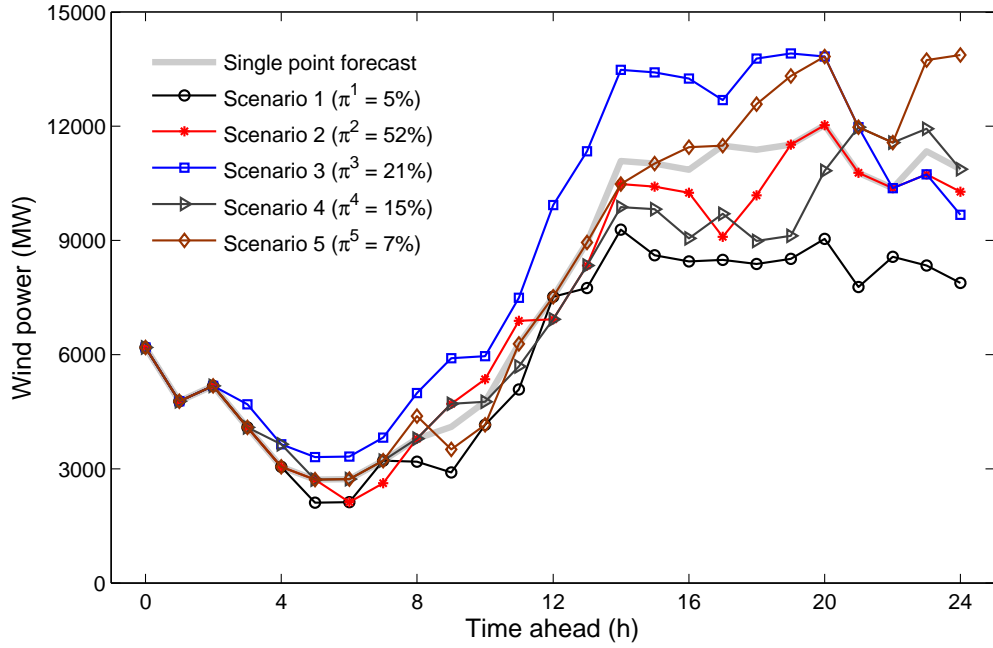
Figure 7.3: Day-ahead wind power forecast scenarios for the GB case study

7.3 Level of spinning reserve used in the Deterministic Model

In the DM, three different levels of reserve were considered to deal with wind uncertainty. The spinning reserve requirement for the single valued wind forecast (Fig. 7.3) for different values of $wu\%$ (refer to Eq. 6.12, Chapter 6) are shown in Fig. 7.4. The greater the capacity of spinning reserve requirement, the greater the cost of operating the electricity network. This is due to a large number of thermal units that have to operate at reduced output which incurs higher generation costs. Also, in response to the

decrease in power generation from these units, more expensive generators are needed to contribute to power supply. The impacts of applying different levels of spinning reserve on the operational cost of the electricity network is shown in Fig. 7.5.

Based on information provided in Figs. 7.4 and 7.5, 20% was considered to be an acceptable value for $wu\%$, due to providing reliable level of reserve [93] at reasonable operational costs. Therefore, results from the DM with $wu\% = 20\%$ was compared to the results from TSM and MSM.
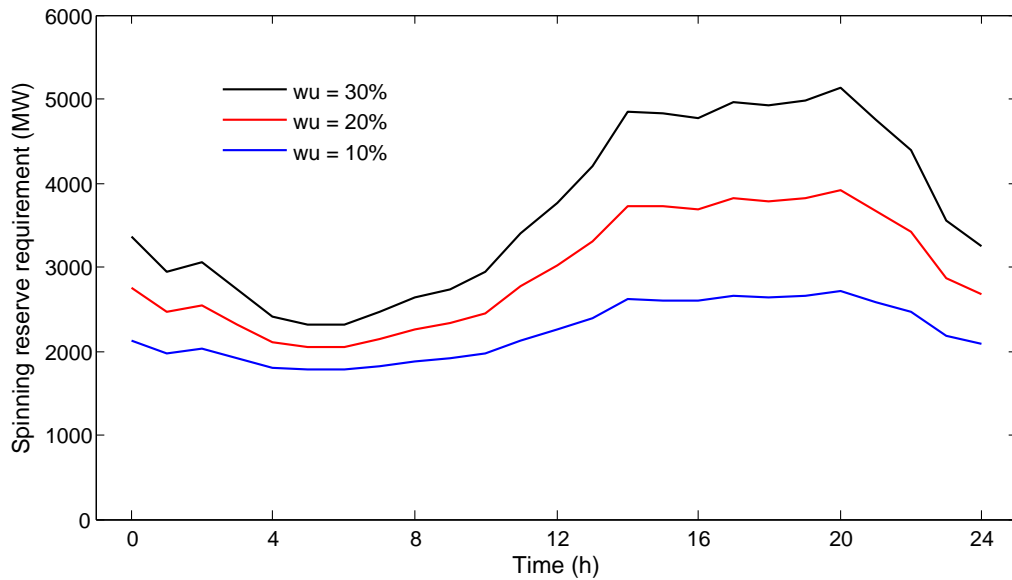
Figure 7.4: Spinning reserve requirement over the time horizon for $wu\% = 10\%, 20\%$ and 30%.
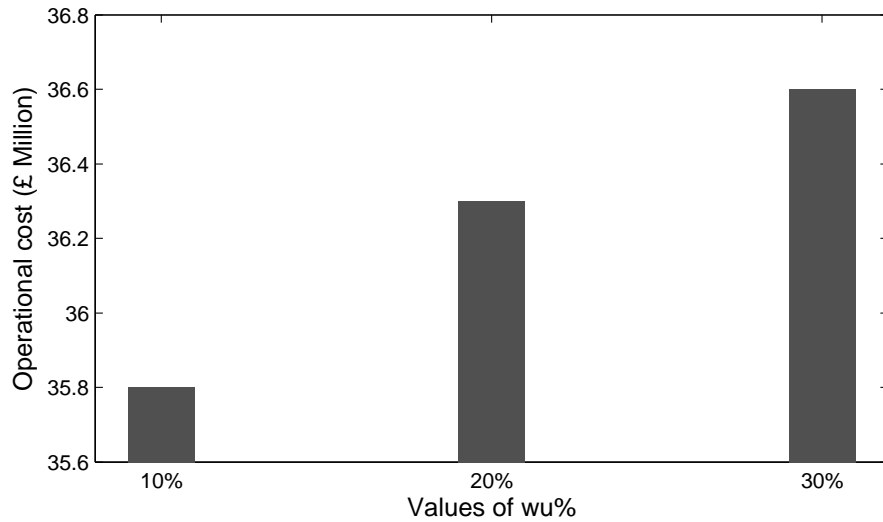
Figure 7.5: Operational cost of electricity network, over the time horizon, for different levels of reserve requirement ($wu\% = 10\%$, 20% and 30%).

7.4   Share of different technologies in power generation

Total electrical energy production over the first three hours of the time horizon is shown in Fig. 7.6 for different generation technologies. Comparison of the solutions obtained from different models up to $t = 2$ is of interest, because the probabilistic scenarios match the single point forecast (no wind uncertainty), and therefore the situation up to this point (in terms of wind generation) is the same for all the models. This period is also considered as the first stage of the multi-stage stochastic programming problem (MSM) i.e. the decision made for this period is actually applied on the system.
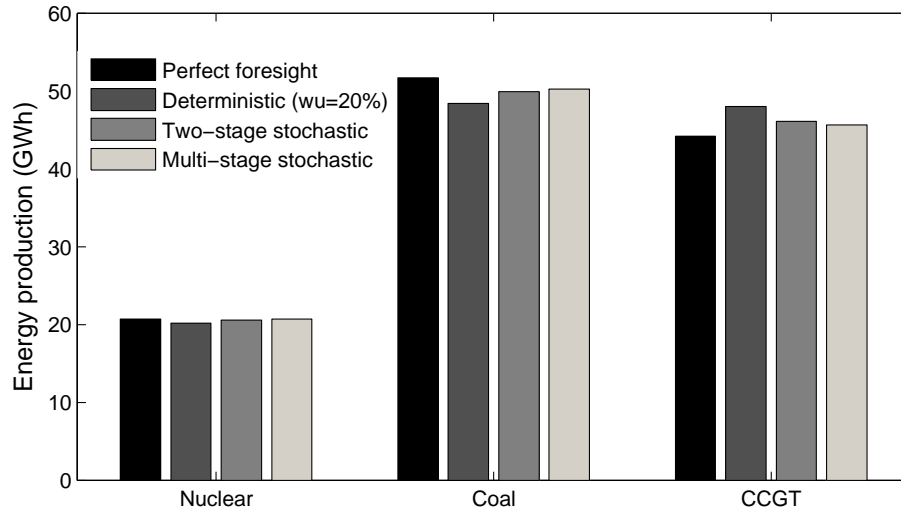
Figure 7.6: Total electrical energy production during the first 3 hours, for different models

Figure 7.7 shows how electricity generation from various technologies and models change with respect to the PFM.
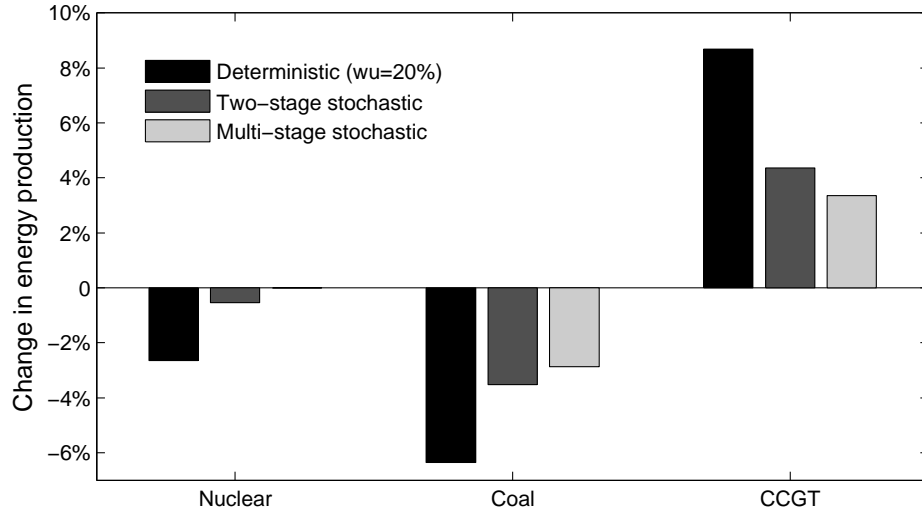
Figure 7.7: Changes of total electrical energy production during the first 3 hours, for different models with respect to the perfect foresight case

The data provided in Figs. 7.6 and 7.7, shows electrical energy production via nuclear plants for the DM and TSM slightly decrease compared to electricity generation from nuclear plants in PFM. There is no change in electricity from nuclear for the MSM compared to the PFM. This is an insignificant change in electricity production compared to the changes in electricity production by Coal and CCGT plants. This suports the common statement that nuclear plants provide negligible contribution in compensating for wind power uncertainty.

In the DM, energy production from a number of Coal-fired generators decrease, compared to the PFM. This shows that a number of coal plants operate at reduced output to contribute in providing reserve requirement that is defined explicitly. In response to the decrease in power generation from Coal plants, the power output from CCGT plants (more expensive option) increase to meet the power demand.

In comparison to the PFM, energy production by coal generators in the stochastic models decrease in order to contribute in providing sufficient spinning reserve to deal

with different possible wind forecast scenarios, and therefore power generation from CCGTs increases to meet the power demand. However, the stochastic models show smaller differences in electricity production in respect to the PFM, compared to the DM. This shows the smaller reserve requirements in the stochastic models.

7.5   Wind curtailment

The total wind curtailed over the time horizon for different models are shown in Fig. 7.8. Higher wind curtailment in the DM is due to the greater cost of providing sufficient spinning reserves, compared to the marginal cost of power generation. Therefore, it is more cost effective to use other generators to meet the demand-supply balance, rather than using the available wind energy along with providing higher reserve requirement.
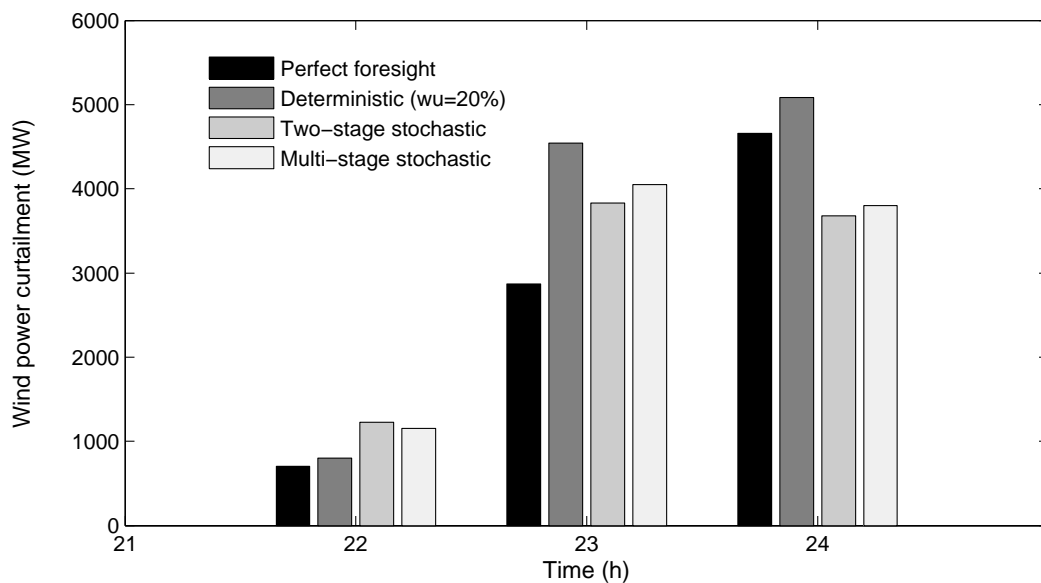
Figure 7.8: Wind curtailment for different models. Data provided for the stochastic models are expected values, i.e. summation of wind energy curtailment in the scenarios multiplied by the probability of the scenarios

For example, in order to avoid wind curtailment over a period of time, a number

of thermal generators are required to shut-down and come on-line again when power output from wind farms decrease. Switching off a number of thermal units and bringing them on-line again after a short period of time, incurs start-up and shut-down costs. These costs could be higher than the costs for power generation that is required to compensate for curtailed wind.

In the TSM, the unit commitment schedule is determined in advance given the possible wind forecast scenarios. The unit commitment solution provides a feasible space for the economic dispatch solution. Therefore, wind energy which leads to infeasible economic dispatch solutions is curtailed.

In the stochastic models a lower amount of wind is curtailed compared to DM and therefore shows better utilisation of the available wind energy.

A large amount of wind energy is curtailed during the later hours of the time horizon, when low electricity demand coincides with high wind generation.

7.6 Pumped storage operation

Hydro pumped storage plants are very effective in compensating for wind uncertainty and variability. It can use electricity to pump water when the total power generated through conventional plants and wind farms is higher than demand, and then use the stored water to generate electricity during high demand and low wind periods. Therefore, having an appropriate capacity of hydro pumped storage in a generation portfolio smooths the net electricity demand that need to be met by conventional generators. The capacity of pumped storage plants in GB is around 2.7 GW and is projected to remain the same in 2020 [4].

Figures 7.9 to 7.12 show the pumping energy, level of storage and energy output for pumped storage plants for different models. It was assumed that at the beginning of the time horizon the storage reservoir is empty. Because of the high electricity demand

from $t=8$ to $t=20$, energy is stored in the storage reservoirs during the previous periods in order to be used when demand is high.
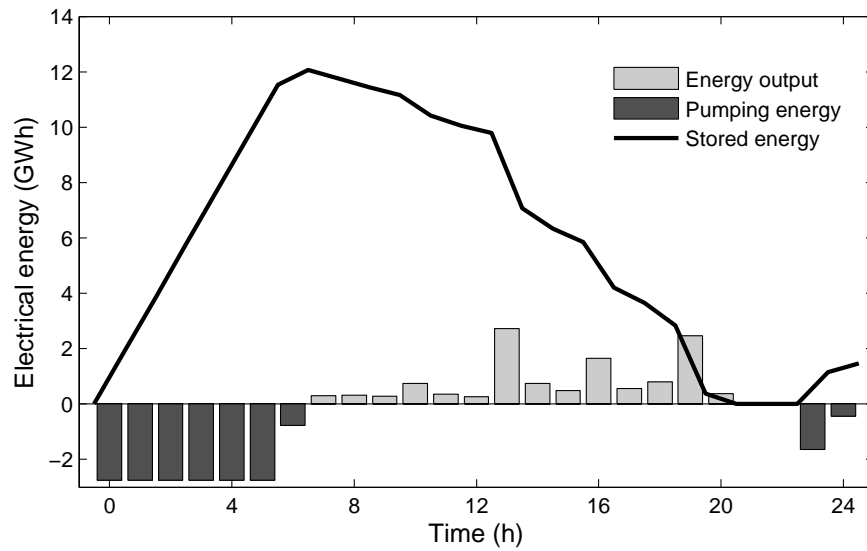
Figure 7.9: Pumped storage operation in PFM. The columns represent the total pumping energy/energy output at each time step.
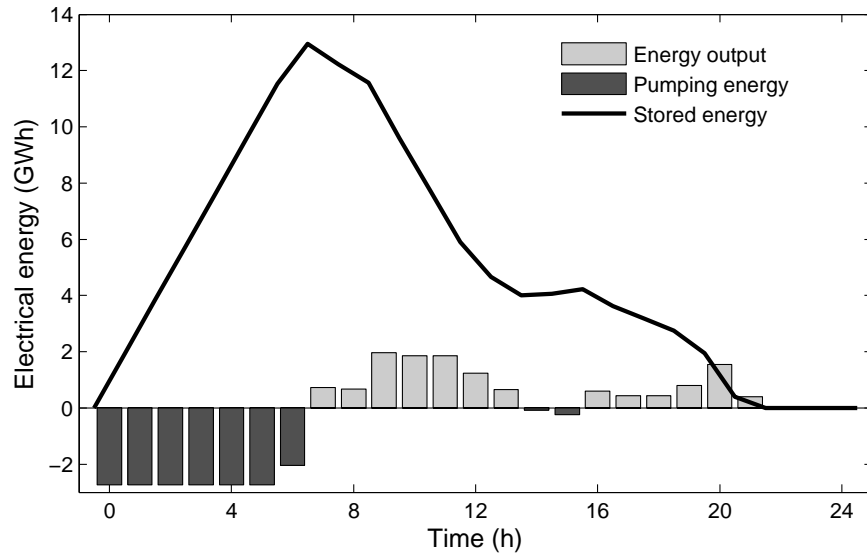
Figure 7.10: Pumped storage operation in DM. The columns represent the total pumping energy/energy output at each time step.

For TSM and MSM (Figs. 7.11 and 7.12) there are significant differences between operation of the pumped storage plants in different scenarios. This shows performance of the pumped storage plants depend on the wind forecasts.
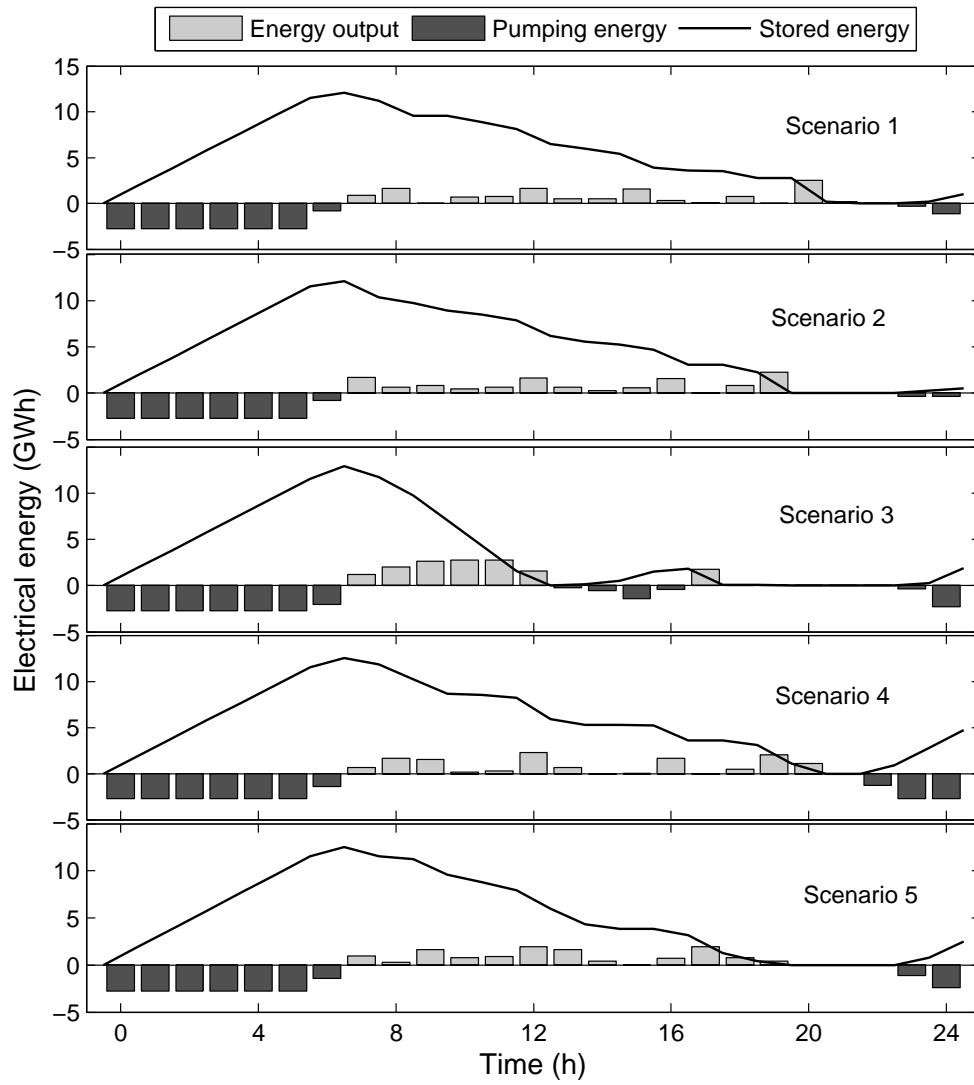
Figure 7.11: Pumped storage operation in different scenarios of TSM. The columns represent the total pumping energy/energy output at each time step.
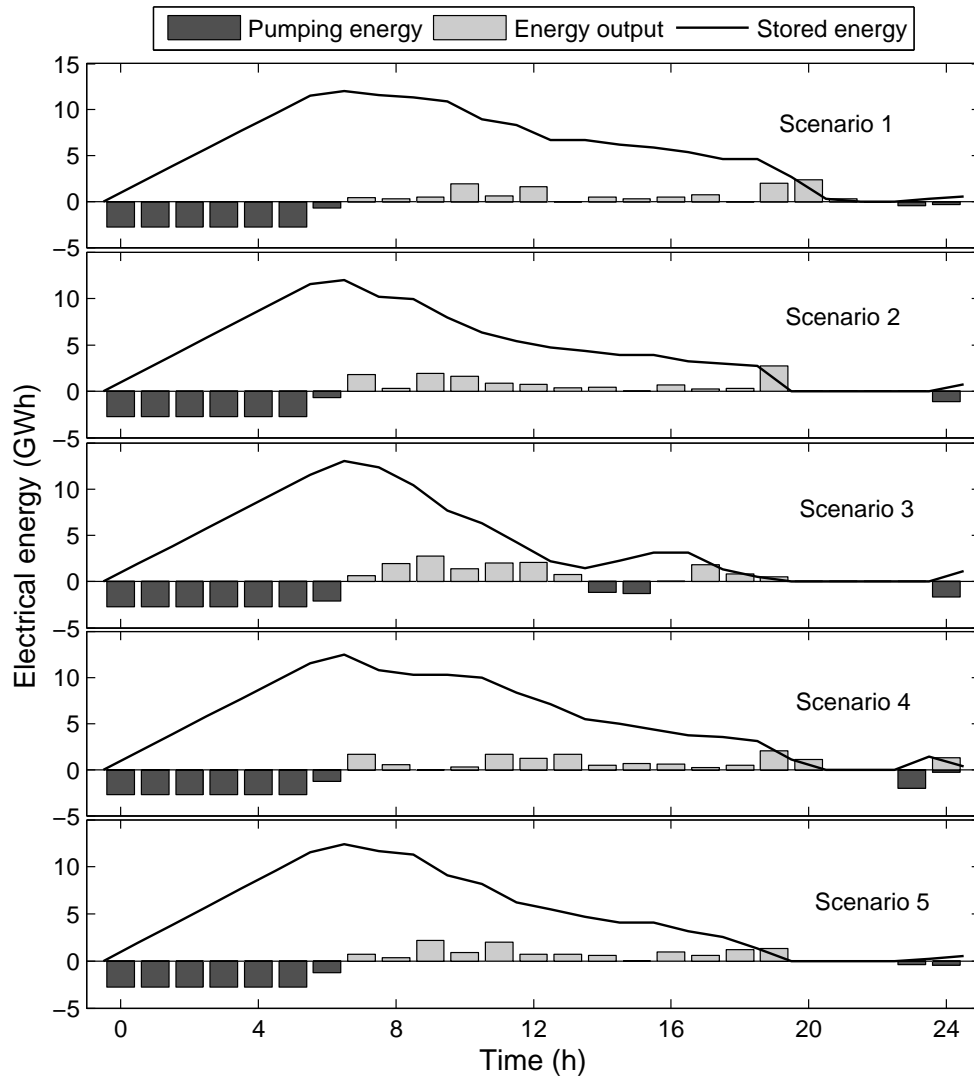
Figure 7.12: Hydro pumped storage operation in different scenarios of MSM. The columns represent the total pumping energy/energy output at each time step.

7.7 Committed thermal plants

The number of committed thermal units for TSM and MSM are shown in Fig. 7.13. Unit commitment solution for TSM is unique and is made in advance for the whole horizon (first stage decision), while for MSM there are as many solutions as the number of scenarios. In the TSM, unit commitment solution provides a feasible space for economic dispatch solutions for different scenarios.

The fact that unit commitment decisions in MSM can be updated when new information on wind forecast is acquired, makes this approach capable of dealing with uncertainties in wind power forecasts.
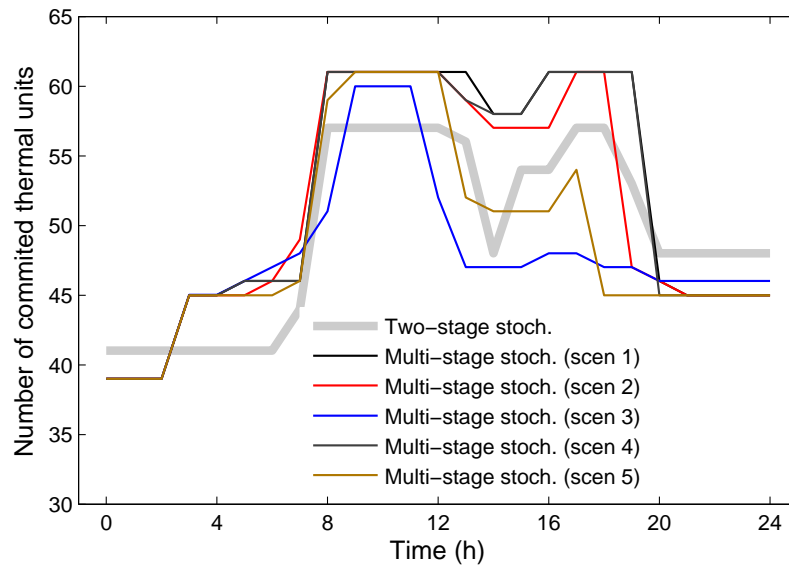
Figure 7.13: Number of committed thermal plants for TSM and scenarios of MSM

7.8 Gas network

7.8.1 Gas demand for electricity generation

Due to compensating for wind variability and uncertainty, output of gas-fired generators is influenced greatly by integration of wind energy into the electricity network. Gas demand for electricity generation for PFM and DM are presented in Fig. 7.14. Gas demand for electricity generation for different scenarios of TSM and MSM are shown in Figs. 7.15 and 7.16, respectively.

In the stochastic approaches, gas demand for every scenario is significantly different from the others. This, subsequently, causes different total gas demand for different scenarios. Although the gas network is less vulnerable against sudden changes in demand, having the most probable scenarios for demand helps the system operator to decide on the least expensive operational strategies for maintaining gas delivery.
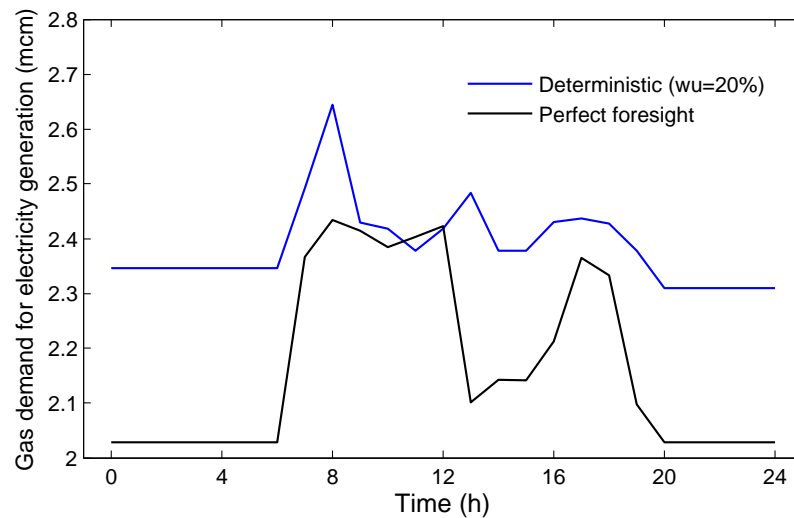
Figure 7.14: Gas demand for electricity generation for the PFM and DM
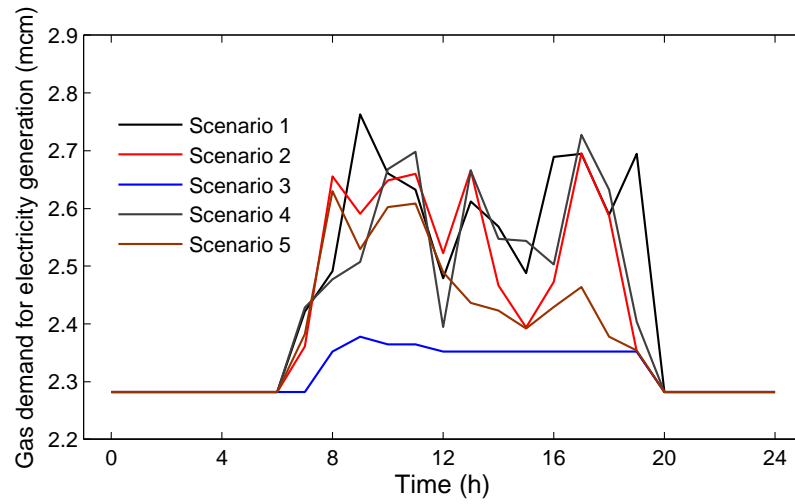
Figure 7.15: Gas demand for electricity generation for different scenarios of the TSM
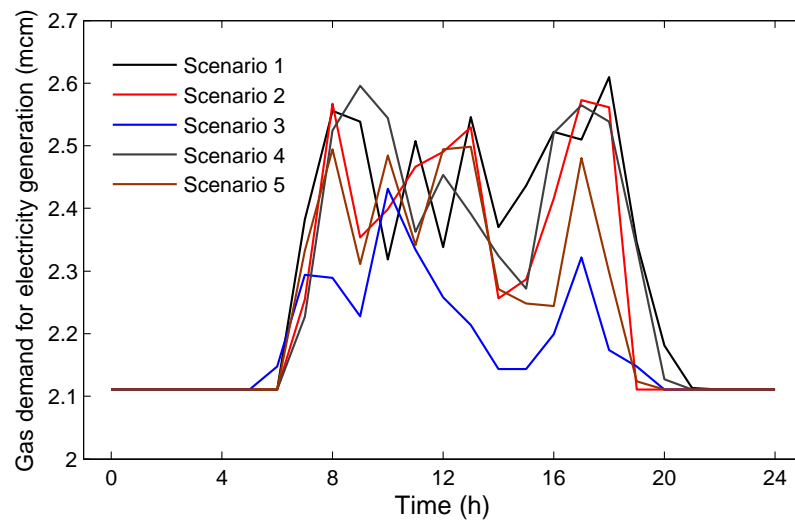
Figure 7.16: Gas demand for electricity generation for different scenarios of the MSM

7.8.2 Performance of gas compressors

Different gas demand for power generation for various approaches leads to different total gas demand profiles. This affects gas pressure in the network and causes compressors to compensate for any pressure drop. Energy consumed by gas compressors for different approaches are presented from Figs. 7.17 to 7.19.
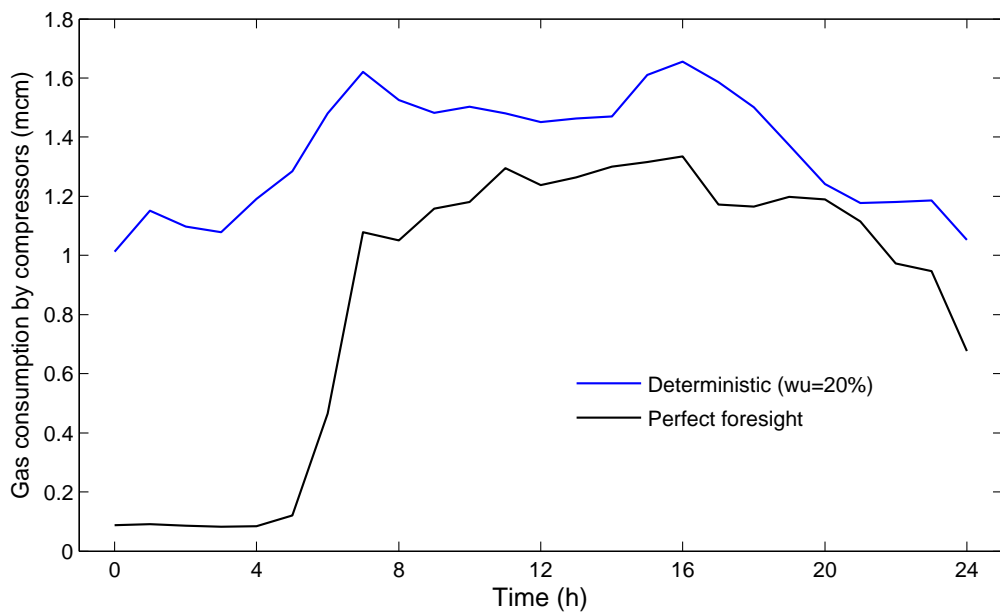
Figure 7.17: Gas consumption by compressors for the PFM and DM

Energy consumption by compressors for different scenarios of TSM and MSM (Figs. 7.18 and 7.19) show significant differences between compressors' energy consumption. Lower expected energy consumption by compressors in the stochastic approaches compared to DM, is due to the larger gas demand for electricity generation in DM.

Results of analysing wind uncertainty impacts on the gas network helps to optimise operation of the network. For instance, for different wind scenarios there is an optimal operation regime for compressors to maintain gas network pressure while meeting demand.
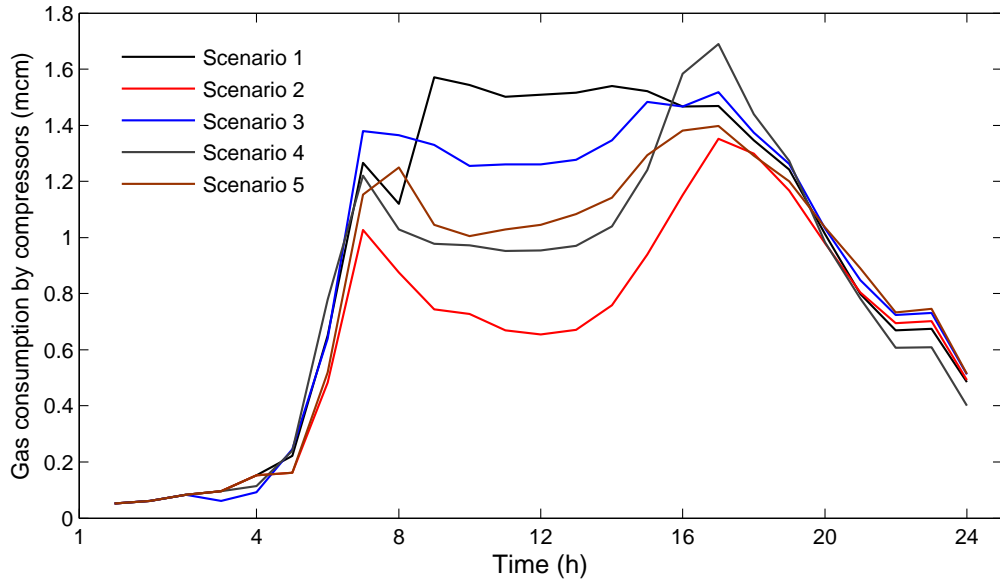
Figure 7.18: Gas consumption by compressors for different scenarios of the TSM
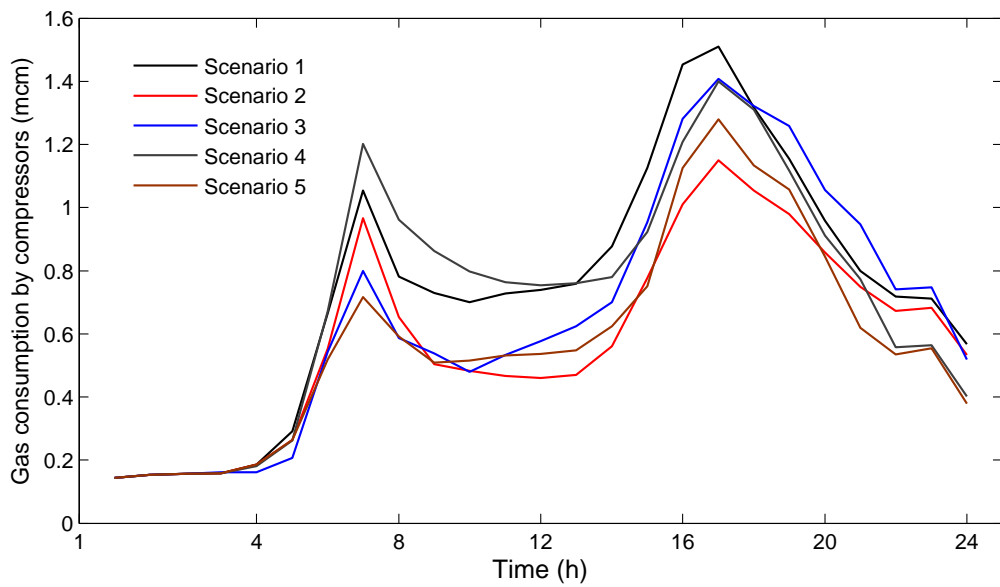
Figure 7.19: Gas consumption by compressors for different scenarios of the MSM

7.9 Operational cost

The changes in operational costs for different approaches with respect to the PFM are shown in Figs. 6.18 and 6.19, for the electricity network and the integrated network, respectively.
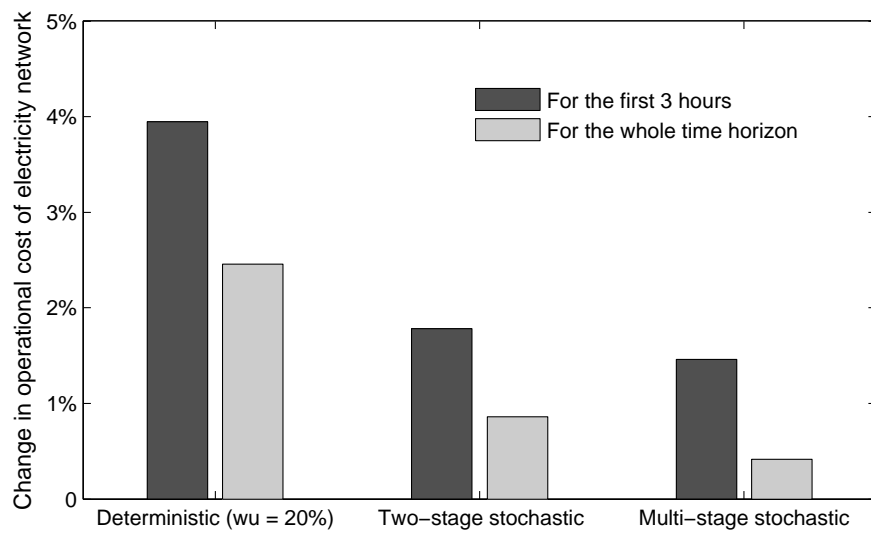
Figure 7.20: Changes of the operational costs of the GB electricity network for different models with respect to PFM
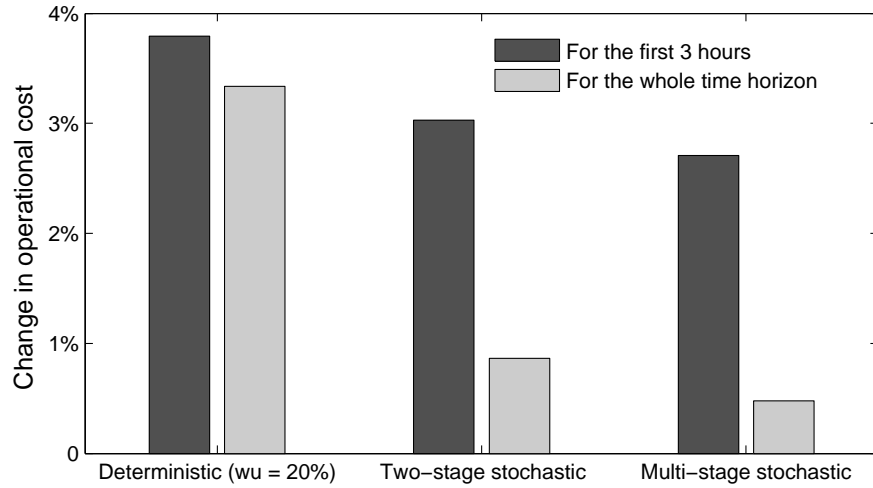
Figure 7.21: Changes of the total operational costs of the GB gas and electricity network for different models with respect to the PFM

In the stochastic models, operational costs during the early time steps, when the wind power is known, and also over the time horizon is lower compared to DM. The total operational costs for the TSM and MSM are 0.11 and 0.12 million pounds lower with respect to DM, respectively (see Table 7.1). This is a significant reduction in the total operational cost over the time horizon.

Table 7.1: Operational costs of the GB integrated gas and electricity networks for different models (£million)

PFM	DM	TSM	MSM
92.3	93.7	92.6	92.5

7.10 Discussion

Two-stage and multi-stage stochastic programming models were used to investigate operation of the GB integrated gas and electricity network in the presence of wind uncertainty. The advantages of adopting stochastic approach for network operation were highlighted such as reduction in wind curtailment and operational costs.

Analysis performed shows that even perfect foresight on wind power does not prevent wind curtailment when low electricity demand periods coincides with high wind periods. This is due to the lack of flexible generation capacity and large scale electricity storage devices to compensate for wind variability. Although pumped storage plants were shown to be responsive to sudden changes of wind power output, their capacity in the GB network (2.7 GW) is not sufficient to deal with 29 GW wind generation capacity.

Impacts of wind uncertainty on the gas network operation were investigated through gas demand for electricity generation. It was shown that different wind forecast scenarios lead to various states of gas network operation. For example, there is an inverse relationship between level of wind power generation and energy consumed by compressors. During the analysis no instance of gas supply security was resulted.

Operational costs of the GB integrated network in the presence of large capacity of wind generation, with uncertain wind output, were calculated for different approaches. Applying the stochastic approaches to operate the integrated network results in significant reduction in operational costs.

Chapter 8

Conclusions

8.1 Conclusions

Large scale integration of wind generation capacity into the energy system was investigated from different perspectives including impacts on the power transmission network, gas network and unit commitment integrated with economic dispatch. For the challenges introduced by large wind generation capacity appropriate measures were proposed and their effectiveness were analysed through detailed modelling of each measure. Developing western and Eastern HVDC links and gas storage facilities are two solutions proposed to deal with impacts of geographically dispersed wind farms on the transmission network and wind variability on the gas network, respectively. Use of new operational planning models, such as two- and multi-stage stochastic programming models also is a solution for operating the gas and electricity network under wind uncertainty.

8.1.1 Dispersed wind generation capacity and the transmission network

Wind farms location in GB is not distributed uniformly across the country. A large capacity of onshore and offshore wind generation is expected to be installed in Scotland while large power demand centres are in the South. Therefore power transmission capacity reinforcement is required to deliver generated power.

The electricity part of the CGEN model was used to analyse the adequacy of the GB power transmission network in 2020 to deal with power delivery from wind farms to demand centres. The role of Eastern and Western HVDC submarine links were investigated.

It was shown that both HVDC links connecting Scotland to England result in greater use of available wind generation (reduction in curtailment), lower gas use for electricity generation and therefore reduced operating costs. Investment in either HVDC link gave favourable pay back periods. This conclusion is supported by National Grid current initiatives to develop the HVDC submarine links.

8.1.2 Impacts of wind variability on the gas network

Impacts of wind power variations on the GB gas network were investigated and bottle-necks of the network were identified. Subsequently, the efficacy of appropriate measures was analysed.

Given the large amount of wind generation and low coal-fired generation capacity anticipated in the UK by 2020, gas-fired generators will be used to compensate for wind power variability due to their fast ramping rates and sizable generation capacity. However, this could lead to significant power swings on the gas network as gas-fired generators ramp up and down.

The simulation results showed that the simultaneous occurrence of low wind generation and peak electricity demand in 2020 will result in rapid and large increases in gas consumption, mainly due to the demand from gas-fired generation. The insufficiency of local linepack in the gas network will constrain gas supply to some gas-fired generators. Consequently these generators will operate at reduced output and more expensive sources of electricity will be employed to meet shortfalls in generation. The gas interconnectors and LNG terminals will have a crucial role in supplying gas to GB in 2020.

It was shown that additional gas storage facilities could enhance gas availability and increase linepack during periods of high gas demand and low wind generation.

8.1.3 Stochastic programming models of an integrated gas and electricity network

Wind uncertainty becomes more challenging when the capacity of wind generation increases. Uncertainty in wind forecasts can be mitigated through large scale electricity storage devices that allow excess electricity generated from wind to be stored, and therefore supply electricity during low wind periods. But the problem is the economic feasibility of introducing such facilities. Applying new models for optimal system operation that take into account the wind uncertainty is necessary.

Two- and multi-stage stochastic programming models were developed for optimising the operation of the GB gas and electricity networks, take into account the wind uncertainty. A method for producing probabilistic wind power forecasts was also developed and used along with the stochastic models of gas and electricity network to obtain the optimal strategies to operate the system under wind uncertainty.

Applying the stochastic programming models resulted in lower wind curtailment compared to the deterministic calculation. Analysis showed wind energy curtailment occurs even when using the perfect foresight model, which illustrates the lack of large scale electricity storage devices or flexible generation plants with low Start-up/Shutdown costs to accommodate wind generation during low demand periods.

Impacts of wind uncertainty on gas network operation were investigated through gas demand for electricity generation. It was shown that different levels of wind generation lead to various states of gas network operation. For example, there is an inverse relationship between level of wind generation and energy consumed by compressors.

Using the stochastic models resulted in lower operational costs of the case studied, without compromising on the security of the system. The total expected operational

costs for the two- and multi-stage stochastic models were 0.11 and 0.12 million pounds lower compared to the deterministic calculation, respectively. This is a significant reduction in total operational costs over a day.

8.2   Contributions of the thesis

- Role of new Western and Eastern HVDC links on the operation of the GB electricity network in 2020 was investigated, using CGEN electricity model.

- Impacts of wind variability on the operation of the GB gas and electricity network in 2020 was analysed, using CGEN model. Bottlenecks of the gas network were identified and appropriate solutions were proposed through detailed technical modelling.

- Developing a computer code to produce probabilistic wind power forecast scenarios, usable in stochastic optimisation of gas and electricity network operation.

- Developing two-stage and multi-stage stochastic programming models to optimise an integrated gas and electricity network.

- the operation of the GB integrated gas and electricity network, taking account of wind uncertainty.

8.3   Future work

Modelling the detailed dynamic behaviour of gas flow through a pipe results in more accurate investigation of the interdependencies between gas and electricity network. In particular, taking into account the effects of temperature on the gas flow is important. Because of the negative correlation between temperature and gas demand (especially during winter), it is crucial to also analyse sensitivity of gas flow to temperature.

The stochastic model, developed in this research, consists of gas and electricity network models which are non-linear and mixed integer mathematical programming problems, respectively. Hence, the computational cost of the model is of concern, especially when running a multi-stage stochastic programming problem with a number of scenarios. More efficient solution algorithms are required in order to reduce the simulation run time and obtain more accurate solution sets. Given the extensive use of lagrangian relaxation technique in the literature, it is suggested as a possible solution method.

Wind uncertainty in generation portfolios that are exposed to a competitive electricity market leads to uncertainty in energy prices. A stochastic model that can help individual owners of the thermal generators with decision making on time-ahead scheduling and bidding would be of interest. A mixed Complementary Programming (MCP) approach integrated with the stochastic recourse is suggested for developing a model.

Appendix A: Comparison of the simplified and complete gas network

An example of gas network simplification is shown in Fig. 1. The simplified and complete gas networks are compared over a single time step. See Fig 2 and Tables 1 and 2.
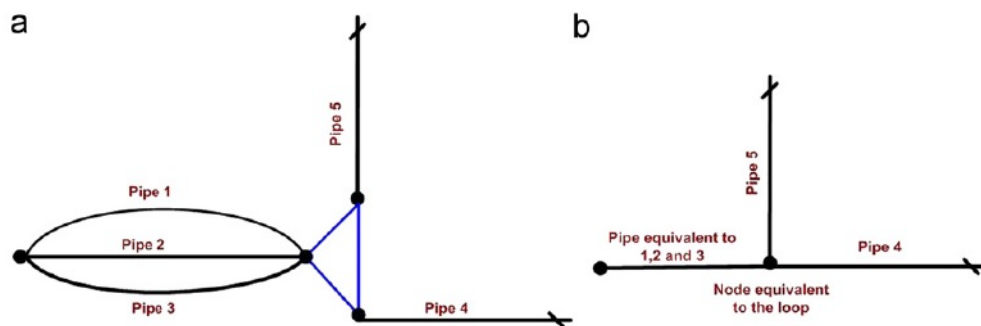
Figure 1: An example of gas network simplification. Part of the (a) original network and (b) simplified network.
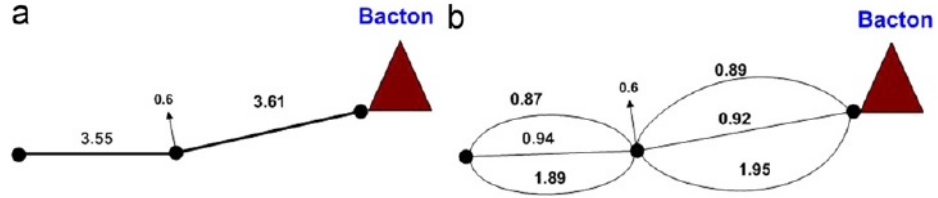
Figure 2: Comparison of gas flow in parallel pipes with the equivalent pipe. Part of the (a) simplified network and (b) complete gas network (NTS).

Table 1: Comparison of gas supply from different terminals (mcm).

Gas terminals	NTS	Simplified
St Fergus	0.978	0.923
Teesside	1.678	2.016
Barrow	1.377	1.35
Burton point	0	0.003
Easington	2.652	2.797
Theddlethorpe	1.272	1.413
Bacton	6.669	6.235
Isle of Grain	1.367	1.6
Milford Haven	1.89	1.63

Table 2: Comparison of gas deliverability and pressure at different storage facilities.

	Gas deliverability (mcm)		Gas pressure (bar)	
	NTS	Simplified	NTS	Simplified
Glenmavis	0.76	0.77	65.25	66.74
Horn sea	1.53	1.53	76.17	71.7
Hatfield moore	0.2	0.2	69.94	69.59
Partington	1.65	1.67	66.45	66.73
Hole house	0.23	0.23	65.81	66.32
Humbly grove	0.31	0.31	74.51	76.03
Avonmouth	1.19	1.2	85	70.74
Dynevor Arms	0.37	0.37	67.22	78.83
Rough	3.66	3.66	82.05	78.34

References

[1] PelaFlow Consulting. Windpower program - wind turbine power output variation with steady wind speed. `http://www.wind-power-program.com/turbine_characteristics.htm`. viii, 40

[2] J. Oswald, M. Raine, and H. Ashraf-Ball. Will british weather provide reliable electricity? *Energy Policy*, 36(8):3212 – 3225, 2008. viii, 6, 7, 39, 40, 41, 47

[3] International Energy Agency. World energy outlook 2010. `http://www.iea.org/weo/2010.asp`, 2010. xii, 1, 2

[4] National Grid plc. Initial consultation: operating the electricity transmission networks in 2020. `http://www.nationalgrid.com/NR/rdonlyres/32879A26-D6F2-4D82-9441-40FB2B0E2E0C/39517/Operatingin2020Consulation1.pdf`, 2009. xii, 3, 4, 38, 46, 124

[5] UKERC. Ukerc energy 2050 report, 2009. xii, 30

[6] PB Power. The cost of generating electricity. `http://www.raeng.org.uk/news/publications/list/reports/Cost_of_Generating_Electricity.pdf`. xii, 45

[7] S. Bisanovic, M. Hajro, and M. Dlakic. Mixed integer linear programming based thermal unit commitment problem in deregulated environment. *Journal of Electrical Systems*, 6(4):466–479, 2010. xii, 96

[8] Redpoint Energy Ltd. Decarbonising the gb power sector: evaluating investment pathways, generation patterns and emissions through to 2030. `http://hmccc.s3.amazonaws.com/docs/FINAL%2520Decarbonising%2520the%2520GB%2520power%2520sector_v1.pdf`. xii, 28, 97

[9] A. Gerber, J. B. Ekanayake, B. Awad, and N. Jenkins. Operation of the 2030 gb power generation system. *Proceedings of the ICE - Energy*, 164(1):25–37, February 2011. xiii, 28, 96, 99

[10] Mott MacDonald. *UK Electricity Generation Costs Update.* 2010. xiii, 102

[11] Department of Energy and Climate Change (DECC). The uk renewable energy strategy. `http://www.renewableseast.org.uk/uploads/TheUKRenewableEnergyStrategy2009[1].pdf`, 2009. 3, 38

145

[12] European Parliament. Directive 2001/80/ec of the european parliament and of the council. `/http://eur-lex.europa.eu/LexUriServ/site/en/oj/2001/l_309/l_30920011127en00010021.pdfS`, 2001. 3, 39

[13] National Grid plc. Gb ten year statement. `/https://www.nationalgrid.com/uk/Gas/TYS/archive/`, 2010. 4

[14] R. Rubio, D. Ojeda-Esteybar, O. Ano, and A. Vargas. Integrated natural gas and electricity market: A survey of the state of the art in operation planning and market issues. In *Transmission and Distribution Conference and Exposition: Latin America, 2008 IEEE/PES*, pages 1 –8, aug. 2008. 4, 7

[15] M. Chaudry, N. Jenkins, and G. Strbac. Multi-time period combined gas and electricity network optimisation. *Electric Power Systems Research*, 78(7):1265 – 1279, 2008. 4, 5, 7, 10, 11

[16] J. Munoz, N. Jimenez-Redondo, J. Perez-Ruiz, and J. Barquin. Natural gas network modeling for power systems reliability studies. In *Power Tech Conference Proceedings, 2003 IEEE Bologna*, volume 4, page 8 pp. Vol.4, june 2003. 4, 5

[17] D. Berry. Renewable energy as a natural gas price hedge: the case of wind. *Energy Policy*, 33(6):799 – 807, 2005. 4, 7

[18] M.S. Morals and J.W.M. Lima. Natural gas network pricing and its influence on electricity and gas markets. In *Power Tech Conference Proceedings, 2003 IEEE Bologna*, volume 3, page 6 pp. Vol.3, 2003. 4

[19] B. Lu and M. Shahidehpour. Unit commitment with flexible generating units. *Power Systems, IEEE Transactions on*, 20(2):1022 – 1034, may 2005. 4

[20] Z. Li. Natural gas for generation: a solution or a problem? *Power and Energy Magazine, IEEE*, 3(4):16 – 21, july-aug. 2005. 5

[21] Fulvio Fontini and Lorenzo Paloscia. The impact of the new investments in combined cycle gas turbine power plants on the italian electricity price. *Energy Policy*, 35(9):4671 – 4676, 2007. 5

[22] T. Li, M. Eremia, and M. Shahidehpour. Interdependency of natural gas network and power system security. *Power Systems, IEEE Transactions on*, 23(4):1817 –1824, nov. 2008. 5

[23] M. Shahidehpour, Y. Fu, and T. Wiedman. Impact of natural gas infrastructure on electric power systems. *Proceedings of the IEEE*, 93(5):1042 –1056, may 2005. 5, 7

[24] H. Holttinen, P. Meibom, F. v. Hulle, B. Lange, M. O'Malley, J. Pierik, J. O. Tande, A. Estanqueiro, E. Gomez, L. Soder, G. Strbac, J. C. Smith, and M. Milligan. *Design and operation of power systems with large amounts of wind power*. IEA Wind Task 25, Final report, Phase one 2006-08, 2009. 6

[25] Electricity network strategy group (ensg). `http://www.decc.gov.uk/assets/decc/11/meeting-energy-demand/future-elec-network/2032-electricity-networks-strategy-group-ensg.pdf`. 6, 8, 24

[26] Frank Graves and Julia Litvinova. Hedging effects of wind on retail electric supply costs. *The Electricity Journal*, 22(10):44 – 55, 2009. 7

[27] Pavlos S. and Georgilakis. Technical challenges associated with the integration of wind power into power systems. *Renewable and Sustainable Energy Reviews*, 12(3):852 – 863, 2008. 7

[28] Parsons B Milligan M Smith J C, DeMeo E A. Wind power impacts on electric power system operating costs: summary and perspective. In *American wind energy association global wind power conference*, 2004. 7

[29] Zavadil R Santoso S Smith J Brooks D, Lo E. Characterizing the impact of significant wind generation facilities on bulk power system operations planning. In *Utility Wind Integration Group*, 2003. 7

[30] Electrotek ConceptsInc. Systems operations impacts of wind generation integration study. `http://www.uwig.org/WeEnergiesWindImpacts_FinalReport.pdf`, 2003. 7

[31] Barry W and Kennedy. Integrating wind power: Transmission and operational impacts. *Refocus*, 5(1):36 – 37, 2004. 7

[32] M. Urbina and Z. Li. Modeling and analyzing the impact of interdependency between natural gas and electricity infrastructures. In *Power and Energy Society General Meeting - Conversion and Delivery of Electrical Energy in the 21st Century, 2008 IEEE*, pages 1 –6, july 2008. 7

[33] F. Palacios-Gomez, L. Lasdon, and M. Engquist. Nonlinear optimization by successive linear programming. *Management Science*, 28(10):1106 – 1120, 1982. 11

[34] A. Osiadacz. Simulation and analysis of gas networks. *Gulf Publishing Company*, 1987. 13, 14, 15, 16, 18

[35] F. Corraro and L. Verde. A component oriented modelling approach for fluid-dynamic piping system simulation (fluidys). In *Computer-Aided Control System Design, 2000. CACSD 2000. IEEE International Symposium on*, pages 214 –219, 2000. 13

[36] I. Cameron. Using an excel-based model for steady-state and transient simulation. In *Pipeline Simulation Interest Group (PSIG), 31st annual meeting*, pages 20 –22, 1999. 15

[37] S. An, Q. Li, and T.W. Gedra. Natural gas and electricity optimal power flow. In *Transmission and Distribution Conference and Exposition, 2003 IEEE PES*, volume 1, pages 138 – 143 Vol.1, sept. 2003. 18

[38] M. Thompson, M. Davison, and H. Rasmussen. Natural gas storage valuation and optimization: A real options application. *Naval Research Logistics (NRL)*, 56(3):226–238, 2009. 19, 20

[39] A. J. Wood and B. F. Wollenberg. *Power Generation, Operation, and Control.* 1996. 20, 96

[40] X. Wang and J. McDonald. *Modern Power System Planning.* 1994. 20

[41] ENSG. Our electricity transmission network: a vision for 2020. `http://webarchive.nationalarchives.gov.uk/20100919181607/http:/www.ensg.gov.uk/assets/ensg_transmission_pwg_full_report_final_issue_1.pdf`, 2009. 24, 28, 29

[42] Consultation document. Western hvdc link - preparing our energy network for the future. `http://www.westernhvdclink.co.uk/files/consultation.pdf`. 24

[43] National Grid Electricity Transmission plc. 2009 offshore development information statement, and appendixes. `http://www.nationalgrid.com/uk/Electricity/ODIS/Archive/`, 2009. 28

[44] A. Gerber, M. Qadrdan, M. Chaudry, J. Ekanayake, and N. Jenkins. A 2020ăgb transmission network study using dispersed wind farm power output. *Renewable Energy*, 37(1):124 – 132, 2012. 28

[45] Enterprise & Regulatory Reform (BERR) Department for Business. Atlas of uk marine renewable energy resources: technical report. http://www.renewables-atlas.info/downloads/documents/$R1432_Final_15May08.pdf$. 28

[46] Hsu SA. *Meteorology.* London: Academic Press, 1988. 28

[47] D. McQueen and S. Watson. Validation of wind speed prediction methods at offshore sites. *Wind Energy*, 9:75–85, 2009. 28

[48] National Grid plc. `/http://www.nationalgrid.com/uk/Electricity/Data/Demand+Data/`, 2009. 30, 46

[49] Jesse D. Maddaloni, Andrew M. Rowe, and G. Cornelis van Kooten. Wind integration into various generation mixtures. *Renewable Energy*, 34(3):807 – 814, 2009. 39

[50] National Grid plc. Gb ten year statement. `/https://www.nationalgrid.com/uk/Gas/TYS/archive/`, 2008. 42, 46

[51] M. Qadrdan, M. Chaudry, J. Wu, N. Jenkins, and J. Ekanayake. Impact of a large penetration of wind generation on the gb gas network. *Energy Policy*, 38(10):5684 – 5695, 2010. 42

[52] National Grid plc. Gb seven year statement. `/https://www.nationalgrid.com/uk/Gas/TYS/archive/`, 2008. 47

[53] S. Lefton and P. Besuner. Power plant cycling operations and unbundling their effect on plant heat rate. /http://www.aptecheng.com, 2001. 58

[54] K. Methaprayoon, C. Yingvivatanapong, W.J. Lee, and J.R. Liao. An integration of ann wind power estimation into unit commitment considering the forecasting uncertainty. *Industry Applications, IEEE Transactions on*, 43(6):1441 –1448, nov.-dec. 2007. 61, 78

[55] H. Holttinen G. Giebel, P. Sorensen. Forecast error of aggregated wind power. http://www.trade-wind.eu/fileadmin/documents/publications/D2.2_ Estimates_of_forecast_error_for_aggregated_wind_power_Final.pdf, 2007. 61

[56] B. Ernst, B. Oakleaf, M.L. Ahlstrom, M. Lange, C. Moehrlen, B. Lange, U. Focken, and K. Rohrig. Predicting the wind. *Power and Energy Magazine, IEEE*, 5(6):78 –89, nov.-dec. 2007. 61

[57] A. Botterud, J. Wang, C. Monterio, and V. Miranda. Wind power forecasting and electricity market operations. http://www.usaee.org/usaee2009/submissions/ OnlineProceedings/Botterud_etal_paper.pdf. 61, 78

[58] C. Monterio, R. Bessa, V. Miranda, A. Botterud, J. Wang, and G. Conzelmann. Wind power forecasting: State-of-the-art 2009. http://www.dis.anl.gov/pubs/65613.pdf, 2009. 61, 62

[59] Y. V. Makarov, P. V. Etingov, Z. Huang, J. Ma, B. B. Chakrabarti, K. Subbarao, C. Loutan, and R. T. Guttromson. Integration of wind generation and load forecast uncertainties into power grid operations. In *Transmission and Distribution Conference and Exposition, 2010 IEEE PES*, pages 1 –8, april 2010. 62

[60] J. Juban, N. Siebert, and G.N. Kariniotakis. Probabilistic short-term wind power forecasting for the optimal management of wind generation. In *Power Tech, 2007 IEEE Lausanne*, pages 683 –688, july 2007. 62

[61] P. Pinson, H. Madsen, H. A. Nielsen, G. Papaefthymiou, and B. Klockl. From probabilistic forecasts to statistical scenarios of short-term wind power production. *Wind Energy*, 12(1):51–62, Sep 2008. 62

[62] J. B. Bremnes. Probabilistic wind power forecasts using local quantile regression. *Wind Energy*, 7(1):47–54, 2004. 62

[63] H. Hassani. Singular spectrum analysis: Methodology and comparison. *Journal of Data Science*, 5:239–257, 2007. 62

[64] Nekrutkin V. Golyandina, N. and A Zhigljavsky. *Analysis of Time Series Structure: SSA and related techniques*. 1996. 63, 65

[65] ELEXON Ltd. http://www.bmreports.com/bsp/bsp_home.htm. 66

[66] H. Brand, E. Thorin, and C. Weber. *Scenario reduction algorithm and creation of multi-stage scenario trees*. OSCOGEN, 2002. 73

[67] J. Dupacová, N. Gröwe-Kuska, and W. Römisch. Scenario reduction in stochastic programming: An approach using probability metrics, 2003. 73

[68] V.S. Pappala, I. Erlich, K. Rohrig, and J. Dobschinski. A stochastic model for the optimal operation of a wind-thermal power system. *Power Systems, IEEE Transactions on*, 24(2):940 –950, May 2009. 77

[69] P. Beraldi, D. Conforti, and A. Violi. A two-stage stochastic programming model for electric energy producers. *Comput. Oper. Res.*, 35:3360–3370, October 2008. 77

[70] L. Wu, M. Shahidehpour, and T. Li. Cost of reliability analysis based on stochastic unit commitment. *Power Systems, IEEE Transactions on*, 23(3):1364 –1374, 2008. 77, 78

[71] J. Garcia-Gonzalez, R.M.R. de la Muela, L.M. Santos, and A.M. Gonzalez. Stochastic joint optimization of wind generation and pumped-storage units in an electricity market. *Power Systems, IEEE Transactions on*, 23(2):460 –468, May 2008. 77

[72] P. Carpentier, G. Gohen, J.-C. Culioli, and A. Renaud. Stochastic optimization of unit commitment: a new decomposition framework. *Power Systems, IEEE Transactions on*, 11(2):1067 –1073, May 1996. 77

[73] F. Bouffard and F.D. Galiana. Stochastic security for operations planning with significant wind power generation. *Power Systems, IEEE Transactions on*, 23(2):306 –316, May 2008. 77

[74] A. Tuohy, P. Meibom, E. Denny, and M. O'Malley. Unit commitment for systems with significant wind penetration. *Power Systems, IEEE Transactions on*, 24(2):592 –601, May 2009. 77

[75] J. Wang, M. Shahidehpour, and Z. Li. Security-constrained unit commitment with volatile wind power generation. *Power Systems, IEEE Transactions on*, 23(3):1319 –1327, aug. 2008. 77

[76] A. Shapiro, D. Dentcheva, and A. Ruszczynski. *Lectures on Stochastic Programming; Modelling and Theory*. Pereqrinus Ltd., Stevenage, U.K., 1981. 79, 81

[77] A. Ruszczynski and A. Shapiro, editors. *Stochastic Programming*, volume 10 of *Handbooks in Operations Research and Management Science*. Elsevier, 2003. 79

[78] K. Marti. *Stochastic Optimization Methods*. Springer, second edition edition, 2008. 79

[79] P. Kall and J. Mayer. *Stochastic Linear Programming: Models, Theory, and Computation*, volume 80 of *International Series in Operations Research & Management Science*. Springer, 2005. 79

[80] J. Mayer. On the numerical solution of jointly chance constrained problems. In *Probabilistic constrained optimization*, volume 49 of *Nonconvex Optim. Appl.*, pages 220–235. Kluwer Acad. Publ., Dordrecht, 2000. 79

[81] A. Charnes and W. W. Cooper. Chance constrained programming. *Management Science*, 6:73 – 79, 1959. 79

[82] Y. Ermoliev, , and R. J-B Wets. *A Computer Code for Solution of Probabilistic-Constrained Stochastic Programming Problems, by T. Szantai.* Berlin: Springer-Verlag, 1988. 79

[83] A. Prekopa. On probabilistic constrained programming. Princeton: Princeton University Press, 1970. 79

[84] U.A. Ozturk, M. Mazumdar, and B.A. Norman. A solution to the stochastic unit commitment problem using chance constrained programming. *Power Systems, IEEE Transactions on*, 19(3):1589 – 1598, aug. 2004. 79

[85] R. Zorgati, W. van Ackooij, and R. Apparigliato. Supply shortage hedging: Estimating the electrical power margin for optimizing financial and physical assets with chance-constrained programming. *Power Systems, IEEE Transactions on*, 24(2):533 –540, may 2009. 79

[86] W. Jiekang, Z. Jianquan, C. Guotong, and Z. Hongliang. A hybrid method for optimal scheduling of short-term electric power generation of cascaded hydroelectric plants based on particle swarm optimization and chance-constrained programming. *Power Systems, IEEE Transactions on*, 23(4):1570 –1579, nov. 2008. 79

[87] P. Couchman, B. Kouvaritakis, M. Cannon, and F. Prashad. Gaming strategy for electric power with random demand. *Power Systems, IEEE Transactions on*, 20(3):1283 – 1292, aug. 2005. 79

[88] T. Shiina. Numerical solution technique for joint chance-constrained programming problem; an application to electric power capacity expansion. *Journal of the Operations Research Society of Japan*, 42:128 – 140, 1999. 79

[89] J. Anders, G. Generation planning model with reliability constraints. *IEEE Transactions on Power Apparatus and Systems*, PAS-100:4901 – 4908, 1981. 79

[90] M. Carrion and J.M. Arroyo. A computationally efficient mixed-integer linear formulation for the thermal unit commitment problem. *Power Systems, IEEE Transactions on*, 21(3):1371 –1378, aug. 2006. 94

[91] N. Growe-Kuska, K.C. Kiwiel, M.P. Nowak, W. Romisch, and I. Wegner. Power management in a hydro-thermal system under uncertainty by lagramgian relaxation. *Decision Making under Uncertainty: Energy and Power*, 2005. 95, 98

[92] Y. Rebours and D. Kirschen. What is spinning reserve? `http://www.eee.manchester.ac.uk/research/groups/eeps/publications/reportstheses/aoe/rebours%20et%20al_tech%20rep_2005A.pdf`, 2005. 97, 98

[93] T.Y. Lee. Optimal spinning reserve for a wind-thermal power system using eipso. *Power Systems, IEEE Transactions on*, 22(4):1612 –1621, nov 2007. 105, 119